Available online at www.sciencedirect.com
ScienceDirect
Materials Letters 61 (2007) 3984–3987
materials letters
www.elsevier.com/locate/matlet

Biosynthesis of gold nanoparticles using the bacteria *Rhodopseudomonas capsulata*

Shiying He, Zhirui Guo, Yu Zhang, Song Zhang, Jing Wang, Ning Gu *

State Key Laboratory of Bioelectronics, Southeast University, Nanjing, 210096, PR China
Jiangsu Laboratory for Biomaterials and Devices, Southeast University, Nanjing, 210096, PR China

Received 10 October 2006; accepted 1 January 2007
Available online 13 January 2007

Abstract

The use of microorganisms in the synthesis of nanoparticles emerges as an eco-friendly and exciting approach. In this study, the bacteria *Rhodopseudomonas capsulata* was screened and found to successfully produce gold nanoparticles of different sizes and shapes. The important parameter, which controls the size and shape of gold nanoparticles, was pH value. The *R. capsulata* biomass and aqueous $HAuCl_4$ solution were incubated at pH values ranging from 7 to 4. The results demonstrated that spherical gold nanoparticles in the range of 10–20 nm were observed at pH value of 7 whereas a number of nanoplates were observed at pH 4.

© 2007 Elsevier B.V. All rights reserved.

Keywords: Biosynthesis; Nanomaterials; Gold; Enzyme; Microorganism; Electron microscopy

1. Introduction

The optoelectronic and physicochemical properties of nanoscale matter are size- and shape-dependent [1–3]. So the synthesis of gold nanoparticles of different sizes and shapes is of great importance for their applications in optical devices, electronics, biotechnologies and catalysis [4–6]. Conventional synthetic methods of gold nanoparticles have involved a number of chemical methods [7–10]. There is an increasing pressure to develop clean, nontoxic and environmentally benign synthetic technologies. Microbial resistance against heavy metal ions has been exploited for biological metal recovery via reduction of the metal ions or formation of metal sulfides [11]. So the attractive procedure is using microorganisms such as bacteria and fungi to synthesize gold nanoparticles recently. An earlier study found that *Bacillus subtilis* 168 [12] were able to reduce Au^{3+} ions to gold nanoparticles with a size range of 5–25 nm inside the cell walls. *Shewanella algae* were found to reduce Au^{3+} ions forming 10–20 nm gold nanoparticles extracellularly with the assistance of hydrogen gas [13]. Fungi (*Verticillium* sp [14] and *Fusarium oxysporum* [15]) and actinomycete (*Thermomonospora* sp [16] and *Rhodococcus* sp [17]) were also used to synthesize nanoparticles intra- or extracellularly. However, the biosynthesis of gold nanoplate extracellularly is still scarce. In this study, prokaryote bacteria *Rhodopseudomonas capsulata*, recognized as one of the ecologically and environmentally important microorganisms, commonly existing in the natural environment, were investigated for reducing Au^{3+} ions at room temperature with a single step process. Especially gold nanoplates were formed under the lower starting pH.

2. Experiment

2.1. Synthesis

Photosynthetic bacteria *R. capsulata* were cultured in the medium containing purvate, yeast extract, NaCl, NH_4Cl and K_2HPO_4 at pH 7 and 30 °C. The bacteria were cultured for 72 h and separated from broth by centrifugation (5000 rpm) at 4 °C

---

* Corresponding author. State Key Laboratory of Biolectronics, Southeast University, Nanjing, 210096, PR China. Tel.: +86 25 8379 2576; fax: +86 25 8379 4960.

E-mail address: guning@seu.edu.cn (N. Gu).

0167-577X/$ - see front matter © 2007 Elsevier B.V. All rights reserved.
doi:10.1016/j.matlet.2007.01.018

for 10 min. The collected bacteria were washed five times with distilled water to obtain about 1 g wet weight of bacteria and then resuspended in 20 mL of 1×10^{-3} M aqueous $HAuCl_4$ solution in a test tube. The reactants were adjusted to neutral pH using 0.1 M NaOH solution. In other experiments, the starting pH of the 1×10^{-3} M aqueous $HAuCl_4$ solution added with biomass was adjusted to 6, 5 and 4 using 0.1 M NaOH and HCl solutions respectively in test tubes. All the experiments were conducted at room temperature for a period of 48 h.

The UV–Visible spectra of gold nanoparticles synthesized were measured on a Shimadzu spectrophotometer (model UV-3150PC). The products were dropped on a carbon-coated grid and then analyzed by transmission electron microscopy (TEM) (JEOL, JEM-200EX) and electronic diffraction (ED, JEOL, JEM-200EX) was used to determine the crystal structure of the samples. X-ray diffraction (XRD) measurements were carried out on a Shimadzu XD-3A instrument. The reaction solution was inoculated on the agar plate to detect the viability of bacteria after reacting with aqueous $HAuCl_4$ solution.

3. Results and discussion

The aqueous chloroaurate ions were reduced during exposure to the bacteria *R. capsulata* biomass. The color of the reaction solution turned from pale yellow to purple (as shown in Fig. 1A), which indicated the formation of gold nanoparticles extracellularly. The reaction was completed after 48 h of incubation indicating that it was a slow process. The color of the reaction solution remained purple without any changes, and the gold nanoparticles analyzed by UV–Vis spectra and TEM were stable after 48 h of reaction. Control experiments without biomass addition stayed pale yellow, indicating that the production of gold nanoparticles was obtained by the reduction of microorganisms indeed. Fig. 1B shows the UV–Vis absorption spectra recorded from the gold nanoparticles solution after 48 h of reaction (curve 1). The results indicate that the reaction solution has an absorption maximum at about 540 nm attributed to the surface plasmon resonance band (SPR) of the gold nanoparticles. After the reaction, the gold nanoparticles solution was filtered from the bacteria *R. capsulata* biomass and aged for three months. Then the gold NPs solution was tested for stability using UV–Vis spectra measurement. The results as shown in Fig. 1B (curve 2) indicate that the solution was stable for at least three months with only little aggregation of particles in the solution.

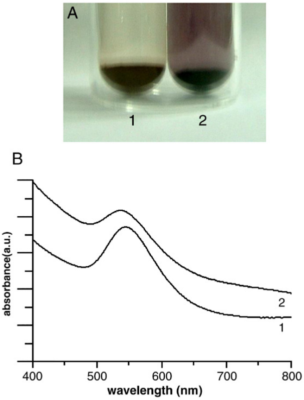

Fig. 1. (A) Picture of test tubes containing the bacteria *R. capsulata* biomass before (test tube 1) and after 48 h (test tube 2) incubation in an aqueous of $AuCl_4^-$ solution at neutral pH; (B) UV–Vis absorption spectra of gold nanoparticles after the reaction of 10^{-3} M aqueous $HAuCl_4$ solution at neutral pH with the bacteria *R. capsulata* for 48 h (curve 1) and kept for three months after reaction (curve 2).

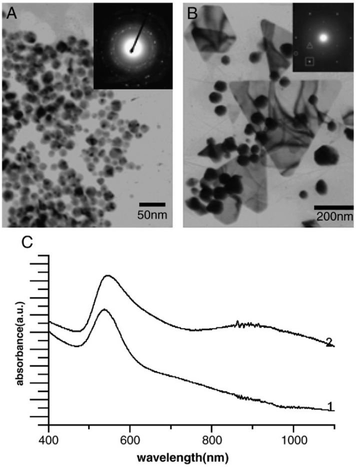

Fig. 2. (A) TEM image of the gold nanoparticles produced by the reaction of 10^{-3} M aqueous $HAuCl_4$ solution with bacteria *R. capsulata* biomass at pH 7. The inset shows their ED pattern. (B) TEM image of the gold nanoparticles produced by the reaction of 10^{-3} M aqueous $HAuCl_4$ solution with bacteria *R. capsulata* biomass at pH 4. The inset shows a typical SAED pattern of a gold nanoplate. (C) UV–Vis absorption spectra of gold nanoparticles produced at pH 7 (curve 1) and pH 4 (curve 2).

Experiments were performed to detect the viability of the bacteria to the gold ions and gold NPs. Bacteria *R. capsulata* were found to proliferate when a small drop of solution containing bacteria and gold NPs was inoculated on agar plates demonstrating that the bacteria are resistant to the gold ions and gold NPs.

Transmission electron microscopy (TEM) measurements show the various shapes and sizes of gold nanoparticles formed with the changes of pH. As shown in Fig. 2A, well-separated gold nanoparticles with occasional aggregation are mainly spherical in the size range 10–20 nm at pH 7. This is consistent with the optical spectrum (Fig. 2C). The diffraction ring, as can be seen from the electron diffraction (ED) pattern recorded from the gold nanoparticles, is consistent with nanocrystalline gold. With the decrease of pH, gold nanoplates appeared. When the pH was adjusted to 4, there were a number of nanoplates observed in addition to the spherical gold nanoparticles in the reaction solution. Fig. 2B shows the representative TEM image of gold nanoparticles obtained. It is clearly seen that the predominantly larger nanoparticles are triangular nanoplates. The single-crystalline structure of these nanoplates was further confirmed by their corresponding selected-area electron diffraction (SAED) analysis. From many TEM images similar with Fig. 2B, statistical analysis of the gold nanoparticles was performed. The results indicate that nearly 60% of the total nanoparticle population is due to triangular gold nanoplates in the size of 50–400 nm. And most of the other nanoparticles are spherical with a size range of 10–50 nm. Fig. 2C shows typical UV–Vis–NIR spectrum of gold nanoparticles at pH 4. Two SPR bands of the gold nanoplates centering respectively at about 540 nm (band I) and 900 nm (band II) are clearly visible. Band I is a common feature corresponding to the traverse surface plasmon resonance and band II that occurs in the NIR region indicates the longitudinal plasmon resonance of the gold nanoplates.

As shown by the XRD pattern in Fig. 3, which corresponds to the gold nanoparticles in Fig. 2B, Bragg reflections are present, which could be indexed on the basis of the face-centered cubic (fcc) gold structure. No spurious diffractions due to crystallographic impurities were found. An overwhelmingly strong diffraction peak located at 38.09° is ascribed to the {1 1 1} facets of face-centered cubic metal gold structures, while diffraction peaks of other four facets are much weak. It is worth pointing that the ratio of intensity between the {2 0 0} and {1 1 1} peaks is much lower than the standard value (0.068 versus 0.53). The ratio between the {2 2 0} and {1 1 1} peaks is also much lower than the standard value (0.039 versus 0.33). These observations indicate that the gold nanoplates formed by the reduction of Au (III) by bacteria *R. capsulata* are dominated by the {111} facets, and most of the {111} planes parallel to the surface of the supporting substrate were sampled.

These results show that the starting pH could have an important effect on the size and shape of gold nanoparticles. Different pH would regulate the proton concentration resulting in the control of gold nanoparticles morphology. The main groups of the enzyme secreted by biomass that may play an important role in reducing the $AuCl_4^-$ ions include amino, sulfhydryl and carboxylic groups [14–16,18]. And the $AuCl_4^-$ ions could bind to biomass through these functional groups. These groups of the biomass might carry more positive charge at low pH values, which weakens the reducing power of the biomass and allows the $AuCl_4^-$ ions to get closer to the binding sites. So the reaction rate of gold ions is very slow and Au-biomass biosorbent is strong, which would contribute to the formation of nanoplate morphologies. On increasing pH values, the reducing power and reaction rate increase correspondingly and could contribute to the formation of thermodynamic-favored spherical particles.

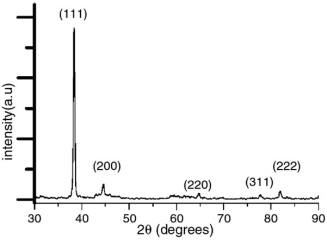

Fig. 3. Representative XRD pattern of gold nanoplates synthesized by the reaction of 10^{-3} M aqueous $HAuCl_4$ solution with bacteria *R. capsulata* biomass at pH 4.

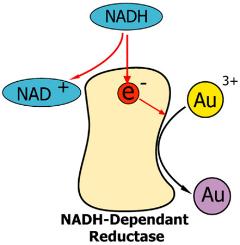

Scheme 1. Possible mechanisms of gold ions bioreduction.

The possible role as shown in Scheme 1 is involved in the electron shuttle enzymatic metal reduction process. Previous studies [15,19,20] have indicated that NADH- and NADH-dependent enzymes are important factors in the biosynthesis of metal nanoparticles. Bacteria *R. capsulata* are known to secrete cofactor NADH- and NADH-dependent enzymes that may be responsible for the bioreduction of Au (3+) to Au (0) and the subsequent formation of gold nanoparticles. The reduction seems to be initiated by electron transfer from the NADH by NADH-dependent reductase as electron carrier. Then the gold ions obtain electrons and are reduced to Au (0). The exact mechanism of the reduction of gold ions is yet to be elucidated for bacteria *R. capsulata*. Our current research focuses on the biological reduction mechanism of gold ions and our findings will be reported later.

4. Conclusion

In conclusion, it has been demonstrated that the bacteria *R. capsulata* are capable of producing gold nanoparticles extracellularly and the gold nanoparticles are quite stable in solution. And this is an efficient, eco-friendly and simple process. The shape of the gold nanoparticles is controlled by pH. Work is continuing for the study of the biological mechanism for the nanoparticles formation and more detailed study of controlling the shapes and sizes of nanoparticles. The NIR absorbance of the gold nanotriangles could find interesting applications in cancer hyperthermia. This report will also lead to the development of a rational biosynthetic procedure for other metal nanomaterials such as silver and platinum with the bacteria *R. capsulata*.

Acknowledgements

The authors gratefully acknowledge the financial support given to this research from the National Natural Science Foundation of China (Nos. 60371027, 60171005 and

90406023). We are also grateful to Mr. Aiqun Xu and Xun Xiao from the Analysis and Testing Centre of Southeast University for their kind help with the measurements.

References

[1] A.P. Alivisatos, J. Phys. Chem. 100 (1996) 13226.

[2] R. Jin, Y. Cao, C.A. Mirkin, K.L. Kelly, G.C. Schatz, J.G. Zheng, Science 294 (2001) 1901.

[3] J. Aizpurua, P. Hanarp, D.S. Sutherland, M. Kall, G.W. Bryant, F.J.G. de Abajo, Phys. Rev. Lett. 90 (2003) 057401-1.

[4] C.N.R. Rao, A.K. Cheetham, J. Mater. Chem. 11 (2001) 2887.

[5] M. Moreno-Manas, R. Pleixats, Acc. Chem. Res. 36 (2003) 638.

[6] M. Han, X. Gao, J.Z. Su, S. Nie, Nat. Biotechnol. 19 (2001) 631.

[7] W.M. Tolles, Nanotechnology 7 (1996) 59.

[8] P.R. Selvakannan, S. Mandal, R. Pasricha, S.D. Adyanthaya, M. Sastry, Chem. Commun. 13 (2002) 1334.

[9] K. Okitsu, A. Yue, S. Tanabe, H. Matsumoto, Y. Yobiko, Langmuir 17 (2001) 7717.

[10] Y. Sun, Y. Xia, Science 298 (2002) 2176.

[11] J.R. Stephen, S.J. Maenaughton, Curr. Opin. Biotechnol. 10 (1999) 230.

[12] T.J. Beveridge, R.G.E. Murray, J. Bacteriol. 141 (1980) 876.

[13] Y. Konish, N. Deshmukh, T. Tsukiyama, N. Saitoh, Trans. Mater. Res. Soc. Jpn. 29 (2004) 2341.

[14] P. Mukherjee, A. Ahmad, M. Mandal, S. Senapati, S.R. Sainkar, M.I. Khan, R. Ramani, R. Parischa, P.V. Ajayakumar, Angew. Chem., Int. Ed. 40 (2001) 3585.

[15] P. Mukherjee, S. Senapati, A. Ahmad, M.I. Khan, M. Sastry, ChemBiochem 3 (2002) 293.

[16] A. Ahmad, S. Senapati, M.I. Khan, R. Kumar, M. Sastry, Langmuir 19 (2003) 3550.

[17] A. Ahmad, S. Senapati, M.I. Khan, R. Ramani, V. Srinivas, M. Sastry, Nanotechnology 14 (2003) 824.

[18] V. Armendariz, I. Herrwra, J.R.P. Visea, M.J. Yacaman, J. Nanopart. Res. 6 (2004) 377.

[19] A. Ahmad, P. Mukherjee, M. Mandal, S. Senapati, M.I. Khan, R. Kumar, M. Sastry, J. Am. Chem. Soc. 124 (2002) 12108.

[20] S. Senapati, A. Ahmad, M.I. Khan, M. Sastry, R. Kumar, Small 1 (2005) 517.

Bioresource Technology 113 (2012) 132–135

Contents lists available at SciVerse ScienceDirect

Bioresource Technology

journal homepage: www.elsevier.com/locate/biortech

Green synthesis of gold nanoparticles using palm oil mill effluent (POME): A low-cost and eco-friendly viable approach

Pei Pei Gan, Shi Han Ng, Yan Huang, Sam Fong Yau Li *

Department of Chemistry, National University of Singapore, 3 Science Drive 3, Singapore 117543, Singapore

ARTICLE INFO

Article history:
Available online 14 January 2012

Keywords:
Palm oil mill effluent
Biosynthesis
Gold nanoparticles
Bioreduction
Agro waste

ABSTRACT

The present study reports the synthesis of gold nanoparticles (AuNps) from gold precursor using palm oil mill effluent (POME) without adding external surfactant, capping agent or template. The biosynthesized AuNps were characterized by using UV–vis spectroscopy, transmission electron microscopy (TEM), X-ray diffraction (XRD), and Fourier transform infrared spectroscopy (FTIR). According to the image analysis performed on a representative TEM micrograph by counting 258 particles, the obtained AuNps are predominantly spherical with an average size of 18.75 ± 5.96 nm. In addition, some triangular and hexagonal nanoparticles were also observed. The influence of various reaction parameters such as reaction pH, concentration of gold precursor and interaction time to the morphology and size of biosynthesized AuNps was investigated. This study shows the feasibility of using agro waste material for the biosynthesis of AuNps which is potentially more scalable and economic due to its lower cost.

© 2012 Elsevier Ltd. All rights reserved.

1. Introduction

Gold nanoparticles (AuNps) are found to be useful in many applications such as biomedicine, catalysis, biosensing, electronic and magnetic devices. Although existing chemical and physical methods have successfully produced well-defined nanoparticles, these processes are usually costly and involve the use of toxic chemicals. In addition, synthesis of AuNps using chemical methods could still lead to the presence of some toxic chemical species being adsorbed on the surface of nanoparticles which may cause adverse effects in medical applications. In this case, synthesis of nanoparticles using microorganisms or plants could be advantageous, in which biomolecules secreted by the biomass can act as both reducing and capping agents during the reaction and resulted in nanoparticles that are more biocompatible (Lukman et al., 2011).

Over the past several years, biological synthesis of nanoparticles by using microorganisms such as bacteria (Taheri Otaqsara, 2011), fungi (Pradhan et al., 2011), and yeast (Sathish Kumar et al., 2011) have been reported by several research groups. However, a major drawback of microbial synthesis is the difficulty to provide good control over size distribution, shape and crystallinity of nanoparticles (Narayanan and Sakthivel, 2010). The manipulation of reaction parameters such as pH and temperature might inactivate the microbes and hinder the bioreduction process. In addition, the requirements of specialized facilities and long incubation time could limit the scale of production as well. In contrast, plant-mediated synthesis of nanoparticles is comparatively simpler and more cost-effective, in which nanoparticles with morphology comparable to those synthesized by chemical and physical methods were obtained (Parsons et al., 2007).

To the best of our knowledge, the use of agro waste from lignocellulosic plant biomass has not been investigated so far for their ability in biosynthesis of nanoparticles. POME is a residue generated during the production of palm oil. Approximately 0.5–0.75 ton of POME was generated from every ton of oil palm fresh fruit produced and discharged in soil and natural waters as waste (Alam et al., 2009; Chou et al., 2010). In the present study, we have demonstrated the ability of POME to synthesize AuNps without addition of any external surfactant, capping agent or template. The biosynthesized AuNps were found to be predominantly spherical, with some triangular and hexagonal shapes observed. The influence of various reaction parameters to the morphology and size of biosynthesized AuNps was also investigated.

2. Methods

POME was collected from a palm oil mill in Kluang, Johor, Malaysia. It was dried at 60 °C for 24 h before it was ground by an electrical blender and subsequently sieved. The portion of ground POME with diameter of particles $\leqslant$53 µm was used. Chloroauric acid ($HAuCl_4{\cdot}3H_2O$) was procured from Sigma–Aldrich and used as received.

---

* Corresponding author. Tel.: +65 6516 2681; fax: +65 6779 1691.
E-mail address: chmlifys@nus.edu.sg (S.F.Y. Li).

0960-8524/$ - see front matter © 2012 Elsevier Ltd. All rights reserved.
doi:10.1016/j.biortech.2012.01.015

2.1. Synthesis of AuNps

The source of gold precursor used in all the experiments was $HAuCl_4{\cdot}3H_2O$ in deionized water. Typical reaction mixtures contained 0.1 g of POME powder in 10 ml of 1.0 mM $HAuCl_4$ solution unless otherwise stated. The reaction mixtures were stirred at 300 rpm for 48 h at room temperature. At the end of reaction, the mixture was drawn and filtered for analysis. The effect of pH on the formation of AuNps was investigated by adjusting the pH of reaction mixtures (0.1 g POME, 1.0 mM $HAuCl_4$ solution) from 2.0 to 11.0 by using 0.1–1.0 M HCl and NaOH. Subsequent tests were performed at the optimum pH as determined. The effect of initial gold salt concentration was determined by changing the concentration of $HAuCl_4$ to 0.10, 0.25, 0.50, 1.0 and 2.0 mM. To study the effect of temperature on the formation of AuNps, reaction mixtures containing 0.1 g POME powder, and 10 ml of 1.0 mM $HAuCl_4$ were incubated at 25, 40 and 60 °C, respectively.

2.2. Characterization of AuNps

AuNps were characterized by using a Shimadzu UV2450 UV–vis Spectrophotometer operated at a resolution of 1 nm by using deionized water as blank for each of the sample sets. XRD diffractogram of dry nanoparticles powder was obtained using Bruker-AXS Smart Apex CCD single-crystal diffractometer with CuK_α radiation ($\lambda = 0.1542$ nm). The measurement was carried out using thoroughly dried thin films of nanoparticles on Si(1 1 1) wafers. The morphology of the AuNps was analyzed using high resolution images obtained with a JEOL 3010 TEM.

2.3. FTIR analysis

Samples of POME powder before and after reaction with $HAuCl_4$ as well as the AuNps produced were analyzed. The FTIR spectra were obtained on a Shimadzu IR Prestige-21 operated in transmission mode (400–4000 cm^{-1}) at a resolution of 4.0 cm^{-1} with the sample as KBr pellets.

2.4. Synthesis of AuNps using POME extracts

POME powder (0.1 g) was suspended in 2 ml of extraction solvent, sonicated for 2 h and centrifuged at 14,000 rpm for 10 min at room temperature using the corresponding solvent. The supernatant solutions were collected and kept for future use. During the biosynthesis, the extracted fractions were added to appropriate amount of $HAuCl_4$ and made up to a final volume of 10 ml to obtain a concentration of 1 mM solution. The reaction mixture was stirred for 48 h at room temperature. For the extraction using boiling water, 1 g of the POME powder was suspended in 50 ml of water and the mixture was boiled for 10 min.

3. Results and discussion

3.1. Effects of initial pH on the biosynthesis of AuNps

The initial pH value of the aqueous $HAuCl_4$ solutions was an important parameter in the synthesis of AuNps using POME. It was observed that the color of gold solutions changed from pale yellow to purplish-pink (pH 2.0, 3.0) and wine red (pH 4.0, 5.0) followed by violet and grayish blue (pH 6.0, 7.0, 8.0, 9.0) when the initial pH of solution was increased. However, no color change was observed for gold solutions at highly alkaline pH (pH 10.0 and 11.0). The color change would be an indication of gold bioreduction mediated by POME and the subsequent formation of AuNps after 48 h of reaction. The UV–vis spectra obtained from solutions at different initial pH after 48 h of reaction shows characteristic absorption bands of AuNps at around 530–560 nm except for pH 10.0 and 11.0 (Supplementary data Fig. S1a). The shift of wavelength could be an indication of the increasing aggregation of AuNps occurred at higher pH.

In addition to biosynthesis of AuNps, the capability of POME to bind and concentrate gold from aqueous solutions was also observed at acidic pH. It was found by ICP-MS analysis, the maximum efficiency of gold biosorption reached ~95% at pH 2.0 after 2 h of reaction. However, the solution turned to pink color after 24 h, suggesting the formation of AuNps in solution after long contact time. Similar result was also observed by Antunes et al., where the optimal removal of gold ions was found at pH 2.0 within 3 h of reaction time (Antunes et al., 2001). In general, biosorption mechanism of gold is ionic rather than covalent due to the dependence of gold binding with pH. At pH 2.0, gold is present in solution in anionic form $[AuCl_4]^-$ and the functional groups of active biocompounds on the biomass surface such as hydroxyl groups tend to undergo protonation and become positively charged. The overall positively charged surface could promote the interaction between protonated functional groups and the negatively charged $[AuCl_4]^-$ through electrostatic attraction or electrovalent bond (Zhou et al., 2010). As a result, biosorption was preferred over bioreduction of gold ions. The bioreduction of gold could occur through the oxidation of hydroxyl to carbonyl groups as shown in Eq. (1):

$$AuCl_4^- + 3R{-}OH \rightarrow Au^0 + 3R{=}O + 3H^+ + 4Cl^- \tag{1}$$

POME has a high content of phenolic acids and flavonoids. The abundant hydroxyl groups available in these compounds could participate in the gold bioreduction. The formation of AuNps at pH 2.0 after 24 h suggested that the bioreduction of gold ions is a slow process at acidic pH due to the protonation of hydroxyl groups and the competing biosorption process.

At higher initial pH values (10.0 and 11.0), the increasing amount of OH^- could act as strong complexing agents of gold ions that interfere with the capping ability of biomolecules in POME and also compete with the $[AuCl_4]^-$ for binding to the biomolecules.

3.2. Effect of the of $HAuCl_4$ concentration and temperature on the biosynthesis of AuNps

According to LaMer model, it is predicted that the formation of nanoparticles could only happen when the precursor concentration is within a suitable range for nucleation. However, this range might vary amongst different biomass-assisted synthesis approaches. Therefore, the effect of precursor concentration on this POME-mediated synthesis was studied (Supplementary data Fig. S1b). It was found that there was no formation of AuNps by using 0.10 and 0.25 mM of gold chloride. The formation of AuNps increased as the concentration of gold chloride increased from 0.50 to 2.0 mM. This is in agreement with the range of initial precursor concentration ($\leqslant 10^{-3}$ M) that was generally used by most of the biological methods reported in the literature (Ghodake et al., 2010; Shankar et al., 2003; Zhou et al., 2010).

The effect of temperature on the formation of AuNps was also investigated (Supplementary data Fig. S1c). The solution changed from pink to grayish blue followed by dark brown as the temperature increased. The darkening of solution indicates that the process of aggregation of smaller AuNps to form larger particles was favored over nucleation to form new nanoparticles at higher temperature. The slight shift of absorption wavelength from 530 to 545 nm when the temperature was increased from 25 to 60 °C suggested the increasing size of AuNps. This phenomenon may due to the increased rate of reduction at higher temperature which may hinder the capping process and resulted in the aggregation of AuNps. In fact, the effect of temperature in directing the shape and size of nanoparticles has been reported by several research groups (Ghodake et al., 2010; Lukman et al., 2011; Njagi et al., 2011). The ability of POME to biosynthesize well-dispersed AuNps at room temperature could not only increase the ease of handling but also provide the advantage of energy-saving.

3.3. Characterization of AuNps

The morphology of AuNps synthesized at pH 3.0 and pH 8.0 was observed by using TEM. The TEM images revealed that AuNps formed at pH 3.0 were predominantly spherical with some others having occasionally triangular, truncated triangular and hexagonal shapes. When the pH was increased to 8.0, the edges of the nanostructures became not well-defined which could be a result of aggregation. It was found that pH 3.0 appears to be an optimum pH for this biosynthesis process due to the well-dispersed and uniform nanostructures obtained. AuNps with well-defined structures were observed after 1 h of reaction which suggested that the biosynthesis process mediated by POME was relatively rapid. As the reaction proceeded for about 9 and 48 h, aggregation of AuNps became dominant with some of the nanoparticles overlapped with each other and clustered together. This observation revealed that reaction time could be an important factor in controlling the size and morphology of AuNps. In fact, the formation of AuNps could be a result of heterogeneous nucleation and growth followed by Ostwald ripening. The heterogeneous nucleation could be catalyzed by extraneous material released by POME, in which the foreign particles act as a scaffold for the crystal to grow on. Since there is no requirement for the incipient surface energy, this nucleation process is kinetically favored. Along with the crystal growth, Ostwald ripening took place and responsible for the coarsening of size distribution. During Ostwald ripening, small crystals tend to dissolve in the solution and transfer their mass to grow larger particles which lead to a greater stability with lower energy state. The excess Gibb's free energy associated with the nanoparticles could then be minimized by transformation into more energetically favorable shapes, which was directed by the bioorganic capping molecules (Fiehn et al., 2000).

Fig. 1 shows the histogram of particle size distribution of the AuNps obtained after 3 h of reaction time at pH 3.0. The average particle size was determined to be 18.75 ± 5.96 nm by counting 258 particles on a representative TEM micrograph. The co-existence of AuNps in smaller and larger size was due to the AuNps formed in early and later stages of the reaction, which shows that both nucleation to form new nanoparticles and aggregation to form larger particles happened consecutively. Crystalline nature of the biosynthesized AuNps was investigated by XRD technique and the corresponding XRD-diffractogram was analyzed. Diffraction peaks observed at 38.1°, 44.1°, 64.7° and 77.8° can be indexed to the (1 1 1), (2 0 0), (2 2 0) and (3 1 1) Bragg's reflections of cubic structure of metallic gold respectively (JCPDS No. 04-0784). Another series of diffraction peaks at 45.9°, 57.0°, 71.6° and 76.1° which can be indexed to the (1 0 0), (1 0 3), (0 0 6) and (1 0 5) Bragg's reflections of hexagonal phases (JCPD No. 41-1402) were also observed (data not shown). XRD analysis suggested that the biosynthesized AuNps are composed of crystalline gold and they are biphasic in nature. In addition to the assigned Bragg peaks, additional yet unassigned peaks found at 28.4° and 32.1° were also noticed, which might be a result of crystallization of some bioorganic compounds or proteins that are present in the POME on the surface of AuNps. Similar results were also reported by Shankar et al. (2003) and Philip (2009) in the synthesis of Ag nanoparticles using geranium leaf and mushroom extract.

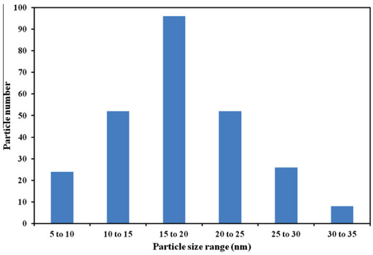

Fig. 1. Histogram of particle size distribution of AuNps synthesized using POME at pH 3 with reaction time of 3 h.

The stability of the AuNps synthesized by POME was examined by comparing the UV–vis spectra of AuNps that were freshly prepared and stored at 4 °C for more than 6 months (Supplementary data Fig. S1d). There is no obvious change of solution color and SPR peaks observed after 6 months of storage which would suggest the AuNps synthesized have considerately good stability.

3.4. Possible functional groups involved in the biosynthesis of POME

The involvement of surface functional groups in biosynthesis of AuNps was studied by FTIR (data not shown). The main difference between the spectrum of POME before and after gold reduction is the disappearance of N–H or C=O stretching vibrations band at 2351 cm^{-1}. This phenomenon revealed that biomolecules in the POME such as proteins or flavonoids that contain abundant of C=O or N–H groups might play an important role in the bioreduction and stabilization of AuNps during the synthetic process. FTIR analysis of AuNps shows the presence of five bands at 1056, 1645, 2376, 2924 and 3453 cm^{-1}. The first two absorption bands are attributed to the C–N stretching of aliphatic amines or amines/phenols and amide I bands, respectively. The other two bands at 2376 and 2924 cm^{-1} are characteristic of N–H or C=O and C–H stretching vibrations. The reappearance of 2376 cm^{-1} in the spectrum of AuNps suggested the attachment of some C=O or N–H groups onto AuNps during the biosynthesis process. In addition, the band at 3453 cm^{-1} indicates the presence of polyphenolic OH group. Hence, it was deduced that AuNps might be capped and stabilized by functional groups on the POME surface such as proteins and polyphenols through the interactions of free amine groups in the proteins as well as the carbonyl groups in the polyphenols.

In order to further investigate the compounds involved in the bioreduction of gold ions, reducing capability of various polarity based fractions of POME extracted using *n*-hexane, ethyl acetate, butanol, unboiled and boiled water were analyzed. Formation of AuNps was found by using both boiled and unboiled water extracts of POME. This observation suggested that most of the bioorganic compounds involved in the synthesis of AuNps are polar and water-soluble, such as flavonoids, proteins, reducing sugars, and water-soluble alkaloids present in plant systems. The minor amount of AuNps formed by using ethyl acetate extract was believed to be mediated by polyphenols and alkaloids extracted by this medium polar solvent. No formation of AuNps was observed by using the butanol extract. In fact, butanol is more polar than ethyl acetate. However, the bioactive polyphenols present in the POME might be more soluble in polar-aprotic solvent such as ethyl acetate rather than polar-protic solvent such as butanol. It was also found that AuNps were not formed by using hexane extract which may due to the inability of this non-polar solvent to extract alkaloids and polyphenols.

3.5. Interaction of biosynthesized AuNps with mercury ions

AuNps could form alloys with mercury with varying composition such as Au_3Hg, AuHg, $AuHg_3$ (Pradeep and Anshup, 2009). The potential use of AuNps for the removal of mercury from water through amalgamation of these two metals have been demonstrated (Lisha et al., 2009). The interaction of these biosynthesized AuNps with mercury was examined, which will correspond to its potential use in water purification. For the treatment of AuNps with mercury, 50 mg of $HgCl_2$ was added into 5 ml of the as prepared AuNps. According to the UV–vis spectra, shift in peak position was observed for AuNps before and after mercury treatment, which suggested that AuNps were consumed to form Au–Hg amalgam with different morphology (data not shown). A rapid color change of AuNps solution from wine red to grayish after the addition of Hg(II) was observed within seconds. The interaction of AuNps with Hg(II) shows the chemical reactivity of the biosynthesized AuNps and its potential use for mercury removal in water purification.

4. Conclusions

Biosynthesis of AuNps using POME was demonstrated to be a simple, low-cost and non-toxic method. The AuNps synthesized were predominantly spherical with an average size of 18.75 nm. The morphology and size of AuNps could be controlled by varying the reaction conditions such as initial pH of the $HAuCl_4$ solution and reaction temperature. Bioactive compounds involved in the biosynthesis are most likely proteins and water soluble polyphenols in POME that contains amine and carbonyl groups. Interaction of biosynthesized AuNps with Hg(II) was investigated which demonstrates the chemical reactivity of these nanoparticles.

Acknowledgements

We acknowledge financial support from the National University of Singapore, National Research Foundation and Economic Development Board (SPORE, COY-15-EWI-RCFSA/N197-1), Ministry of Education (R-143-000-382-112, and R-143-000-416-232, and R-143-000-441-112), A-STAR (SERC PSF 052 101 0044), Ministry of Defense (R-143-000-416-646) and Environment and Water Industry Development Council (0601-IRIS- 093-08).

Appendix A. Supplementary data

Supplementary data associated with this article can be found, in the online version, at doi:10.1016/j.biortech.2012.01.015.

References

- Alam, M.Z., Kabbashi, N.A., Hussin, S.N.I.S., 2009. Production of bioethanol by direct bioconversion of oil-palm industrial effluent in a stirred-tank bioreactor. Journal of Industrial Microbiology and Biotechnology 36, 801–808.
- Antunes, A.P.M., Watkins, G.M., Duncan, J.R., 2001. Batch studies on the removal of gold(III) from aqueous solution by *Azolla filiculoides*. Biotechnology Letters 23, 249–251.
- Chou, K.W., Norli, I., Anees, A., 2010. Evaluation of the effect of temperature, NaOH concentration and time on solubilization of palm oil mill effluent (POME) using response surface methodology (RSM). Bioresource Technology 101, 8616–8622.
- Fiehn, O., Kopka, J., Trethewey, R.N., Willmitzer, L., 2000. Identification of uncommon plant metabolites based on calculation of elemental compositions using gas chromatography and quadrupole mass spectrometry. Analytical Chemistry 72, 3573–3580.
- Ghodake, G.S., Deshpande, N.G., Lee, Y.P., Jin, E.S., 2010. Pear fruit extract-assisted room-temperature biosynthesis of gold nanoplates. Colloids and Surfaces B: Biointerfaces 75, 584–589.
- Sathish Kumar, K., Amutha, R., Arumugam, P., Berchmans, S., 2011. Synthesis of gold nanoparticles: an ecofriendly approach using *Hansenula anomala*. ACS Applied Materials & Interfaces 3, 1418–1425.
- Lisha, K., Anshup, A., Pradeep, T., 2009. Towards a practical solution for removing inorganic mercury from drinking water using gold nanoparticles. Gold Bulletin 42, 144–152.
- Lukman, A.I., Gong, B., Marjo, C.E., Roessner, U., Harris, A.T., 2011. Facile synthesis, stabilization, and anti-bacterial performance of discrete Ag nanoparticles using Medicago sativa seed exudates. Journal of Colloid and Interface Science 353, 433–444.
- Narayanan, K.B., Sakthivel, N., 2010. Biological synthesis of metal nanoparticles by microbes. Advances in Colloid and Interface Science 156, 1–13.
- Njagi, E.C., Huang, H., Stafford, L., Genuino, H., Galindo, H.M., Collins, J.B., Hoag, G.E., Suib, S.L., 2011. Biosynthesis of iron and silver nanoparticles at room temperature using aqueous sorghum bran extracts. Langmuir 27, 264–271.
- Parsons, J.G., Peralta-Videa, J.R., Gardea-Torresdey, J.L., 2007. Chapter 21 Use of plants in biotechnology: synthesis of metal nanoparticles by inactivated plant tissues, plant extracts, and living plants. Developments in Environmental Science, 463–485.
- Philip, D., 2009. Biosynthesis of Au, Ag and Au–Ag nanoparticles using edible mushroom extract. Spectrochimica Acta – Part A: Molecular and Biomolecular Spectroscopy 73, 374–381.
- Pradeep, T., Anshup, A., 2009. Noble metal nanoparticles for water purification: a critical review. Thin Solid Films 517, 6441–6478.
- Pradhan, N., Nayak, R.R., Pradhan, A.K., Sukla, L.B., Mishra, B.K., 2011. In situ synthesis of entrapped silver nanoparticles by a fungus – *Penicillium purpurogenum*. Nanoscience and Nanotechnology Letters 3, 659–665.
- Shankar, S.S., Ahmad, A., Sastry, M., 2003. Geranium leaf assisted biosynthesis of silver nanoparticles. Biotechnology Progress 19, 1627–1631.
- Taheri Otaqsara, S.M., 2011. Biosynthesis of quasi-spherical Ag nanoparticle by*Pseudomonas aeruginosa* as a bioreducing agent. EPJ Applied Physics 56, 30402.
- Zhou, Y., Lin, W., Huang, J., Wang, W., Gao, Y., Lin, L., Li, Q., Du, M., 2010. Biosynthesis of gold nanoparticles by foliar broths: roles of biocompounds and other attributes of the extracts. Nanoscale Research Letters 5, 1351–1359.

DOI: 10.1002/anie.200904359

Nanotechnology

Gold Nanoparticles for Biology and Medicine

*David A. Giljohann, Dwight S. Seferos, Weston L. Daniel, Matthew D. Massich, Pinal C. Patel, and Chad A. Mirkin**

Keywords:
cytotoxicity · DNA · drug delivery · gold · nanoparticles

© 2010 Wiley-VCH Verlag GmbH & Co. KGaA, Weinheim

Gold colloids have fascinated scientists for over a century and are now heavily utilized in chemistry, biology, engineering, and medicine. Today these materials can be synthesized reproducibly, modified with seemingly limitless chemical functional groups, and, in certain cases, characterized with atomic-level precision. This Review highlights recent advances in the synthesis, bioconjugation, and cellular uses of gold nanoconjugates. There are now many examples of highly sensitive and selective assays based upon gold nanoconjugates. In recent years, focus has turned to therapeutic possibilities for such materials. Structures which behave as gene-regulating agents, drug carriers, imaging agents, and photoresponsive therapeutics have been developed and studied in the context of cells and many debilitating diseases. These structures are not simply chosen as alternatives to molecule-based systems, but rather for their new physical and chemical properties, which confer substantive advantages in cellular and medical applications.

From the Contents

1. Introduction	3281
2. Citrate and Transferrin	3281
3. Amines	3283
4. Oligonucleotides	3284
5. Peptides	3288
6. Antibodies	3289
7. Lipids	3290
8. Summary and Outlook	3290

1. Introduction

Gold nanoparticles (AuNPs) have a rich history in chemistry, dating back to ancient Roman times where they were used to stain glasses for decorative purposes. The modern era of AuNP synthesis began over 150 years ago with the work of Michael Faraday, who was possibly the first to observe that colloidal gold solutions have properties that differ from bulk gold.[1,2] Reliable and high-yielding methods for the synthesis of AuNPs, including those with spherical and nonspherical shapes, have been developed over the last half-century.[3] The resulting AuNPs have unique properties, such as size- and shape-dependent optical and electronic features, a high surface area to volume ratio, and surfaces that can be readily modified with ligands containing functional groups such as thiols, phosphines, and amines, which exhibit affinity for gold surfaces.[3] By using these functional groups to anchor the ligands, additional moieties such as oligonucleotides, proteins, and antibodies can be used to impart even greater functionality. The realization of such gold nanoconjugates has enabled a broad range of investigations, including programmed assembly and crystallization of materials,[4,5] arrangement of nanoparticles into dimers and trimers onto DNA templates,[6] bioelectronics,[7–9] and detection methods.[10,11] The application of gold nanoconjugates for biodetection and biodiagnostics have been reviewed elsewhere.[12–14]

In recent years, gold nanoconjugates and their properties have led to new and exciting developments with enormous potential in biology and medicine. These investigations represent a new direction that greatly deviates from the more established use of gold nanoconjugates as labels for electron microscopy.[15] Our recent studies, as well as those of several other research groups, have shown that gold nanoconjugates, when functionalized with appropriate surface moieties, can readily enter living cells. These developments have forged a new frontier in nanoparticle research, including the broader use of gold nanoconjugates in cellular biology and the promise for their eventual use as therapeutic agents.

In this Review we describe the current status of gold nanoconjugates for cellular and therapeutic uses. As surface chemistry is one of the key features that controls the properties and functionality, we have divided this Review into sections based on the type of surface functionalization, including citrate, amine, nucleic acid, peptide, antibody, and lipid ligands (Table 1). In each section, our discussion focuses on chemical synthesis, physical and chemical properties, as well as investigations and applications in cells. In Section 8, we also propose key opportunities and open questions that have yet to be addressed by the scientific community. These questions should inspire future investigations and lead to discoveries that continue the development of the rich chemistry of gold nanoparticles.

2. Citrate and Transferrin

Citrate-functionalized gold nanoparticles can be prepared on a relatively large scale and with a high degree of monodispersity by using the methods of Frens[16] as well as Enustun and Turkevich.[17] These methods allow for the synthesis of citrate-capped spherical nanoparticles with

---

[*] Dr. D. A. Giljohann,[+] Dr. D. S. Seferos,[++] [+] W. L. Daniel,
M. D. Massich, P. C. Patel, Prof. C. A. Mirkin
Department of Chemistry and International Institute for Nanotechnology, Northwestern University
2145 Sheridan Road, Evanston, IL 60208-3113 (USA)
Fax: (+1) 847-467-5123
E-mail: chadnano@northwestern.edu

[++] Current Address:
Department of Chemistry, University of Toronto
80 St. George Street, Toronto, Ontario M5S 3H6 (Canada)

[+] These authors contributed equally to this work.

© 2010 Wiley-VCH Verlag GmbH & Co. KGaA, Weinheim

WILEY InterScience® DISCOVER SOMETHING GREAT

Table 1: Au NP surface functionalites.

Surface functionality	Application	Reference
citrate	cell uptake	[18,19]
transferrin	cell uptake	[20,21]
CTAB	cell uptake	[14,94]
amine	gene transfection	[26,30,31]
	antiviral activity	[34]
	drug delivery	[34]
	oligonucleotide transfection	[36]
oligonucleotide	antisense gene regulation	[25,77,88,102]
	mRNA detection	[87,88]
	small-molecule detection	[89]
	RNA interference	[90]
	cancer cell detection	[93]
peptide	nuclear translocation	[23,100]
	antisense gene regulation	[102]
antibody	imaging	[15,106,107,110]
	photothermal therapy	[108,109,110]
lipid	imaging	[112]
	cholesterol binding	[111]

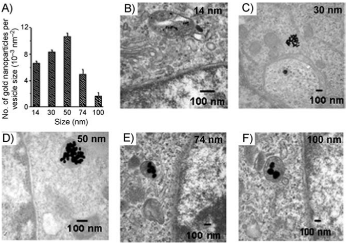

Figure 1. Transmission electron microscopy imaging and measurements of gold nanoparticles in cells. A) Graph of number of gold nanoparticles per vesicle diameter for various nanoparticle sizes. B–F) TEM images of gold nanoparticles with sizes of 14, 30, 50, 74, and 100 nm, respectively, trapped inside vesicles of a HeLa cell. Adapted from Ref. [19], with permission from the American Chemical Society; Copyright 2006.

diameters ranging from 5 to 250 nm.[16,17] This well-established synthesis and the ability to finely control size has contributed to citrate-functionalized nanoconjugates forming the basis of recent investigations of the uptake of gold nanoparticles by cells.[18] In one such study, Chan and coworkers determined how the size and shape of the particles influence their ability to be internalized by cells.[19] Their study demonstrates that, in a HeLa cell model, the amount of time that the citrate particles remain internalized is independent of the particle size when they have diameters between 14 and 74 nm. However, the size does affect the total number of nanoparticle conjugates internalized during the experiment. By using inductively coupled plasma atomic emission spectroscopy (ICP-AES) to determine the intracellular gold content, these researchers determined that citrate-capped gold nanoconjugates with diameters of 50 nm are most readily internalized by HeLa cells (Figure 1). They found that the maximum number of citrate-stabilized gold nanoconjugates taken up by a HeLa cell is 3000, 6160, and 2988 for gold nanoconjugates with diameters of 14, 50, and 74 nm, respectively.

Chad A. Mirkin is the Director of the Northwestern University International Institute for Nanotechnology, the George B. Rathmann Prof. of Chemistry, Prof. of Chemical and Biological Engineering, Prof. of Biomedical Engineering, Prof. of Materials Science and Engineering, and Prof. of Medicine. He has authored over 400 manuscripts and has over 350 patents and applications. He is the founder of the companies Nanosphere, NanoInk, and AuraSense, and he cofounded the journal Small. He has received over 60 national and international awards for his contributions to chemistry, materials science, and nanoscience.

Weston Daniel studied chemistry at the University of Minnesota, Twin Cities and graduated in 2005. He is now conducting PhD research at Northwestern University under the mentorship of Chad Mirkin. His research focuses on developing detection schemes by using biomolecule-functionalized gold nanoparticles.

David Giljohann studied at Northwestern University and obtained his Bachelor's Degree in 2003. He completed his PhD there under the mentorship of Chad Mirkin in 2009. His research is focused on the development of oligonucleotide-modified nanoparticles, including nanoflares as well as antisense DNA and RNA gold nanoparticles.

Pinal Patel completed his undergraduate studies at Towson University in 1999. He then worked at the United States Department of Defense before returning to academia. He is currently pursuing PhD research at Northwestern University under the guidance of Chad Mirkin. His research is focused on determining the cellular uptake and intracellular localization of oligonucleotide-modified gold nanoparticles.

The mechanism by which the citrate-capped gold nanoconjugates enter cells has been the subject of investigation. Chan and co-workers recorded transmission electron microscopy images of internalized "bare" citrate nanoconjugates and showed that the particles were mainly localized within vesicles inside of the cells.[19] They correlated cell uptake with the nonspecific adsorption of proteins to the citrate-capped nanoparticle surfaces.

The negatively charged citrate surface provides a convenient scaffold to attach positively charged proteins such as transferrin, which is expected to facilitate and improve entry into cells. In one study, atomic force microscopy was used to image transferrin-coated citrate-functionalized gold nanoconjugates on the cell surface.[20] The images obtained suggest vesicle formation at the cell surface and nanoconjugate internalization through endocytosis. A series of experiments by Chithrani and Chan further determined that transferrin-coated citrate-functionalized gold nanoconjugates enter cells through the clathrin-mediated endocytosis pathway.[21]

Many investigations in cells use citrate-capped AuNPs as important precursors of covalent conjugates with additional functionality, because further derivatization has been shown to increase uptake ability,[22] alter intracellular localization,[23,24] or impart functionality that can be used to affect a cellular response.[25,26] Indeed, citrate-coated particles are generally not ideal structures for investigations and internalization studies on cells. They are susceptible to environmentally induced aggregation and can be quite difficult to work with. In the next sections we describe the major classes of gold nanoconjugates that are functionalized with designer ligands, which have been developed and used for experiments on cells.

Dwight Seferos completed his PhD at the University of California, Santa Barbara in 2006 under the guidance of Guillermo Bazan, and then carried out postdoctoral research at Northwestern University in the laboratory of Chad Mirkin. He is currently an Assistant Professor in the Department of Chemistry at the University of Toronto.

Matthew Massich completed his undergraduate studies in 2004 at the University of St. Thomas. He is currently carrying out PhD research at Northwestern University with Chad Mirkin. His research investigates the biological response to the use of oligonucleotide-functionalized gold nanoparticles for therapeutic and diagnostic applications.

3. Amines

In addition to the methods of Enustun and Turkevich and of Frens, alternative methods for the synthesis of gold nanoparticles have been developed. The Brust–Schiffrin method allows for the synthesis of monodisperse gold nanoparticles ranging from 1 to 3 nm in diameter.[27] The resultant nanoparticles are stabilized by a monolayer of alkanethiolates. The composition of the monolayer can be changed through a substitution reaction to include specific functionalities, depending on the intended use of the nanoparticles.[28] Accordingly, gold nanoconjugates functionalized with a monolayer of amine-terminated alkanethiolates (hereafter referred to as amine-functionalized) have been prepared for various biological applications.

3.1. Gene Transfection

The ability to induce control over biological systems at the genetic level is a fundamental concept in experimental biology, and holds great promise for developing new treatments of disease.[29] The search for the best method for controlling gene expression is ongoing. Their straightforward synthesis and high-degree of chemical tunability has resulted in amine-functionalized nanoparticles having been developed as a means to transfer genetic material into cell models.[26,30]

Amine surface groups are positively charged at physiological pH values, and thus amine-functionalized nanoconjugates electrostatically interact with negatively charged nucleic acids. Studies by Rotello and co-workers have demonstrated that 2 nm gold nanoparticles functionalized with a mixed monolayer containing quaternary amines and uncharged surface groups are able to bind DNA plasmids and deliver them efficiently to 293T cells.[26] In fact, these nanoconjugates are able to transfect these cells with a greater efficiency than the commonly used cationic polymer transfection agent polyethylenimine (PEI, 60 kDa). These researchers also found that the efficiency of the nanoparticle-mediated gene transfection was affected by the ratio of positively charged quaternary amines to negatively charged phosphate groups on the DNA, as well as the relative amount and length of the surface-bound uncharged thiol chain. Building on these observations, these researchers have recently shown that gold nanoparticles functionalized with lysine moieties are highly efficacious at delivering DNA plasmids, and outperform a commercial vector by a factor of 28.[31]

The utility of amine-functionalized nanoconjugates for gene delivery was also demonstrated by Thomas and Klibanov.[30] In this study, combinations of thiol-modified PEI (2 kDa) and dodecyl-PEI (2 kDa) were used as surfactants or complexing agents during AuNP synthesis. The concentration of PEI was used to control the size of the functionalized nanoparticles from 2.3 to 4.1 nm in diameter. The resultant nanoconjugates deliver plasmid DNA to COS-7 cells more efficiently than PEI alone.

© 2010 Wiley-VCH Verlag GmbH & Co. KGaA, Weinheim

3.2. Drug Delivery

Site-specific delivery, stability, and the programmed release of the drugs to physiological targets have been major challenges for molecular and macromolecular therapeutics.[32] The highly tunable and multivalent surface architecture of gold nanoconjugates offers the potential to incorporate multiple therapeutic agents as well as to target and protect molecules on the surface of a single nanoparticle, and thus are expected to improve the delivery and efficacy of therapeutic payloads. New generations of novel nanoconjugates with AuNPs as their cores have been designed and synthesized.[33] A recent study by Feldheim and co-workers has shown how multivalent AuNPs functionalized with derivatives of an important HIV antagonist are highly effective at silencing viral production in a cell model.[34]

Rotello and co-workers have developed a cationic 2 nm gold nanoconjugate functionalized with thiol-modified alkyl amines that possess photoactive *o*-nitrobenzyl ester linkages, which can be cleaved with near-UV irradiation (Figure 2).[35] Irradiation releases the positively charged alkyl amine from the particle, thereby resulting in a net negatively charged carboxylate-functionalized nanoparticle. The reversal in charge provides an effective means of releasing a negatively charged payload such as an oligonucleotide from the nanoparticle surface. These cationic nanoparticles with photocleavable ligands were shown to inhibit transcription of the bound oligonucleotide; however, the transcription activity can be recovered following the cleavage reaction. Intracellular delivery of the bound oligonucleotide was also demonstrated in MEF cells. Fluorescence-based experiments show that, upon photoinduced cleavage, the bound DNA is released from the nanoparticle surface to the intracellular environment where it then localizes in the nucleus. A similar strategy has been developed to deliver anticancer drugs.[36]

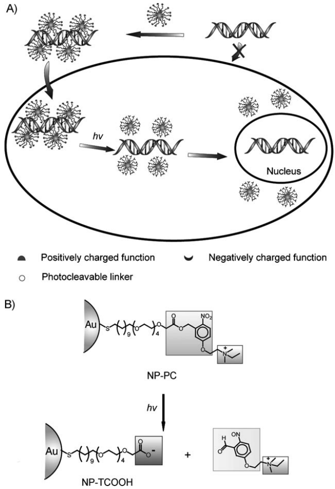

Figure 2. A) Schematic illustration of the release of DNA from a photocleavable AuNP complex (NP-PC) upon UV irradiation within the cell. B) Schematic presentation of light-induced surface transformation of NP-PC. Adapted from Ref. [35].

Another study by Rotello and co-workers demonstrates an alternative method of releasing molecules from gold nanoparticle drug carriers. In this method, gold nanoparticles functionalized with a mixed monolayer of amine-terminated and fluorophore-labeled alkyl thiol ligands were internalized by either HepG2 or MEF cells. Exposure to intracellular environments containing an elevated glutathione concentration (a thiol-possessing peptide) results in substitution and the passive release of the nanoconjugate ligands.[37]

3.3. Stability

In addition to providing functional groups, surface-bound ligands also contribute to the stability of the AuNPs. The stability of the nanoconjugates is an important consideration for their potential use as therapeutic agents because they must maintain their stability under harsh conditions such as in the cell or in the bloodstream. In a study by Rotello and co-workers, the effect of surface charge on the stability of amine-functionalized gold nanoparticle was characterized.[38] In this study, 2 nm gold nanoparticles functionalized with combinations of positively charged amines, negatively charged carboxylates, and fluorescent ligands were used. Various thiol species were tested for their ability to displace ligands bound to the nanoparticle surface. It was found that increasing the net positive charge on the nanoparticle surface caused a more rapid displacement of ligands, whereas more negatively charged nanoconjugates did not display measurable displacement of surface-bound ligands.[38] This result is consistent with studies by our research group on the stability of 13 nm oligonucleotide/gold nanoparticle conjugates which found that the negatively charged thiolated oligonucleotide ligands are not easily displaced in intracellular environments or by small molecules such as glutathione.[25]

4. Oligonucleotides

Over the past decade, our research group and others have synthesized, characterized, and applied polyvalent DNA-functionalized gold nanoconjugates (DNA-AuNPs).[4] This unique class of nanomaterial consists of a gold nanoparticle core that is functionalized with a dense shell of synthetic oligonucleotides. DNA-AuNPs exhibit cooperative properties that result from their polyvalent surfaces,[39–43] and these properties have been applied to areas such as programmable

© 2010 Wiley-VCH Verlag GmbH & Co. KGaA, Weinheim

crystallization[44–46] and enzyme-free biodiagnostic assays.[47,48] Indeed, the optical, catalytic, and binding properties of DNA-AuNPs have been used for a variety of colorimetric,[11,49,50] electronic,[7] scanometric,[51] and Raman-based[52] detection strategies, some of which have recently been commercialized and approved by the American Food and Drug Administration.[51]

4.1. Synthesis

Nanoconjugates densely functionalized with synthetic oligonucleotides are prepared by mixing alkanethiol-terminated oligonucleotides and citrate-capped AuNPs. Oligonucleotide ligands displace the citrate from the AuNPs through formation of a gold–thiol bond. NaCl is added to the reaction mixture to shield charge repulsion, thus allowing a greater number of oligonucleotides to chemically adsorb to the nanoparticle surface, thereby resulting in a dense monolayer of oligonucleotides (Figure 3). Approximately 250 oligonucleotides can be chemisorbed to the surface of 15 nm diameter AuNPs, thus creating polyvalent structures.[53] Methods have been optimized for functionalizing particles with diameters ranging from 2 to 250 nm.[54,55] This polyvalent material has a number of emergent properties that are unique from the properties of the oligonucleotides or the AuNPs alone.

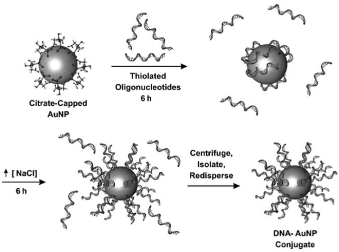

Figure 3. The synthesis of the oligonucleotide gold nanoconjugates: Alkanethiol-terminated oligonucleotides are added to citrate-stabilized AuNPs, thereby displacing the capping citrate ligands through formation of a gold–thiol bond. Subsequent addition of a salt shields repulsion between the strands, thus leading to a dense monolayer of oligonucleotides.

4.2. Properties

One unusual but now fairly well understood property of DNA-AuNPs is their ability to bind complementary nucleic acids with a high affinity.[56] In fact, polyvalent particles exhibit binding constants as large as two orders of magnitude greater than the analogous molecular oligonucleotides of the same sequence.[40] Experimental data and later theoretical models show that this property likely arises from the dense packing and high local concentration of oligonucleotides on the gold surface.[41,57] Additionally, the oligonucleotides on the AuNP surface are close enough such that the counterions associated with one oligonucleotide also act to screen negative charges on adjacent oligonucleotides. This additional charge screening causes increased stabilization of the oligonucleotide duplex, thereby increasing the effective binding constants associated with the DNA-AuNP compared with molecular oligonucleotides. Consistent with this observation, larger particles that have more DNA per particle, but less DNA per unit area exhibit affinities comparable to the molecular system and lower than the gold nanoconjugate structures.[58] In the context of cellular applications, it was hypothesized and subsequently demonstrated that the higher binding constant of the DNA-AuNP would lead to better intracellular binding of the target molecule, thereby increasing the effectiveness of antisense gene regulation (see Section 4.4.1).[25]

Nucleic acids are often hampered in biological investigations by enzymatic hydrolysis, which leads to degradation and renders them inactive.[59,60] Another emergent property of DNA-AuNPs is resistance to degradation by enzymes such as DNase I.[25] Two explanations have been proposed as the origin of this enhanced stability: First, the dense packing of DNA on the surface of the particle could result in steric inhibition of enzyme binding, so that the inaccessible, particle-bound DNA would not be engaged or cleaved by the enzyme. An alternate hypothesis is that the high local ion concentration associated with the densely packed DNA inhibits enzyme activity, since it is known that high concentrations of Na^+ ions result in a reduction of enzymatic activity.[61,62] Experiments elucidating these two possibilities have recently been carried out.[63] Molecular DNA and DNA-AuNPs have similar enzymatic degradation rates under conditions where salt concentrations do not affect the enzymatic activity. However, the DNA-AuNP reaction rate is greatly slowed relative to that of molecular DNA under conditions where the salt concentrations affect enzymatic activity. The study concluded that the local Na^+ concentration is the dominant factor that contributes to the enhanced stability of DNA. The resistance of DNA-AuNPs to enzymatic degradation is an important property that renders these structures extremely promising candidates for introducing nucleic acids into cells, where oligonucleotide degradation has historically been a major challenge.

4.3. Cellular Uptake

Perhaps the most surprising property of DNA-AuNPs is their ability to enter a wide variety of cell types. The facile uptake of these structures into cells was not predicted, given that these structures contain a densely functionalized shell of polyanionic DNA (ca. 100 DNAs on the surface of each 13 nm gold particle), and that strategies for the introduction of oligonucleotides typically require that DNAs are com-

© 2010 Wiley-VCH Verlag GmbH & Co. KGaA, Weinheim

Table 2: Cell types that internalize polyvalent DNA gold nanoconjugates. Cellular internalization was determined using mass spectrometry and cell-associated fluorescence measurements.

Cell type	Designation or source
breast	SKBR3, MDA-MB-321, AU-565
brain	U87, LN229
bladder	HT-1376, 5637, T24
colon	LS513
cervix	HeLa, SiHa
skin	C166, KB, MCF, 10 A
kidney	MDCK
blood	Sup T1, Jurkat
leukemia	K562
liver	HepG2
kidney	293T
ovary	CHO
macrophage	RAW 264.7
hippocampus neurons	primary, rat
astrocytes	primary, rat
glial cells	primary, rat
bladder	primary, human
erythrocytes	primary, mouse
peripheral blood mononuclear cell	primary, mouse
T cells	primary, human
beta islets	primary, mouse
skin	primary, mouse

plexed with positively charged agents to effect cellular internalization. Indeed, because of their high negative charge, most researchers at the time would have predicted that the nanoparticles would not enter cells.[64] Remarkably, it has been shown in all the cell types examined to date (which include over 30 cell lines, primary cells, and neurons, Table 2) that DNA-AuNPs can be added directly to cell culture media and are subsequently taken up by cells in high numbers (Figure 4). Quantification of uptake using ICP-MS shows that while the number of internalized particles varies as a function of cell type, concentration, and incubation time, the cellular internalization of DNA-AuNPs is a general property of these materials. Importantly, the density of DNA on the particle surface was found to be the deciding factor of DNA-AuNP uptake. At DNA surface loadings of greater than about $18\ \mathrm{pmol\,cm^{-2}}$, cellular uptake can exceed one million DNA-AuNPs per cell.[65] The importance of the polyvalent arrangement of oligonucleotides to cellular uptake can be further emphasized when comparing DNA-AuNPs to other types of AuNPs. For example, HeLa cells internalize only a few thousand citrate-coated gold particles,[19] compared to over one million DNA-AuNPs under nearly identical conditions.[65] Importantly, fluorescence spectroscopy studies reveal that the thiolated oligonucleotides remain bound to the AuNPs after cellular internalization (Figure 4).

Given the surprising ability of DNA-AuNPs to enter cells, the mechanism of uptake is of great interest. Interestingly, biophysical characterization of DNA-AuNPs after exposure to serum-containing media reveals changes in the charge and size of the nanoconjugates. Exposure to cell culture conditions results in greater positive charge and larger nanoparticle diameter (as measured by zeta potential and light scattering), which was further shown to be caused by the adsorption of proteins.[65] The interaction of polyvalent nanoparticle conjugates with proteins provides a possible mechanism of recognition and subsequent internalization of these highly negatively charged particles, the details of which are still under intensive investigation.

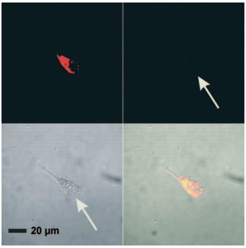

Figure 4. Fluorescent microscopy images of C166-EGFP cells incubated for 48 h with gold nanoconjugates functionalized with dual-fluorophore-labeled oligonucleotides (3′-Cy3 and 5′-Cy5.5) only reveal fluorescence from Cy5.5 (706–717 nm, upper left). Negligible fluorescence is observed in the emission range of Cy3 (565–615 nm, upper right). Transmission and composite overlay images are shown in the lower left and lower right quadrants, respectively. The arrows indicate the location of the cell. Adapted from Ref. [25], with permission from the American Association for the Advancement of Science; Copyright 2006.

4.4. Applications in Cells

Methods based on nucleic acids for detecting and controlling gene expression have had a significant impact on fundamental studies of gene pathways and functions.[29] Methods for controlling gene expression include the use of antisense oligonucleotides[66] and small interfering RNA (siRNA),[67] which can be directed against messenger RNA (mRNA) through Watson–Crick pairing. While the promise of "gene therapy" based on nucleic acids was recognized over 20 years ago, its development has faced challenges with regard to entry into cells, delivery of intact oligonucleotides, and efficacy.[68] Various transfection agents, such as cationic lipids and polymers,[69] modified viruses,[70] dendrimers,[71] liposomes,[72] and nanoparticles,[26,73] have thus been developed to shuttle nucleic acids into cells. Despite the use of these materials, the toxicity of these agents and their off-target effects limit the amount of oligonucleotides that can be delivered safely. An ideal gene regulation system—from a research standpoint—should feature high uptake efficiencies across all cell types, high intracellular stability, strong binding affinity for target nucleic acids, and very low toxicity. Recently DNA-AuNPs were used as agents to alleviate

© 2010 Wiley-VCH Verlag GmbH & Co. KGaA, Weinheim

several of the challenges that are commonly associated with the application of nucleic acids in cells.[25]

4.4.1. *Antisense Gene Control*

We hypothesized that, because of their enhanced binding properties, DNA-AuNPs could act as potent "sponges" for binding mRNA and preventing translation into proteins. As a demonstration of this concept, we developed DNA-AuNPs that target the mRNA sequences that code for enhanced green fluorescent protein (eGFP) expressed in mouse endothelial cells. An antisense sequence complementary to an internal coding region of the mRNA for eGFP was used in the design and synthesis of "antisense nanoparticles".[25] Quantitative measurement of expression by using fluorescence assays demonstrates that these particles outperform lipid-complexed DNA used in a direct comparison. Initial experiments demonstrate a silencing of approximately 20%, but further optimization of the experimental parameters and conjugate structure has increased the gene silencing ability to greater than 75% (Figure 5).

Although more than a decade of studies have been dedicated to the synthesis and characterization of DNA-AuNPs, functionalization is not limited to DNA-type oligomers. Indeed, AuNPs can be encoded with a suite of designer oligonucleotides that confer enhanced properties, ranging from increased target specificity to catalytically enhanced biological processing.[74,75] In a recent example, locked nucleic acid (LNA) nanoparticle conjugates have been synthesized and investigated.[76,77] LNAs incorporate bridged sugars in their backbones, which have been shown to increase binding affinity and increase duplex stability.[78] AuNPs densely functionalized with LNA form remarkably stable duplexes with complementary nucleic acids, and can be easily handled and manipulated under biologically relevant conditions. For application in cells, the use of LNA-modified AuNPs increases the effectiveness of gene knockdown compared to analogous DNA-modified AuNPs.[77]

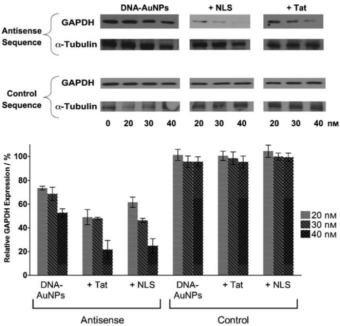

Figure 5. A) Representative Western blots showing the expression of glyceradlehyde 3-phosphate dehydrogenase (GAPDH) in HeLa cells treated with various concentrations and compositions of the gold nanoconjugates. GAPDH expression is reduced in a dose- and sequence-dependent manner. α-Tubulin is shown as the loading control. B) Relative decrease in GAPDH expression in HeLa cells. α-Tubulin was used as a loading control and for subsequent normalization of GAPDH knockdown. The error bars represent the standard deviation from at least three Western blots. Adapted from Ref. [102], with permission from the National Academy of Sciences; Copyright 2008.

4.4.2. *Intracellular Detection and Imaging*

Oligonucleotide-based probes to visualize and detect intracellular RNA, including those used for in situ staining,[79,80] molecular beacons,[81,82] and fluorescence resonance energy transfer (FRET) probes[83,84] are important biological tools to measure and quantify biological activity in living systems. However, cells do not readily internalize molecular probes, they require the use of transfection agents or microinjection for uptake. In addition, as a consequence of their oligonucleotide structure, such imaging agents can have limited stability to nuclease degradation, which can lead to a high background signal and decreased ability to specifically detect target structures.

Much work has thus gone into the development of structures that overcome these limitations, including chemically modified molecular beacons[85] or their corresponding peptide conjugates.[86] Recently, our research group has developed novel intracellular detection probes termed "nanoflares" that take advantage of the properties of DNA-AuNPs.[87–89] Nanoflares are oligonucleotide-functionalized gold nanoparticles that are hybridized to short, fluorophore-labeled complements designed to provide an intracellular fluorescence signal that correlates with the concentration of a specific nucleic acid or molecular target. In the absence of a target, the fluorophore is close to the nanoparticle surface, which quenches its fluorescence. Target binding releases the fluorophore, thereby generating a signal that can be detected inside a live cell. Nanoflares can distinguish between different cell types on the basis of the expression profile, and give a semiquantitative real-time readout of gene expression in a living sample (Figure 6).

Several problems commonly associated with intracellular RNA detection, including the difficulty associated with cell entry, toxicity, and intracellular instability, are obviated as these nanoparticles are densely functionalized with oligonucleotides. These probes do not require microinjection or auxiliary reagents to enter cells and are more resistant than molecular nucleic acids towards enzymatic degradation, thus lowering background signal and improving detection ability.

4.4.3. *RNA Interference*

Additional work is now underway on conjugates functionalized with RNA-capping ligands that are capable of acting in the highly potent RNA interference (RNAi) pathway. Recently, we determined that RNA-AuNPs can be

© 2010 Wiley-VCH Verlag GmbH & Co. KGaA, Weinheim

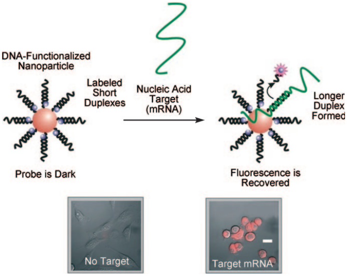
DNA-Functionalized Nanoparticle
Labeled Short Duplexes
Nucleic Acid Target (mRNA)
Longer Duplex Formed
Probe is Dark
Fluorescence is Recovered
No Target
Target mRNA

Figure 6. "Nanoflares" are gold nanoconjugates functionalized with oligonucleotide sequences complementary to a specific nucleic acid target (messenger RNA) hybridized to short fluorescent sequences. In the absence of a target the nanoflares are dark, because of quenching by the gold nanoparticle. In the presence of a target binding displaces the short flare through the formation of a longer (more energetically favorable) duplex. The result is a fluorescence signal inside the cell, which indicates the target has been detected. Scale bar: 20 μm. Adapted from Ref. [87], with permission from the American Chemical Society; Copyright 2007.

synthesized and subsequently introduced into cells without the use of transfection agents.[90] Traditional RNAi uses molecular RNAs, which have extremely short half-lives as a result of the instability of ribonucleotides to RNase-type enzymes, thus limiting their efficacy.[91,92] In the case of RNA-gold nanoconjugates, a dense monolayer of surface-immobilized RNA increases the protection from nonspecific degradation both in cell culture media and in the intracellular environment. These structures are over six times more stable than molecular RNA in serum-containing media, and this enhanced stability does not rely on chemical modifications to the RNA molecular structure. We have further shown that the RNA-gold nanoconjugates have a more persistent ability to silence genes. The enhanced stability and high cellular uptake should result in these structures playing an important role in future fundamental studies as well as in the therapeutic application of RNAi.

4.4.4. *Cellular Detection*

In addition to intracellular applications, Tan and co-workers have developed a colorimetric assay that uses DNA-AuNPs for the detection of cancer cells. Specifically, AuNPs were functionalized with a monolayer of aptamers selected to have a high affinity for surface receptors expressed by a cancer cell line (CCRF-CEM).[93] The aptamer-functionalized nanoconjugates assemble on the cell surfaces, which causes their surface plasmon resonances to interact. This results in a red shift in the extinction spectra, thus providing a direct readout of target binding. The strong extinction of AuNPs means that the presence of cancer cells can be detected by the naked eye or by using a spectrometer, which eliminates the need for expensive and complicated instrumentation and makes the assay potentially useful for cancer diagnosis or disease screening.

5. *Peptides*

The targeting portions of many proteins are short stretches of oligopeptides. Peptide-based nuclear localization signals have been used to alter the intracellular localization and increase efficacy of conjugated biomolecules.[94] Such peptide signaling sequences are often composed of a stretch of positively charged amino acids such as arginine and lysine, which interact with Importin A for transport across the nuclear envelope.[95] Sequences derived from the HIV Tat protein (CYGRKKRRQRRR) and integrin binding domain (CKKKKKKGGRGDMFG) have been studied extensively for delivery of exogenous proteins and synthetic materials to the nucleus.[23,96–99]

5.1. *Peptide Nanoconjugates*

Recently, examples of peptide–gold nanoparticle conjugates have been reported. Feldheim, Franzen, and co-workers conjugated peptides to gold nanoparticles through attachment to bovine serum albumin (BSA) and subsequent electrostatic association.[23,100] The resulting nanoconjugates enter the nucleus of HepG2 cells in culture. Interestingly, only nanoconjugates functionalized with peptides containing both

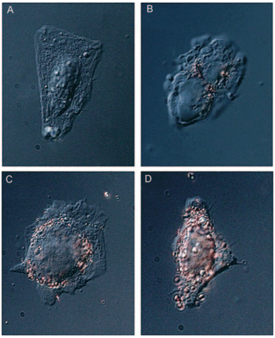

Figure 7. Images of nanoparticle–peptide complexes incubated with HepG2 cells for 2 h. Complexes were: A) nuclear localization peptide, B) receptor-mediated endocytosis peptide, C) adenoviral fiber protein, and D) both nuclear localization and receptor-mediated endocytosis peptides. Adapted from Ref. [23], with permission from the American Chemical Society; Copyright 2003.

© 2010 Wiley-VCH Verlag GmbH & Co. KGaA, Weinheim

a receptor-mediated endocytosis (RME) and nuclear localization signal (NLS) are able to enter the nucleus of these cells (Figure 7). The same researchers recently investigated the ability of AuNPs modified with both peptides and polyethylene glycol (PEG) to enter cells. Interestingly, the particles are actively internalized even if the PEG molecule within the monolayer is large (molecular weight: 5000).[101] These studies point to exciting opportunities in the design of multifunctional conjugates.

5.2. Peptide/DNA-Gold Nanoparticle Conjugates

We recently prepared gold nanoconjugates functionalized with both antisense oligonucleotides and NLS or HIV Tat peptides.[102] Our synthetic strategy uses thiolated oligonucleotides and cysteine-terminated peptides to functionalize the AuNP surfaces. As the oligopeptides and oligonucleotides are oppositely charged, the addition of salt is required to screen oppositely charged biomolecules during synthesis. When tested in cell culture, the resultant conjugates are internalized and localized in the perinuclear region. Consequently, these particles have a high gene silencing ability (> 75 % decrease in expression of the target protein).

5.3. Multifunctional and Multicomponent DNA Nanoconjugates

The versatility of nanoconjugates can be increased by incorporating multiple functional groups into each construct, or by rationally designing it to have multiple functions. Recently, our research group has demonstrated that nanoflares (see Section 4.4.2) can be adapted for both intracellular mRNA detection and gene knockdown.[88] These nanoflares enter cells and bind mRNA in a location suitable for gene knockdown, thereby decreasing the relative abundance of mRNA, while simultaneously releasing a fluorescent flare. Here, the nanoflare provides a read-out of gene regulation inside the cell. Such capabilities will provide valuable feedback, as the results of manipulating a cellular system can be observed in real time. In addition, one can, in principle, create all sorts of cell-sorting genetic screening asays by using the nanoflare approach.

Other therapeutic nanoconstructs have been designed to take advantage of the uptake of DNA-AuNPs by cells. For example, Pt^{IV} complexes are being explored for chemotherapy in an effort to reduce the side effects of cisplatin. Studies by the research groups of Lippard and Mirkin have shown that AuNPs can be modified with both oligonucleotides and cisplatin prodrugs. These constructs, similar to their cannonical DNA counterparts, deliver the drug payload effectively to cells.[127] The prodrug consists of a Pt^{IV} complex designed to be reduced and released as active cisplatin in the acidic endosomes of cells. In addition, synthetic handles (in this case, a carboxylic acid) can be added to the cisplatin precursor to allow for straightforward conjugation to the oligonucleotides through amide linkages. Future work in this area will examine regulating gene expression to chemosensitize the cells while delivering drugs. Such multicomponent conjugates should decrease the amount of chemotherapeutic agent needed for therapeutic efficacy while simultaneously reducing systemic toxicity.

6. Antibodies

Antibody-labeled gold nanoconjugates have been used in immunohistochemistry for almost 40 years.[15] Recently, however, there has been a resurgence in their use as a consequence of the development of gold nanoconjugates for live cell studies. Synthetic methods to produce antibody-gold nanoconjugates include adsorption,[15] *N*-hydroxysuccinimide (NHS) ester chemistry,[103] and oligonucleotide-directed immobilization.[104] Antibodies can adsorb to AuNPs through hydrophobic and ionic interactions, or through chemisorption of native thiol groups present in their chemical structure.[105] However, conjugates synthesized with this method have limited stability because the proteins are easily desorbed.[106] AuNPs functionalized with monolayers containing NHS esters can be reacted with the primary amine groups of the antibody to form more stable structures. Alternatively, DNA-AuNPs can be hybridized with antibodies that have been conjugated to complementary oligonucleotides.[106]

6.1. Imaging

AuNPs modified with antibodies specific to cancer-associated proteins have been used to image cancerous cells. In one example, conjugates with antibodies to epithelial growth factor receptor (EGFR) were incubated with oral epithelial cancerous and noncancerous epithelial cells. Light microscopy experiments show that conjugates bind to cancerous cells with a six times greater affinity than the noncancerous controls, thus making this technique potentially useful for the detection of cancer cells.[107]

6.2. Photothermal Therapy

Gold nanorods[108] and nanoshells[109] conjugated with antibodies are being developed as photothermal therapy agents that use antibody-coated surfaces to hone in on cancerous cells. For example, nanoshells conjugated to antibodies against human epidermal growth factor receptor 2 (HER2) were incubated with cancerous cells over-expressing HER2 receptors. These cells were then irradiated with near-IR light at a frequency that is resonant with the surface plasmon resonance of the nanoshell. Light absorption leads to heating, which causes cell death.[110] Nanoshells conjugated to control antibodies did not display this affect, because of the lack of nanoshell binding on the cell surfaces. These conjugates are also being developed as materials that combine photothermal therapy with near-IR imaging capabilities.[107,110]

© 2010 Wiley-VCH Verlag GmbH & Co. KGaA, Weinheim

7. Lipids

Recently, lipids have joined oligonucleotides, peptides, and antibodies as biomolecules used to modify AuNPs. Our research group and others have synthesized biomimetic high density lipoprotein (HDL) nanostructures by adsorbing lipids and proteins to the surface of AuNPs.[111] In this synthesis, thiolated lipids or alkanethiols along with apolipoprotein A1 (APOA1), a protein component of HDL, are adsorbed onto the surface of AuNPs. Next, a second lipid is adsorbed onto the AuNP surface through hydrophobic interactions between the lipid tails and thiolated species. Simple methods for synthesizing HDL with control over the size, shape, and composition had not been demonstrated prior to these studies. It is being increasingly appreciated that size, shape, and chemistry of HDL has an impact on its in vivo physiology, and these structures may prove useful as therapeutics and imaging agents.[111,112]

7.1. Therapeutics

Natural HDL is critical for transporting cholesterol from macrophages in atherosclerotic plaques and from the body, and increasing the HDL levels may provide an approach to preventing or reversing atherosclerosis. To that end, our research group synthesized HDL mimics called HDL AuNPs whose size as well as protein and lipid contents are similar to those of natural HDL (Figure 8). Importantly, these nanostructures can be used to determine the strength of interactions between HDL and cholesterol. In our first example using these conjugates we showed that HDL AuNPs are capable of binding a fluorescent cholesterol analogue with a high binding affinity ($K_d = 4$ nM).[111] To the best of our knowledge, this is the first measured binding constant for any form of HDL and a cholesterol derivative. This is important as it provides a key data point from which to evaluate future constructs and their ability to bind cholesterol as well as their potential as new therapeutic candidates.

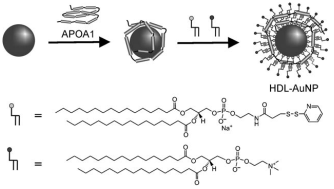

Figure 8. Templated synthesis of spherical HDL nanoparticles through use of thiol-terminated peptides and the protein (APOA1). Adapted from Ref. [111], with permission from the American Chemical Society; Copyright 2009.

7.2. Imaging

In addition to cholesterol transport, HDL-AuNP mimics have been used to image macrophage cells in vivo.[112] Macrophage density is indicative of high-risk atherosclerotic plaque, thus making it an attractive imaging target. Mice fed high cholesterol diets, an established model for atherosclerosis, were injected with HDL-AuNPs. Tomography images of the mice aortas showed a build-up of HDL-AuNPs, thereby indicating that the nanoparticles could be applied to atherosclerotic imaging.

8. Summary and Outlook

Gold nanoconjugates are an important class of materials that have already proven useful in fundamental cell biology applications. As is the case with all nanomaterials, little is known about the interactions of gold nanoconjugates and cells at the molecular level, and the design criteria for research and therapeutic usage are still being formulated. In the next sections, we discuss emerging challenges in the field. In our opinion, these questions will be the key towards the further development of gold nanoconjugates into viable therapeutic agents.

8.1. Mechanism of Uptake in Cells

Several research groups have now confirmed the internalization of gold nanoconjugates in common cell-line models. The mechanism of cellular internalization is likely to differ for different classes of gold nanoconjugates because of differences in their surface chemistry, size, and charge. Indeed, substitution reactions can be used to modulate the ability of an AuNP to be internalized by a cell.[24,113] In the case of AuNPs functionalized with positively charged amines or peptides, the mechanism likely involves the interaction of these positive moieties with the negatively charged cell surface.[26] In the case of antibody conjugates or those that possess peptidic internalization signals, interactions between specific cell-surface antigens are likely mechanistic steps.[23] Negatively charged gold nanoconjugates likely follow yet another uptake pathway. Studies by our research group and others suggest that internalization in the cell may involve the interaction of proteins with the nanoparticle surfaces.[21,65] Identifying the proteins that allow the negatively charged gold nanoconjugates to penetrate cells stands as a formidable challenge.

8.2. Targeting

The use of gold nanoconjugates provides a highly effective method for introducing substances into cells. We have described how the unique ensemble properties of these materials allow for multivalent drug and antisense agents. These agents can be used to control cellular function, regulate gene expression, and detect intracellular analytes with greater

© 2010 Wiley-VCH Verlag GmbH & Co. KGaA, Weinheim

efficiency than molecular systems, which is in part due to composite properties and proven cellular uptake ability across diverse cell types. An important challenge for the continued development of these materials as therapeutics is to target specific cells and eventually tissues and organs. Strategies for targeted delivery may include the use of biomolecules such as antibodies,[108] aptamers,[114] peptides,[23] or small molecule ligands.[115]

Targeting strategies need to be integrated with functionality to create multifunctional particles for delivering oligonucleotides or other therapeutic cargos to target cells. For example, antibodies targeted against surface receptors for appropriate cellular targets should be able to effect cell-specific uptake and limit nonspecific uptake, but they must also maintain the other desired activity and properties of nanoconjugates. In the case of polyvalent DNA-AuNPs, moieties such as antibodies must be attached in a manner that does not limit the degree of DNA functionalization or the properties that result from the density of DNA. While this is not trivial, it is noteworthy that cofunctionalized AuNPs have already been synthesized and preliminarily studied, including structures which successfully incorporate peptides without compromising complementary binding to nucleic acids.[102] These results are promising steps towards the next generation of targeted polyvalent nanoconjugate therapeutics.

8.3. Toxicity

The toxicity of several types and sizes of gold nanoconjugates has been investigated by a number of independent research groups. Although results have varied to date, several important conclusions can be drawn from these studies. Perhaps the most salient is that the toxicity of gold nanoconjugates is dependent on the chemical composition of the surface ligands. In fact, it is often the surface group itself that leads to toxicity. For example, although gold nanoconjugates functionalized with cetyltrimethylammonium bromide (CTAB) were initially thought to be toxic, it was subsequently determined that the particles do not cause cytotoxicity if they are washed to remove excess ligand.[18] Additional work in this area, has shown how the toxicity of a ligand such as CTAB is reduced when complexed with an AuNP,[116] presumably because of an alteration of the cellular localization of the toxic agent. Rotello and co-workers have also shown how the chemical functionality and charge of nanoconjugate surface ligands influence toxicity. These researchers found that while amine-functionalized particles were only mildly toxic, particles functionalized with carboxylic acids were nontoxic under all the conditions examined.[117]

Several recent studies have focused on the toxicity of citrate-capped nanoconjugates. One study investigating human dermal fibroblasts determined that the rate of cell proliferation, spreading, and adhesion is slowed by the presence of citrate-capped nanoconjugates.[118] The authors presented evidence that actin stress is the cause of these effects. A second, independent study also reports decreased cell growth in the presence of citrate-capped nanoconjugates, and in this case, the authors present evidence that this is the result of oxidative damage.[119] Similar results have also been reported when similar particles were used in myeloma cells.[120] Although acute and gross toxicity was not observed in these cases, the adverse effects of citrate-capped nanoconjugates merit further attention.

Intriguing recent investigations demonstrate that the size of the conjugate also determines its toxicity. In a recent study, Simon, Jahnen-Dechent, and co-workers examined a panel of phosphine-functionalized AuNPs with diameters ranging from 0.8 to 15 nm. These researchers found that 1.4 nm diameter particles were toxic, whereas 15 nm diameter particles were nontoxic, even at up to 100-fold higher concentrations.[121] In the case of these 1.4 nm diameter particles, evidence is presented that toxicity results from necrosis; however, neither 1.2 nor 1.8 nm diameter particles display this effect. Chan and co-workers have recently investigated the cell response to herceptin-coated gold nanoparticles within the 2–100 nm size range and found that 40 and 50 nm particles have the greatest effect on cell signaling functions.[122] Clearly, these are important findings that need to be explored further. The challenge will be preparing a range of particle sizes by using a common synthetic strategy and ensuring exact chemical surface functionality for accurate comparison.

Gold nanorods and nanoshells have recently been tested in mouse models. Halas, West, and co-workers have evaluated the photothermal efficacy of PEG-coated nanoshells injected into tumors in a mouse model. These researchers found that tumors could be ablated by treatment with light, and the animals remained healthy after more than 90 days, thus pointing to a low toxicity of nanoconjugates in vivo.[123] A research group investigating the use of CTAB-functionalized gold nanorods as imaging agents found that the particles were rapidly cleared from the blood after injection into the tail vein.[124] Another study on very similar nanorod particles found that they are accumulated in the liver after 72 h.[125] Interestingly, however, when the surface groups were changed to PEG, very few particles remained in the liver after 72 h, and most were cleared. These initial animal studies are indeed promising, and should motivate future studies that investigate the biodistribution of gold nanoconjugates as a function of size, shape, and chemical properties of the ligands.

To date, no cytotoxicity of the DNA-AuNPs has been observed.[25] It is again important to note that these nanoconjugates have unique size, charge, and surface functionality, with properties derived from the combination of the DNA and the AuNP. Extensive toxicology screening of these unique materials will be a necessity, and determining what component or components of the structure contribute to a biological response will be an exciting endeavor. Preliminary work in our research group on the innate immune response, (as characterized by interferon production, one of the first pathways activated in an innate immune response) has shown little interferon-β production caused by the DNA-AuNPs compared to analogous molecular DNA.[126] Further work is required to examine any changes in the gene expression profile that may result from the introduction of these structures. In addition to in vitro assays, preliminary work to examine biodistribution and toxicity in vivo is now

© 2010 Wiley-VCH Verlag GmbH & Co. KGaA, Weinheim

underway. While polyvalent DNA-AuNPs have already shown utility in cell culture assays, such animal studies will be required to assess the feasibility of these nanomaterials becoming possible therapeutic agents.

8.4. Conclusion

Although the properties of colloidal gold have been investigated for over a century, their application as intracellular agents in living cells emerged only prominently a few years ago. These investigations have demonstrated that multivalent and/or composite nanomaterials can provide significant advantages over molecular systems in terms of uptake and efficacy in cellular models. More fundamentally, these studies have reinforced the underlying concept in nanotechnology that composition, surface derivatization, charge, size, and shape are all critical to materials properties, and that this translates into a unique ability to interact with a biological system such as a cell. The highlighted classes of gold nanoconjugates represent a small but important sample of possible conjugate materials. The study of these classes highlights one very important conclusion: Namely, unique nanomaterials must be investigated and evaluated individually. This is exemplified in the studies of nanoparticle toxicity, where surface functionalization has repeatedly been shown to be a key parameter that influences toxicity. If one were to conclude from earlier work using CTAB-functionalized nanoconjugates that all gold nanoconjugates were toxic, then important opportunities would have been missed, for example the use of DNA-AuNPs for genetic regulation[25] or amine-functionalized conjugates for drug delivery,[36] where toxicity has been shown to be lower than polymer delivery systems.[25] As such, we encourage investigators to study and evaluate nanoconjugates on a case-by-case basis and avoid generalization wherever possible.

The preparation and use of functionalized gold nanoconjugates continues to be an extremely active and important area of research. This field continues to tantalize the chemical research community with major discoveries as well as new scientific challenges, while also involving cross-disciplinary investigators including materials scientists, biologists, engineers, and clinicians. The work carried out thus far provides only a glimpse of the wide range of potential applications for gold nanoparticles in biology and medicine.

C.A.M. acknowledges a Cancer Center for Nanotechnology Excellence (CCNE) award, the NSF-NSEC, and a U.S. Army Medical Research and Material Command Grant W81XWH-08-1-0766 for support of this work. C.A.M. is also grateful for a NIH Director's Pioneer Award. D.S.S. was supported by the LUNGevity Foundation—American Cancer Society Postdoctoral Fellowship in Lung Cancer. P.C.P. was supported by a Ryan Fellowship.

Received: August 4, 2009

[1] M. A. Hayat, *Colloidal gold: principles, methods, and applications*, Academic Press, San Diego, **1989**.
[2] P. P. Edwards, J. M. Thomas, *Angew. Chem.* **2007**, *119*, 5576; *Angew. Chem. Int. Ed.* **2007**, *46*, 5480.
[3] M.-C. Daniel, D. Astruc, *Chem. Rev.* **2004**, *104*, 293.
[4] C. A. Mirkin, R. L. Letsinger, R. C. Mucic, J. J. Storhoff, *Nature* **1996**, *382*, 607.
[5] S. Y. Park, A. K. R. Lytton-Jean, B. Lee, S. Weigand, G. C. Schatz, C. A. Mirkin, *Nature* **2008**, *451*, 553.
[6] A. P. Alivisatos, K. P. Johnsson, X. G. Peng, T. E. Wilson, C. J. Loweth, M. P. Bruchez, P. G. Schultz, *Nature* **1996**, *382*, 609.
[7] S. J. Park, T. A. Taton, C. A. Mirkin, *Science* **2002**, *295*, 1503.
[8] J. Wang, G. D. Liu, A. Merkoci, *J. Am. Chem. Soc.* **2003**, *125*, 3214.
[9] Y. Xiao, F. Patolsky, E. Katz, J. F. Hainfeld, I. Willner, *Science* **2003**, *299*, 1877.
[10] L. He, M. D. Musick, S. R. Nicewarner, F. G. Salinas, S. J. Benkovic, M. J. Natan, C. D. Keating, *J. Am. Chem. Soc.* **2000**, *122*, 9071.
[11] J. Liu, Y. Lu, *J. Am. Chem. Soc.* **2003**, *125*, 6642.
[12] N. L. Rosi, C. A. Mirkin, *Chem. Rev.* **2005**, *105*, 1547.
[13] E. Katz, I. Willner, *Angew. Chem.* **2004**, *116*, 6166; *Angew. Chem. Int. Ed.* **2004**, *43*, 6042.
[14] S. G. Penn, L. He, M. J. Natan, *Curr. Opin. Chem. Biol.* **2003**, *7*, 609.
[15] W. P. Faulk, G. M. Taylor, *Immunochemistry* **1971**, *8*, 1081.
[16] G. Frens, *Nat. Phys. Sci.* **1973**, *241*, 20.
[17] B. V. Enustun, J. Turkevich, *J. Am. Chem. Soc.* **1963**, *85*, 3317.
[18] E. E. Connor, J. Mwamuka, A. Gole, C. J. Murphy, M. D. Wyatt, *Small* **2005**, *1*, 325.
[19] B. D. Chithrani, A. A. Ghazani, W. C. W. Chan, *Nano Lett.* **2006**, *6*, 662.
[20] P. H. Yang, X. S. Sun, J. F. Chiu, H. Z. Sun, Q. Y. He, *Bioconjugate Chem.* **2005**, *16*, 494.
[21] B. D. Chithrani, W. C. W. Chan, *Nano Lett.* **2007**, *7*, 1542.
[22] E. C. Cho, J. W. Xie, P. A. Wurm, Y. N. Xia, *Nano Lett.* **2009**, *9*, 1080.
[23] A. G. Tkachenko, H. Xie, D. Coleman, W. Glomm, J. Ryan, M. F. Anderson, S. Franzen, D. L. Feldheim, *J. Am. Chem. Soc.* **2003**, *125*, 4700.
[24] P. Nativo, I. A. Prior, M. Brust, *ACS Nano* **2008**, *2*, 1639.
[25] N. L. Rosi, D. A. Giljohann, C. S. Thaxton, A. K. R. Lytton-Jean, M. S. Han, C. A. Mirkin, *Science* **2006**, *312*, 1027.
[26] K. K. Sandhu, C. M. McIntosh, J. M. Simard, S. W. Smith, V. M. Rotello, *Bioconjugate Chem.* **2002**, *13*, 3.
[27] M. Brust, M. Walker, D. Bethell, D. J. Schiffrin, R. Whyman, *J. Chem. Soc. Chem. Commun.* **1994**, 801.
[28] M. J. Hostetler, A. C. Templeton, R. W. Murray, *Langmuir* **1999**, *15*, 3782.
[29] S. D. Patil, D. G. Rhodes, D. J. Burgess, *AAPS J.* **2005**, *7*, E61.
[30] M. Thomas, A. M. Klibanov, *Proc. Natl. Acad. Sci. USA* **2003**, *100*, 9138.
[31] P. S. Ghosh, C. K. Kim, G. Han, N. S. Forbes, V. M. Rotello, *ACS Nano* **2008**, *2*, 2213.
[32] V. P. Torchilin, *Adv. Drug Delivery Rev.* **2006**, *58*, 1532.
[33] J. D. Gibson, B. P. Khanal, E. R. Zubarev, *J. Am. Chem. Soc.* **2007**, *129*, 11653.
[34] M. C. Bowman, T. E. Ballard, C. J. Ackerson, D. L. Feldheim, D. M. Margolis, C. Melander, *J. Am. Chem. Soc.* **2008**, *130*, 6896.
[35] G. Han, C. C. You, B. J. Kim, R. S. Turingan, N. S. Forbes, C. T. Martin, V. M. Rotello, *Angew. Chem.* **2006**, *118*, 3237; *Angew. Chem. Int. Ed.* **2006**, *45*, 3165.
[36] C. K. Kim, P. Ghosh, C. Pagliuca, Z. J. Zhu, S. Menichetti, V. M. Rotello, *J. Am. Chem. Soc.* **2009**, *131*, 1360.

© 2010 Wiley-VCH Verlag GmbH & Co. KGaA, Weinheim

[37] R. Hong, G. Han, J. M. Fernandez, B. J. Kim, N. S. Forbes, V. M. Rotello, *J. Am. Chem. Soc.* **2006**, *128*, 1078.
[38] A. Chompoosor, G. Han, V. M. Rotello, *Bioconjugate Chem.* **2008**, *19*, 1342.
[39] J. J. Storhoff, A. A. Lazarides, R. C. Mucic, C. A. Mirkin, R. L. Letsinger, G. C. Schatz, *J. Am. Chem. Soc.* **2000**, *122*, 4640.
[40] A. K. Lytton-Jean, C. A. Mirkin, *J. Am. Chem. Soc.* **2005**, *127*, 12754.
[41] R. C. Jin, G. S. Wu, Z. Li, C. A. Mirkin, G. C. Schatz, *J. Am. Chem. Soc.* **2003**, *125*, 1643.
[42] S. J. Hurst, H. D. Hill, C. A. Mirkin, *J. Am. Chem. Soc.* **2008**, *130*, 12192.
[43] L. M. Demers, C. A. Mirkin, R. C. Mucic, R. A. Reynolds III, R. L. Letsinger, R. Elghanian, G. Viswanadham, *Anal. Chem.* **2000**, *72*, 5535.
[44] D. Nykypanchuk, M. M. Maye, D. van der Lelie, O. Gang, *Nature* **2008**, *451*, 549.
[45] S. Y. Park, A. K. Lytton-Jean, B. Lee, S. Weigand, G. C. Schatz, C. A. Mirkin, *Nature* **2008**, *451*, 553.
[46] H. D. Hill, R. J. Macfarlane, A. J. Senesi, B. Lee, S. Y. Park, C. A. Mirkin, *Nano Lett.* **2008**, *8*, 2341.
[47] J.-M. Nam, C. S. Thaxton, C. A. Mirkin, *Science* **2003**, *301*, 1884.
[48] S. I. Stoeva, J. S. Lee, J. E. Smith, S. T. Rosen, C. A. Mirkin, *J. Am. Chem. Soc.* **2006**, *128*, 8378.
[49] R. Elghanian, J. J. Storhoff, R. C. Mucic, R. L. Letsinger, C. A. Mirkin, *Science* **1997**, *277*, 1078.
[50] J. J. Storhoff, R. Elghanian, R. C. Mucic, C. A. Mirkin, R. L. Letsinger, *J. Am. Chem. Soc.* **1998**, *120*, 1959.
[51] T. A. Taton, C. A. Mirkin, R. L. Letsinger, *Science* **2000**, *289*, 1757.
[52] Y. W. C. Cao, R. C. Jin, C. A. Mirkin, *Science* **2002**, *297*, 1536.
[53] S. J. Hurst, A. K. Lytton-Jean, C. A. Mirkin, *Anal. Chem.* **2006**, *78*, 8313.
[54] J.-S. Lee, D. S. Seferos, D. A. Giljohann, C. A. Mirkin, *J. Am. Chem. Soc.* **2008**, *130*, 5430.
[55] S. J. Hurst, A. K. R. Lytton-Jean, C. A. Mirkin, *Anal. Chem.* **2006**, *78*, 8313.
[56] Y. P. Bao, M. Huber, T. F. Wei, S. S. Marla, J. J. Storhoff, U. R. Muller, *Nucleic Acids Res.* **2005**, *33*, 7.
[57] H. Long, A. Kudlay, G. C. Schatz, *J. Phys. Chem. B* **2006**, *110*, 2918.
[58] A. K. R. Lytton-Jean, C. A. Mirkin, *J. Am. Chem. Soc.* **2005**, *127*, 12754.
[59] C. Cazenave, M. Chevrier, N. T. Thuong, C. Helene, *Nucleic Acids Res.* **1987**, *15*, 10507.
[60] T. M. Woolf, C. G. B. Jennings, M. Rebagliati, D. A. Melton, *Nucleic Acids Res.* **1990**, *18*, 1763.
[61] C. Q. Pan, R. A. Lazarus, *Biochemistry* **1997**, *36*, 6624.
[62] J. Shack, *J. Biol. Chem.* **1959**, *234*, 3003.
[63] D. S. Seferos, A. E. Prigodich, D. A. Giljohann, P. C. Patel, C. A. Mirkin, *Nano Lett.* **2009**, *9*, 308.
[64] T. Niidome, L. Huang, *Gene Ther.* **2002**, *9*, 1647.
[65] D. A. Giljohann, D. S. Seferos, P. C. Patel, J. E. Millstone, N. L. Rosi, C. A. Mirkin, *Nano Lett.* **2007**, *7*, 3818.
[66] E. Uhlmann, A. Peyman, *Chem. Rev.* **1990**, *90*, 543.
[67] Y. Dorsett, T. Tuschl, *Nat. Rev. Drug Discovery* **2004**, *3*, 318.
[68] I. Lebedeva, C. A. Stein, *Annu. Rev. Pharmacol. Toxicol.* **2001**, *41*, 403.
[69] S. J. Hwang, M. E. Davis, *Curr. Opin. Mol. Ther.* **2001**, *3*, 183.
[70] H. Kamiya, H. Tsuchiya, J. Yamazaki, H. Harashima, *Adv. Drug Delivery Rev.* **2001**, *52*, 153.
[71] C. S. Braun, J. A. Vetro, D. A. Tomalia, G. S. Koe, J. G. Koe, C. R. Middaugh, *J. Pharm. Sci.* **2005**, *94*, 423.
[72] M. D. Hughes, M. Hussain, Q. Nawaz, P. Sayyed, S. Akhtar, *Drug Discovery Today* **2001**, *6*, 303.
[73] D. J. Bharali, I. Klejbor, E. K. Stachowiak, P. Dutta, I. Roy, N. Kaur, E. J. Bergey, P. N. Prasad, M. K. Stachowiak, *Proc. Natl. Acad. Sci. USA* **2005**, *102*, 11539.
[74] T. Kubo, Z. Zhelev, H. Ohba, R. Bakalova, *Biochem. Biophys. Res. Commun.* **2008**, *365*, 54.
[75] S. K. Singh, P. Nielsen, A. A. Koshkin, J. Wengel, *Chem. Commun.* **1998**, 455.
[76] F. McKenzie, K. Faulds, D. Graham, *Small* **2007**, *3*, 1866.
[77] D. S. Seferos, D. A. Giljohann, N. L. Rosi, C. A. Mirkin, *ChemBioChem* **2007**, *8*, 1230.
[78] A. A. Koshkin, P. Nielsen, M. Meldgaard, V. K. Rajwanshi, S. K. Singh, J. Wengel, *J. Am. Chem. Soc.* **1998**, *120*, 13252.
[79] A. M. Femino, F. S. Fay, K. Fogarty, R. H. Singer, *Science* **1998**, *280*, 585.
[80] W. P. Kloosterman, E. Wienholds, E. de Bruijn, S. Kauppinen, R. H. Plasterk, *Nat. Methods* **2006**, *3*, 27.
[81] S. Tyagi, F. R. Kramer, *Nat. Biotechnol.* **1996**, *14*, 303.
[82] D. L. Sokol, X. Zhang, P. Lu, A. M. Gewirtz, *Proc. Natl. Acad. Sci. USA* **1998**, *95*, 11538.
[83] S. Sando, E. T. Kool, *J. Am. Chem. Soc.* **2002**, *124*, 9686.
[84] P. J. Santangelo, B. Nix, A. Tsourkas, G. Bao, *Nucleic Acids Res.* **2004**, *32*, e57.
[85] L. Wang, C. Y. J. Yang, C. D. Medley, S. A. Benner, W. H. Tan, *J. Am. Chem. Soc.* **2005**, *127*, 15664.
[86] N. Nitin, P. J. Santangelo, G. Kim, S. Nie, G. Bao, *Nucleic Acids Res.* **2004**, *32*, e58.
[87] D. S. Seferos, D. A. Giljohann, H. D. Hill, A. E. Prigodich, C. A. Mirkin, *J. Am. Chem. Soc.* **2007**, *129*, 15477.
[88] A. E. Prigodich, D. S. Seferos, M. D. Massich, D. A. Giljohann, B. C. Lane, C. A. Mirkin, *ACS Nano* **2009**, *3*, 2147.
[89] D. Zheng, D. S. Seferos, D. A. Giljohann, P. C. Patel, C. A. Mirkin, *Nano Lett.* **2009**, *9*, 3258.
[90] D. A. Giljohann, D. S. Seferos, A. E. Prigodich, P. C. Patel, C. A. Mirkin, *J. Am. Chem. Soc.* **2009**, *131*, 2072.
[91] Y.-L. Chiu, T. M. Rana, *RNA* **2003**, *9*, 1034.
[92] J. Soutschek, A. Akinc, B. Bramlage, K. Charisse, R. Constien, M. Donoghue, S. Elbashir, A. Geick, P. Hadwiger, J. Harborth, M. John, V. Kesavan, G. Lavine, R. K. Pandey, T. Racie, K. G. Rajeev, I. Rohl, I. Toudjarska, G. Wang, S. Wuschko, D. Bumcrot, V. Koteliansky, S. Limmer, M. Manoharan, H.-P. Vornlocher, *Nature* **2004**, *432*, 173.
[93] C. D. Medley, J. E. Smith, Z. Tang, Y. Wu, S. Bamrungsap, W. H. Tan, *Anal. Chem.* **2008**, *80*, 1067.
[94] E. Vives, J. Schmidt, A. Pelegrin, *Biochim. Biophys. Acta Rev. Cancer* **2008**, *1786*, 126.
[95] D. S. Goldfarb, J. Gariepy, G. Schoolnik, R. D. Kornberg, *Nature* **1986**, *322*, 641.
[96] V. Biju, D. Muraleedharan, K. Nakayama, Y. Shinohara, T. Itoh, Y. Baba, M. Ishikawa, *Langmuir* **2007**, *23*, 10254.
[97] A. M. Derfus, A. A. Chen, D. H. Min, E. Ruoslahti, S. N. Bhatia, *Bioconjugate Chem.* **2007**, *18*, 1391.
[98] R. E. Lanford, P. Kanda, R. C. Kennedy, *Cell* **1986**, *46*, 575.
[99] A. K. Oyelere, P. C. Chen, X. Huang, I. H. El-Sayed, M. A. El-Sayed, *Bioconjugate Chem.* **2007**, *18*, 1490.
[100] A. G. Tkachenko, H. Xie, Y. L. Liu, D. Coleman, J. Ryan, W. R. Glomm, M. K. Shipton, S. Franzen, D. L. Feldheim, *Bioconjugate Chem.* **2004**, *15*, 482.
[101] Y. L. Liu, M. K. Shipton, J. Ryan, E. D. Kaufman, S. Franzen, D. L. Feldheim, *Anal. Chem.* **2007**, *79*, 2221.
[102] P. C. Patel, D. A. Giljohann, D. S. Seferos, C. A. Mirkin, *Proc. Natl. Acad. Sci. USA* **2008**, *105*, 17222.
[103] X. Qian, X. H. Peng, D. O. Ansari, Q. Yin-Goen, G. Z. Chen, D. M. Shin, L. Yang, A. N. Young, M. D. Wang, S. Nie, *Nat. Biotechnol.* **2008**, *26*, 83.
[104] C. M. Niemeyer, B. Ceyhan, *Angew. Chem.* **2001**, *113*, 3798; *Angew. Chem. Int. Ed.* **2001**, *40*, 3685.

© 2010 Wiley-VCH Verlag GmbH & Co. KGaA, Weinheim

[105] G. T. Hermanson, *Bioconjugate Techniques*, Academic Press, San Diego, CA, **1996**.

[106] N. Nitin, D. J. Javier, R. Richards-Kortum, *Bioconjugate Chem.* **2007**, *18*, 2090.

[107] I. H. El-Sayed, X. H. Huang, M. A. El-Sayed, *Nano Lett.* **2005**, *5*, 829.

[108] I. H. El-Sayed, X. Huang, M. A. El-Sayed, *Cancer Lett.* **2006**, *239*, 129.

[109] L. R. Hirsch, R. J. Stafford, J. A. Bankson, S. R. Sershen, B. Rivera, R. E. Price, J. D. Hazle, N. J. Halas, J. L. West, *Proc. Natl. Acad. Sci. USA* **2003**, *100*, 13549.

[110] C. Loo, A. Lowery, N. Halas, J. West, R. Drezek, *Nano Lett.* **2005**, *5*, 709.

[111] C. S. Thaxton, W. L. Daniel, D. A. Giljohann, A. D. Thomas, C. A. Mirkin, *J. Am. Chem. Soc.* **2009**, *131*, 1384.

[112] D. P. Cormode, T. Skajaa, M. M. van Schooneveld, R. Koole, P. Jarzyna, M. E. Lobatto, C. Calcagno, A. Barazza, R. E. Gordon, P. Zanzonico, E. A. Fisher, Z. A. Fayad, W. J. Mulder, *Nano Lett.* **2008**, *8*, 3715.

[113] T. B. Huff, M. N. Hansen, Y. Zhao, J. X. Cheng, A. Wei, *Langmuir* **2007**, *23*, 1596.

[114] D. J. Javier, N. Nitin, M. Levy, A. Ellington, R. Richards-Kortum, *Bioconjugate Chem.* **2008**, *19*, 1309.

[115] V. Dixit, J. Van den Bossche, D. M. Sherman, D. H. Thompson, R. P. Andres, *Bioconjugate Chem.* **2006**, *17*, 603.

[116] T. S. Hauck, A. A. Ghazani, W. C. W. Chan, *Small* **2008**, *4*, 153.

[117] C. M. Goodman, C. D. McCusker, T. Yilmaz, V. M. Rotello, *Bioconjugate Chem.* **2004**, *15*, 897.

[118] N. Pernodet, X. H. Fang, Y. Sun, A. Bakhtina, A. Ramakrishnan, J. Sokolov, A. Ulman, M. Rafailovich, *Small* **2006**, *2*, 766.

[119] J. J. Li, L. Zou, D. Hartono, C. N. Ong, B. H. Bay, L. Y. L. Yung, *Adv. Mater.* **2008**, *20*, 138.

[120] R. Bhattacharya, C. R. Patra, R. Verma, S. Kumar, P. R. Greipp, P. Mukherjee, *Adv. Mater.* **2007**, *19*, 711.

[121] Y. Pan, S. Neuss, A. Leifert, M. Fischler, F. Wen, U. Simon, G. Schmid, W. Brandau, W. Jahnen-Dechent, *Small* **2007**, *3*, 1941.

[122] W. Jiang, B. Y. S. Kim, J. T. Rutka, W. C. W. Chan, *Nat. Nanotechnol.* **2008**, *3*, 145.

[123] D. P. O'Neal, L. R. Hirsch, N. J. Halas, J. D. Payne, J. L. West, *Cancer Lett.* **2004**, *209*, 171.

[124] H. F. Wang, T. B. Huff, D. A. Zweifel, W. He, P. S. Low, A. Wei, J. X. Cheng, *Proc. Natl. Acad. Sci. USA* **2005**, *102*, 15752.

[125] T. Niidome, M. Yamagata, Y. Okamoto, Y. Akiyama, H. Takahashi, T. Kawano, Y. Katayama, Y. Niidome, *J. Controlled Release* **2006**, *114*, 343.

[126] M. D. Massich, D. A. Giljohann, D. S. Seferos, L. E. Ludlow, C. M. Horvath, C. A. Mirkin, *Mol. Pharm.* **2009**, *6*, 1934.

[127] S. Dhar, W. L. Daniel, D. A. Giljohann, C. A. Mirkin, S. J. Lippard, *J. Am. Chem. Soc.* **2009**, *131*, 14652.

© 2010 Wiley-VCH Verlag GmbH & Co. KGaA, Weinheim

J Clust Sci (2011) 22:661–665
DOI 10.1007/s10876-011-0412-4

ORIGINAL PAPER

Biological Synthesis of Gold Nanoparticles by Fungus *Epicoccum nigrum*

Zeinab Sheikhloo · Mojtaba Salouti · Farzad Katiraee

Received: 28 May 2011 / Published online: 15 September 2011
© Springer Science+Business Media, LLC 2011

Abstract Gold nanoparticles exhibit unique optical, thermal, chemical and physical properties. The microorganisms have high potential for production of nanoparticles with wide applications. Application of fungi to produce nanoparticles is potentially exciting because of their ability to secrete large amounts of enzymes. In this study, we investigated biosynthesis of gold nanoparticles by the fungus *Epicoccum nigrum* isolated from Andalian gold mine in north-west of Iran. The gold nanoparticles were produced intra and extracellular by reaction of an aqueous solution of chloroauric acid with the biomass of fungus *E. nigrum*. The produced gold nanoparticles were in the size range of 5–50 nm in spherical and rod shapes. This is the first report on the biosynthesis of gold nanoparticles by the fungus *E. nigrum*.

Keywords Nanoparticles · Gold · Biosynthesis · Fungi · *Epicoccum nigrum*

Introduction

Gold nanoparticles have found many potential applications in many fields such as catalysis, sensors, drugs and gene delivery systems [1]. Nanoparticles can be synthesized by physical and chemical methods [2]. The problems of these methods are often experienced with low stability of the nanoparticle preparations, difficult control of the crystal growth and aggregation of the particles [3–5]. One of the most important criteria of nanotechnology is development of clean, nontoxic and

---

Z. Sheikhloo · M. Salouti (✉)
Department of Microbiology, Faculty of Sciences, Zanjan Branch, Islamic Azad University,
Moallem St., Etemadieh, 4515658145 Zanjan, Iran
e-mail: saloutim@yahoo.com

F. Katiraee
Mycology Research Center, Faculty of Veterinary Medicine, University of Tehran, Tehran, Iran

environmentally acceptable green chemistry procedures [6, 7]. Many biological organisms have known to produce inorganic materials either intra or extracellular [8, 9]. Some well-known examples include formation of iron oxides and various metal nanoparticles using bacteria, fungi or plants [10]. The use of eukaryotic organisms such as fungi in the synthesis of nanoparticles with different chemical composition and size is in progress due to their ability to secrete large amounts of enzymes. The fungi possess some advantages over bacteria. The first is that the most filamentous fungi have a high tolerance towards metals and a high wall-binding capacity, as well as intracellular metal uptake capabilities. In addition, they are easy to culture on a large scale, thus making it possible to easily obtain enough biomass for processing [11]. In an interesting study, Bhambure et al. [11] have reported that the fungus *Aspergillus niger* NCIM616, when placed in a concentrated aqueous solution of $HAuCl_4$, resulted in formation of extracellular gold nanoparticles with the size of 12.79 ± 5.61 nm. In an another recent study, Binupriya et al. [12] demonstrated that the fungus *Rhizopus stolonifer*, when placed in aqueous solution of 1 mM $HAuCl_4$, resulted in the extracellular formation of gold nanoparticles. Here, we report the biosynthesis of gold nanoparticles by a novel metal resistance fungus biomass, *Epicoccum nigrum*, isolated from Andalian gold mine in north-west of Iran. *E. nigrum* is an species of fungus that finds in soil and food. Application of fungi for synthesis of gold nanoparticles has already been reported [11, 12]. However, there is no report on the synthesis of gold nanoparticles using *E. nigrum*. The results showed that this fungus is a good candidate for the simple and clean synthesis of gold nanoparticles.

Experimental

Isolation and Growth of Fungi

Many samples of soil were collected from Andalian gold mine in north-west of Iran in sterilized falcon tubes. Five grams of each sample was diluted with 45 mL of sterile distilled water and placed onto the Sabouraud's dextrose agar (SDA) plates. The plates were then incubated at 27 °C for 5–10 days. All of the isolated fungi were tested for synthesis of gold nanoparticles. Then, the fungus that was found to be able to produce gold nanoparticles was identified based on morphological features, slide culture and growth parameters on malt extract agar or oatmeal agar [13, 14]. The emerged colonies on the petri dishes were purified by single spore isolation. The single spores were maintained on SDA slants at 27 °C. The stock cultures were maintained by subculturing at monthly intervals.

Biosynthesis of Gold Nanoparticles

The isolated fungi were grown aerobically in 250 mL Erlenmeyer flasks containing 100 mL MYPG medium (malt extract 0.3%, yeast extract 0.3%, peptone 0.5% and glucose 1% at pH 5.5–6). The culture was agitated on an orbital shaker (160 rpm) at 27–29 °C for 96 h. The biomass was separated from the culture broth by centrifugation (5,000 rpm) at 10 °C for 20 min. The biomass was washed extensively with distilled water to remove medium components. The fresh and clean biomass (5 g of wet biomass) was suspended in 100 mL of 10^{-3} M aqueous $HAuCl_4$ solution at pH 2.5 in 250 mL Erlenmeyer flasks. The whole mixture was put into a shaker at 27–29 °C for 72 h (160 rpm). The reaction was carried out in the dark.

Characterization of Gold Nanoparticles

The bioreduction of the Au ions in solution was monitored by periodic sampling of aliquots of the aqueous component. The scanning was performed in the range of 400–800 nm by a UV–visible spectrophotometer (Shimadzu, UV Pharma spec 1700 with a resolution 0.72 nm). X-Ray diffraction measurement was carried out using (Philips PW 1800) (XRD). The samples for transmission electron microscopy (Philips model EM 208S) analysis were prepared on carbon-coated copper grids.

Results and Discussion

One out of nine kinds of the isolated fungi was found to be able to synthesize gold nanoparticles. This fungus was identified *E. nigrum*, by morphological features, slide culture and growth parameters on malt extract agar. Colonies of *E. nigrum* are fast growing, suede-like to downy, with a strong yellow to orange-brown diffusible pigmentation. When sporulating numerous black sporodochia (aggregates of conidiophores) are visible. Conidia are formed singly on densely compacted, nonspecialized, determinant, slightly pigmented conidiophores. Conidia are globose pyriform, mostly 15–25 μm diameter with a funnel-shaped base and broad attachment scar, often seceding with a protuberant basal cell; i.e. aleuric or rhexolytic dehiscence of conidia. Conidia become multicellular which divide the conidia into up to 15 cells, darkly pigmented and have verrucose external surface. Pelvinate sporodochia was appearing in 8–10 days, visible as black spots and 100–2,000 μm [15].

By mixing the fungus biomass with the aqueous solution of gold ions, the color of the biomass changed from yellow to purple after 32 h. The color change is a signal for the formation of gold nanoparticles. The reduction of the aqueous chloroaurate ions during exposure to the mycelia was followed by UV–vis spectroscopy [11]. The UV–vis spectra, recorded after completion of the reaction, showed a distinct absorption band centered at 543 nm (Fig. 1) that was very specific for gold nanoparticles.

One of the important ways to characterize nanoparticles is evaluating the XRD spectrum of the sample. The XRD pattern clearly showed that the gold nanoparticles have been formed by the bioreduction of gold ions by the fungus XRD patterns of thin films exposed to $HAuCl_4$, broadening of the intense peaks due to (111), (200), (220) and (311) Bragg reflection at $2\theta = 38.26°$, $44.60°$, $64.67°$ and $77.54°$, confirmed the presence of gold nanoparticles (Fig. 2) [9].

The nanostructures synthesized in the fungus cells were further characterized by transmission electron microscopy. The TEM images showed that the gold nanoparticles were formed in spherical and rod shapes both intra and extracellular.

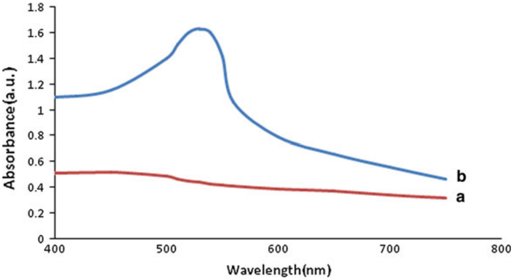

Fig. 1 UV–vis spectra recorded from the fungal cells before (**a**) and after (**b**) exposure to 1 mM aqueous $HAuCl_4$ solution

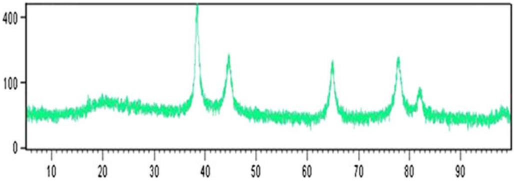

Fig. 2 XRD pattern recorded from an Au nano-*E. nigrum* biofilms

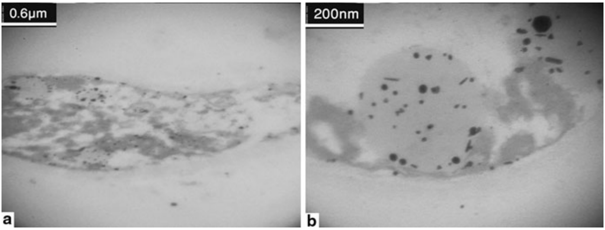

Fig. 3 TEM images at different magnifications of the thin sections of the *E. nigrum* cells after reaction with chloroaurate ions (**a**, **b**). Gold nanoparticles were synthesized both intra and extracellular

The average of nanoparticles size was from 5 to 50 nm. A number of *E. nigrum* cells can be seen in the low magnification of TEM images (Fig. 3). The gold nanoparticles were organized on the cytoplasm and the cell wells.

To our knowledge, this is the first study on the synthesis of gold nanoparticles by *E. nigrum*.

Conclusion

The results showed that the reaction of aqueous chloroaurate ions with the biomass of *E. nigrum* leads to the formation of gold nanoparticles both intra and extracellular.

References

1. S. He, Z. Guo, Z. Yu, and S. Zhang (2007). *Mater. Lett.* **61**, 3984.
2. M. Agnihotri, S. Joshi, K. A. Ravi, S. Zinjarde, and S. Kulkarni (2009). *Mater. Lett.* **63**, 1231.
3. H. Huang and X. Yang (2005). *Colloids Surf. A* **255**, 11.
4. S. Mandal, S. Phadtare, and M. Sastry (2005). *Curr. Appl. Phys.* **5**, 127.
5. D. Mandal, M. E. Bolander, D. G. Mukhopadhyay, and P. Sarkar Mukherjee (2006). *Appl. Microbiol. Biotechnol.* **69**, 485.
6. Z. Ranjbar Navazi, M. Pazouki, and F. Sadat Halek (2010). *Iran. J. Biotechnol.* **8**, 56.
7. I. Maliszewska, L. Aniszkiewicz, and Z. Sadowski (2009). *Acta Phys. Pol. A.* **116**, 163.
8. A. R. Binupriya, M. Sathishkumar, and S. I. Yun (2010). *Colloids Surf. B* **79**, 531.
9. S. S. Shankar, A. Ahmad, R. Pasricha, and M. Sastry (2003). *J. Mater. Chem.* **13**, 1822.
10. P. Mohanpuria, N. K. Rana, and S. K. Yadav (2007). *J. Nanopart. Res.* **10**, 507.
11. R. Bhambure, M. Bule, N. Shaligram, and M. Kamat (2009). *Chem. Eng. Technol.* **32**, 1036.
12. A. R. Binupriya, M. Sathishkumar, and S. I. Yun (2010). *Colloids Surf. B* **79**, 531.
13. R. A. Samson, E. S. Hoekstra, J. C. Frisvad, and O. Filtenborg, *Introduction to Food- and Airborne Fungi*, 6th ed., Chap. 1, p. 118 (Centralbureau voor Schimmelcultures, Delft, 2002).
14. D. H. Larone *Medically Important Fungi—A Guide to Identification*, 3rd ed. (ASM Press, Washington, DC, 1995).
15. D. A. Sutton, A. W. Fothergill, and M. G. Rinaldi *Guide to Clinically Significant Fungi*, 1st ed. (Williams & Wilkins, Baltimore, 1998).

Chapter 3
Biosynthesis of Gold Nanoparticles: A Review

Maggy F. Lengke, Charoen Sanpawanitchakit, and Gordon Southam

3.1 Introduction

Gold is one of the rarest metals on earth, and its importance has been acknowledged since antiquity. Gold is not only used in jewelry industry but also in a diverse range of industrial applications covering the field of biology and medicine, environment, and technology (e.g., Oldenburg et al. 1998; Vieira and Volesky 2000; Salata 2004; Sperling et al. 2008; Cai et al. 2008; Chen et al. 2008; Mohanpuria et al. 2008). Because of the increased demand of gold in many industrial applications, there is a growing need for cost effectiveness as well as to implement green chemistry in the development of new nanoparticles. Although various chemical and physical synthesis methods successfully produce pure and well-defined nanoparticles, these methods remain expensive and involve the use of hazardous chemicals. In consequence, biological processes that lead to the formation of nanoscale inorganic materials are appealing as possible environmentally friendly nanofactories.

The synthesis of gold nanoparticles of different sizes, ranging from <1 to several hundred nanometers, and shapes has been conducted in both aqueous and nonpolar organic solutions (Brust et al. 1994; Handley 1989; Selvakannan et al. 2003; Daniel and Astruc 2004). The usual synthetic route to prepare gold nanoparticles involves the reduction of a gold salt (usually a halide) in solution by various reducing agents in the presence of a stabilizer (Brust et al. 1994; Handley 1989; Selvakannan et al. 2003; Daniel and Astruc 2004; Masala and Seshadri 2004). The use of rapid reductants (e.g., white phosphorus, tannic acid, formamide, *o*-anisidine) results in bigger and generally spherical nanoparticles, while weak reducing agents (e.g., citrate, tartarate)

M.F. Lengke (✉)
Geomega Inc, 2525 28th Street, Suite 200, Boulder, CO 80301, USA
e-mail: maggylengke@yahoo.com

C. Sanpawanitchakit
EnviroGroup Limited, 3561 Stagecoach Road, Suite 205, Longmont, CO 80504, USA

G. Southam
Department of Earth Sciences, University of Western Ontario, London, ON, N6A 5B7, Canada

M. Rai and N. Duran (eds.), *Metal Nanoparticles in Microbiology*,
DOI 10.1007/978-3-642-18312-6_3, © Springer-Verlag Berlin Heidelberg 2011

results in a slow reaction generating small nanoparticles (Handley 1989; Daniel and Astruc 2004). Sulfur-containing ligands (e.g., xanthates, disulfides, dithiols or trithiols), phosphanes, phosphines, amines, chalcogenides, carboxylates, and polymers have all been used to stabilize gold nanoparticles (Brust et al. 1994; Daniel and Astruc 2004).

Biological methods using organisms, such as bacteria and fungi (e.g., Southam and Beveridge 1994, 1996; Canizal et al. 2001; Kashefi et al. 2001; Mukherjee et al. 2001, 2002; Shankar et al. 2003; Keim and Farina 2005; Nair and Pradeep 2002; Ahmad et al. 2005; Lengke and Southam 2005, 2006, 2007; Lengke et al. 2006a, b, c, 2007), plants (e.g., Gardea-Torresdey et al. 2002), plant extracts (e.g., Shankar et al. 2003, 2004), and dead plant biomass (e.g., Gardea-Torresdey et al. 1999, 2000), for the synthesis of gold nanoparticles are relatively new areas, and are currently being explored. Although the biosynthesis of gold nanoparticles is relatively new, the interactions between bacteria and metals have been well documented (e.g., Heath 1981; Nash et al. 1981; Ehrlich 2002) and the ability of bacteria to accumulate metals has been recognized in the bioremediation field (e.g., Lloyd 2002; Dermont et al. 2008). Previous studies of the biosynthesis of gold nanoparticles have been focused on the use of gold (III)–chloride [$AuCl_4^-$] and gold(I)–thiosulfate [$Au(S_2O_3)_2^{3-}$] complexes. Therefore, the objective of this chapter is to review the current state of knowledge concerning the biosynthesis of gold nanoparticles by bacteria, cyanobacteria, and algae using these two gold complexes, based on the existing literature.

3.2 Gold Chemistry

Gold can occur in one of the six oxidation states, from -1 to $+5$ (Puddephatt and Vittal 1994), which can be related to its relatively high electronegativity. The most common form of gold complexes is in aurous [Au(I)] and auric [Au(III)] oxidation states (Emery and Leddicotte 1961). The dissolution of gold in aqueous solution is a combination process of oxidation and complexation. In the presence of a complexing ligand, Au(I) and Au(III) can form stable complexes, otherwise they can be reduced in solution to metallic gold (Nicol et al. 1987). The stability of gold complexes is related not only to the properties of the complexing ligand, but also more specifically to the donor atom of the ligand that is bonded directly to the gold atom. According to Nicol et al. (1987), the first rule is that the stability of gold complexes tends to decrease when the electronegativity of the donor atom increases. For example, the stability of gold halide complexes in solution follows the order $I^- > Br^- > Cl^- > F^-$. The second rule is that Au(III) is generally favored over Au(I) with hard ligands and Au(I) over Au(III) with soft ligands. The soft ligands containing less electronegative donor atoms such as S, C, P, and I form more stable complexes with Au(I), whereas the hard electron donor ligands such as F, Cl, O, and N prefer Au(III). The preferred co-ordination number of Au(I) is 2, tending to form linear complexes, and that of Au(III) is 4, tending to form square planar complexes.

The review of gold complexes below is limited for the gold(III)–chloride and gold(I)–thiosulfate because the published biosynthesis of gold nanoparticles by bacteria, cyanobacteria, and algae mainly utilized these two gold complexes.

3.2.1 Gold(I)–Thiosulfate Complex

Gold(I)–thiosulfate complex is a predominant species at a wide range of pH (acidic to alkaline) and moderate oxidizing to reducing conditions (Senanayake et al. 2003). Sodium thiosulfate is one component of an alternative lixiviant to cyanide for extraction of gold (Aylmore and Muir 2001), and it forms a strong complex with Au(I). The advantage of this approach is that thiosulfate is essentially non-toxic, and ore types that are refractory to gold cyanidation (e.g., carbonaceous or Carlin type ores) can be leached by thiosulfate. Some problems with this alternative process include the high consumption of thiosulfate, and the lack of a suitable recovery technique, because gold(I)–thiosulfate does not adsorb to activated carbon, a standard technique used in gold cyanidation to separate the gold complex from the ore slurry.

3.2.2 Gold(III)–Chloride Complex

Gold (III)–chloride complex is stable under oxidizing and acidic conditions (Ran et al. 2002). It decomposes above 160°C or in light. Many studies of biosynthesis gold nanoparticles had utilized the gold(III)–chloride acid solid as a starting material to form gold(III)–chloride complex (e.g., Nair and Pradeep 2002; Lengke et al. 2006a, b, c, 2007). Gold(III)–chloride acid solid ($HAuC1_4 \cdot xH_2O$) can be produced by dissolving gold in aqua regia and then evaporating nitric acid (HNO_3) with hydrochloric acid (HCl). This solid is also referred to as acid gold trichloride or gold(III)–chloride trihydrate (Emery and Leddicotte 1961; http://en.wikipedia.org/wiki/Gold(III)_chloride). Gold(III)–chloride acid – appearing as long, bright yellow, needle-like crystals – is very hygroscopic and highly soluble in water and ethanol.

3.3 Biosynthesis of Gold Nanoparticles

The interactions between bacteria/cyanobacteria/algae and gold have been well documented since 1986 for biosorption and biorecovery of gold. Our review includes 46 published papers, utilizing bacteria (24), cyanobacteria (8), and algae

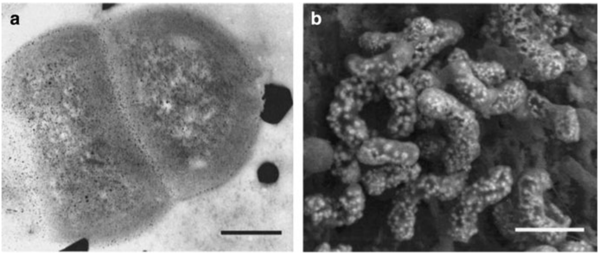

Fig. 3.1 (**a**) A TEM micrograph of a thin section of cyanobacteria cell with the gold nanoparticles inside the cell, (**b**) a SEM micrograph of gold nanoparticles on the surface of sulfate-reducing bacteria (*Desulfovibrio* sp). *Scale bars* in (**a**) and (**b**) are 0.5 and 1.5 μm, respectively

(14) to determine whether gold can be accumulated from gold(I)–thiosulfate and gold(III)–chloride solutions. Because of purposes other than the biosynthesis of gold particles, some studies of biosorption and biorecovery neither included details of the shape and size of gold particles (e.g., Kashefi et al. 2001; Nakajima 2003) nor described the experimental conditions such as pH, temperature, duration, initial gold concentrations, or bacterial population (e.g., Ting et al. 1995; Kashefi et al. 2001). In general, gold nanoparticles were precipitated intracellularly and/or extracellularly depending on the species (Fig. 3.1). The shape of gold particles precipitated by bacteria/cyanobacteria/algae includes spherical, oval, spongy clots, mushroom, irregular, triangular, tetragonal, hexagonal, octahedral, rod, cubic, docahedral, icosahedral, coil or wire, plate, and thin foil, with size ranging from 1 nm to several mm (Fig. 3.2), as discussed below.

3.3.1 Gold(I)–Thiosulfate Complex

The interactions between bacteria and cyanobacteria with a gold–thiosulfate complex have been studied by Lengke and Southam (2005, 2006, 2007) and Lengke et al. (2006a), and are summarized in Table 3.1. *Acidithiobacillus thiooxidans* isolated from the Driefontein Consolidated gold mine in Witwatersrand Basin, Republic of South Africa was able to produce gold particles in the presence of up to 0.26 mmol/L gold at pH ~ 1.9–2.2 and 25°C within a period of 35–75 days (Lengke and Southam 2005). In the presence of dead bacterial cells and in the chemical abiotic experiments, gold was not precipitated under similar experimental conditions and duration. The bacterial system was able to precipitate 87–100% of the gold under diurnal light exposure, while only 11–69% of the gold was precipitated in the dark. The gold nanoparticles were precipitated inside the bacterial cells with the size $<$10 nm,

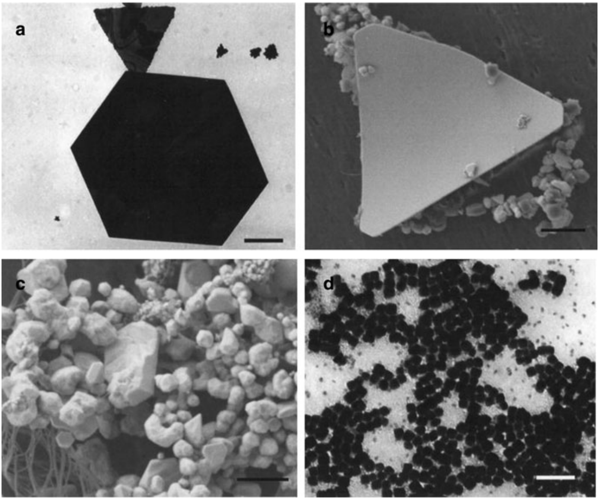

Fig. 3.2 TEM and SEM micrographs of selected gold nanoparticles formed by cyanobacterial interactions with gold(III)–chloride and gold(I)–thiosulfate complexes. *Scale bars* in (**a**), (**b**), (**c**), and (**d**) are 0.5, 2, 1, and 0.1 µm, respectively

forming a spherical shape. Outside the bacterial cells, the gold had formed coiled or wire, irregular, and rounded structures with an approximate size of 0.5–5 µm, and a crystalline octahedral shape.

Heterotrophic sulfate-reducing bacteria (SRB) isolated from the Driefontein Consolidated gold mine in Witwatersrand Basin, Republic of South Africa was able to produce gold particles in the presence of up to 2.6 mmol/L gold at pH ~ 7.4–7.9 and 23–25°C within a period of 6–53 days, in the presence or absence of iron (Lengke and Southam 2006). Only in the presence of live bacterial cells, gold was precipitated from solution. The gold nanoparticles were precipitated inside and at the bacterial cells with the size <10 nm, forming a spherical shape. In bulk solution, the gold had formed spherical, sub-octahedral to octahedral shape with size ranging from 0.5 to 6 µm (Lengke and Southam 2006). The role of SRB in the precipitation of gold was also investigated through column experiments in the presence of up to 2.6 mmol/L gold at pH ~ 7.4–8.5 and 23–25°C within a period of 148 days, in the presence or absence of iron (Lengke and Southam 2007). In the bacterial systems, SRB precipitated gold inside and at the cells, forming spherical nanoparticles (<10 nm). In bulk solution, the formation of octahedral gold crystals,

Table 3.1 A summary of bacterial and cyanobacterial interactions with a gold(I)–thiosulfate complex

No	Bacteria Name	Shape	Extracellular/ Intracellular	Size	pH	Temperature (°C)	Period	Initial gold concentrations (mol/L)	Bacterial population (cells/mL)	Experimental condition	References
Bacteria											
1	*Acidithiobacillus thiooxidans*	Spherical, irregular, coil or wire, octahedral	Extracellular and intracellular	<10 nm (intracellular); 0.5–5 μm (extracellular)	1.9 and 2.2	25	35 days	$(0–0.26) \times 10^{-3}$	$10^7–10^8$	Bacteria stationary growth phase	Lengke and Southam (2005)
		Spherical, irregular, coil or wire, octahedral	Extracellular and intracellular	<10 nm (intracellular); 0.5–5 μm (extracellular)	5.4–1.9	25	75 days	$(0–0.26) \times 10^{-3}$	$10^6–10^8$	Inoculate with bacteria	
			No precipitation		1.9	25	75 days	$(0–0.26) \times 10^{-3}$		Dead cells (autoclaved)	
			No precipitation		1.9 and 5.4	25	75 days	$(0–0.26) \times 10^{-3}$		Abiotic	
2	Heterotrophic sulfate-reducing bacteria (SRB)	Octahedral, spherical	Extracellular and intracellular	<10 nm (intracellular); 0.5–6 μm (extracellular)	7.4–7.9	23–25	53 days	$(0–2.55) \times 10^{-3}$	7×10^6 to 3.5×10^7	Bacteria stationary growth phase	Lengke and Southam (2006)
		Octahedral, spherical	Extracellular and intracellular	<10 nm (intracellular); 0.5–6 μm (extracellular)	7.4–7.9	23–25	6 days	$(0–1.14) \times 10^{-3}$	5×10^3 to 10^6	Inoculate with bacteria	
			No precipitation		7.7	23–25	53 days	$(0–1.14) \times 10^{-3}$		Dead cells (autoclaved)	
			No precipitation		7.4–7.7	23–25	53 days	$(0–2.55) \times 10^{-3}$		Abiotic	

3	Heterotrophic sulfate-reducing bacteria (SRB)	Spherical, octahedral, foil	Extracellular and intracellular	<10 nm (intracellular); 1 µm to several mm (extracellular)	7.4–8.5	23–25	148 days	$(0–2.55) \times 10^{-3}$	4.5×10^8 to 1.4×10^9	Bacteria	Lengke and Southam (2007)
		Spherical		1 µm	7.4–9.1	23–25	148 days	$(0–2.55) \times 10^{-3}$		Abiotic	
Cyanobacteria											
1	*Plectonema boryanum* UTEX 485	Irregular-thin	Extracellular		5.3	25	28 days	$(2–2.8) \times 10^{-3}$	3.8×10^8	Cyanobacteria stationary growth phase	Lengke et al. (2006a)
		Irregular, cubic	Extracellular and intracellular	<10 nm (intracellular); 10–25 nm (extracellular)	5.3	60	28 days	$(2–2.8) \times 10^{-3}$	3.8×10^8	Cyanobacteria stationary growth phase	
		Cubic	Extracellular and intracellular	<10 nm (intracellular); 10–25 nm (extracellular)	5.3–3.9	100	28 days	$(2–2.8) \times 10^{-3}$	3.8×10^8	Cyanobacteria stationary growth phase	
		Irregular	Extracellular and intracellular	<10 nm (intracellular); 10–25 nm (extracellular)	5.3–3.0	200	1 day	$(2–2.8) \times 10^{-3}$	3.8×10^8	Cyanobacteria stationary growth phase	
			No precipitation		5	25	28 days	$(2–2.8) \times 10^{-3}$		Abiotic	
		Cuboctahedral	Precipitation	25 nm	5–3.9	60	28 days	$(2–2.8) \times 10^{-3}$		Abiotic	
		Cuboctahedral	Precipitation	25 nm	5–2.2	100	28 days	$(2–2.8) \times 10^{-3}$		Abiotic	
		Cuboctahedral	Precipitation	25 nm	5–1.9	200	1 day	$(2–2.8) \times 10^{-3}$		Abiotic	

framboid-like structures (~1.5 μm), and gold foil (mm-scale) was observed in the bacterial systems, while only a spherical shape with a size ~1 μm was observed in the chemical abiotic systems.

Plectonema boryanum UTEX 485, a filamentous cyanobacterium, had been reacted with a gold–thiosulfate complex (up to 2.8 mmol/L gold) at 25–100°C for up to 1 month and at 200°C for 1 day (Lengke et al. 2006a). The interaction of cyanobacteria with a gold–thiosulfate complex caused the separation of filaments into their constituent cells and released membrane vesicles after 14 days at 25°C. The precipitation of irregular gold particles on the surface of membrane vesicles was observed. At 60–200°C, nanoparticles of gold and gold sulfide were deposited inside the cells ($<$10 nm) and on the outer surface of the sheaths (~10–25 nm). The larger nanoparticles of gold (~20–25 nm) were distinctly cubic in shape. In the chemical abiotic systems, the gold–thiosulfate were stable for 1 month at 25°C, whereas gold nanoparticles (~25 nm) with a cubohedral habit were precipitated at 60–200°C.

3.3.2 Gold(III)–Chloride Complex

The interactions between bacteria, cyanobacteria, and algae with a gold(III)–chloride complex have been studied using different species, and the results of these studies are summarized in Tables 3.2, 3.3, and 3.4. The first published laboratory study to understand the interaction of a mixed bacteria (*Bacillus mesentericus niger*, *Bacillus oligonitrophilus*, and *Bacterium nitrificans*) with initial elemental gold was conducted by Korobushkina and Korobuskhin (1986). The objective of their study was to determine whether gold can be biologically re-deposited. The elemental gold was dissolved into solution, presumably as gold(III)–chloride or gold–organic complexes, and a reduction process occurred simultaneously, forming spherical/oval (1–2 μm), spongy clots/clusters/nodules (0.1–20 μm), and mushroom (0.1–0.5 μm) shapes. Southam and Beveridge (1994, 1996) employed *Bacillus subtilis* 168 in their experiments at 4, 23–25, 60, and 90°C within 1 week to 8 months. Gold nanoparticles were initially precipitated inside the bacterial cells (5–50 nm) and were released into solution, forming spherical (20 nm) and hexagonal–octahedral (4–20 μm) gold. The formation of crystalline octahedral gold was enhanced by an increase in the experimental duration and temperature. The potential of 14 hyperthermophilic and mesophilic dissimilatory iron(III) reducing bacteria to precipitate elemental gold from solutions was investigated by Kashefi et al. (2001) using hydrogen (H_2), lactate, or acetate electron donor at neutral pH. Of 14 species, 6 were able to precipitate elemental gold only in the presence of H_2 electron donor at 100°C. Most of the six bacteria precipitated gold at the cell surfaces (nm scale), except for *Geovibrio ferrireducens* (ATCC 51996). However, a closer inspection of the thin sections of several species [e.g., *Geobacter sulfurreducens* (ATCC 51573), *Pyrobaculum islandicum* (DSM 4184), *Thermotoga maritima* (DSM 3109)] indicated that gold was also precipitated intracellularly.

Table 3.2 A summary of bacterial interactions with a gold(III)–chloride complex

No	Bacteria name	Shape	Extracellular/ intracellular	Size	pH	Temperature (°C)	Period	Initial gold concentrations (mol/L)	Bacterial population (cells/mL)	Experimental condition	References
1	*Bacillus mesentericus niger*	Spherical, oval	Extracellular	1–2 µm (Extracellular)	7.5	25	360 days	2.5×10^{-3}		Nutrient medium	Korobushkina and Korobuskhin (1986)
	Bacillus oligonitrophilus	Spongy clots/ clusters/ nodules	Extracellular	0.1–20 µm (Extracellular)							
	Bacterium nitrificans	Mushroom	Extracellular	0.1–0.5 µm (extracellular)							
2	*Bacillus subtilis* 168	Irregular, spherical	Extracellular and intracellular	5–50 nm (Intracellular)	2.69	60	7–224 days	2.5×10^{-3}	20 mg/mL dry cell weight	Bacteria late stationary phase	Southam and Beveridge (1994)
		Hexagonal, octahedral		20 µm (Extracellular)							
			No precipitation			60	7–224 days	5×10^{-3}		Abiotic	
3	*Bacillus subtilis* 168	Spherical, irregular, octahedral	Extracellular and intracellular	<20 nm (intracellular)	2.6	4	7–28 days	2.5×10^{-3}	20 mg/mL dry cell weight	Bacteria late stationary phase	Southam and Beveridge (1996)
			Extracellular and intracellular	20 nm(1 h), 4–10 µm (4 weeks) – extracellular	2.6	21–23		2.5×10^{-3}		Bacteria late stationary phase	
			Extracellular and intracellular		2.6	60		2.5×10^{-3}		Bacteria late stationary phase	
			Extracellular and intracellular		2.6	90		2.5×10^{-3}		Bacteria late stationary phase	
			No precipitation		2.6	4		5×10^{-3}		Abiotic	
			No precipitation		2.6	21–23		5×10^{-3}		Abiotic	
			No precipitation		2.6	60		5×10^{-3}		Abiotic	
			No precipitation		2.6	90		5×10^{-3}		Abiotic	
4	*Pyrobaculum islandicum* (DSM 4184)		Extracellular	few nm	6–6.2	100	0.5–3 h		0.025 mg/mL	H_2–CO_2 (80:20 vol/vol) or N_2-CO_2 (80:20 vol/vol) with lactate or acetate	Kashefi et al. (2001)

(*continued*)

Table 3.2 (continued)

No	Bacteria name	Shape	Extracellular/ intracellular	Size	pH	Temperature (°C)	Period	Initial gold concentrations (mol/L)	Bacterial population (cells/mL)	Experimental condition	References
				No precipitation	6–6.2	100	0.5–3 h		0.025 mg/mL	No electron donor	
				No precipitation	6–6.2	30	0.5–3 h		0.025 mg/mL	H_2–CO_2 (80:20 vol/vol) or N_2–CO_2 (80:20 vol/vol) with lactate or acetate	
	Pyrobaculum aerophilum (DSM 7523)			No precipitation	7	100	0.5–3 h		0.025 mg/mL		
	Pyrococcus furiosus (DSM 3638)		Extracellular		7	100	0.5–3 h		0.025 mg/mL	H_2–CO_2 (80:20 vol/vol)	
	Archaeoglobus fulgidus (DSM 4304)			No precipitation	7	100	0.5–3 h		0.025 mg/mL		
	Ferroglobus placidus (DSM 10642)			No precipitation	7	100	0.5–3 h		0.025 mg/mL		
	Shewanella algae strain BRY (ATCC 51181)		Extracellular (also intracellular)		7	100	0.5–3 h		0.025 mg/mL	H_2–CO_2 (80:20 vol/vol)	
				No precipitation	7	100	0.5–3 h		0.025 mg/mL	N_2–CO_2 (80:20 vol/vol) with lactate	
	Desulfuromonas vulgaris (ATCC 35115)		Extracellular		7	100	0.5–3 h		0.025 mg/mL	H_2–CO_2 (80:20 vol/vol)	
				No precipitation	7	100	0.5–3 h		0.025 mg/mL	N_2–CO_2 (80:20 vol/vol) with lactate	
	Desulfuromonas palmitatis (ATCC 51701)			No precipitation	7	100	0.5–3 h		0.025 mg/mL	N_2–CO_2 (80:20 vol/vol) with lactate or acetate	
	Geothrix fermentans (ATCC 700665)			No precipitation	7	100	0.5–3 h		0.025 mg/mL	N_2–CO_2 (80:20 vol/vol) with	

										lactate or acetate	
	Geobacter metallireducens (ATCC 53774)			No precipitation	7	100	0.5–3 h		0.025 mg/mL	H_2–CO_2 (80:20 vol/vol) or N_2–CO_2 (80:20 vol/vol) with acetate	
	Thermotoga maritima (DSM 3109)		Extracellular (also intracellular)		7	100	0.5–3 h		0.025 mg/mL	H_2–CO_2 (80:20 vol/vol)	
				No precipitation	7	30	0.5–3 h		0.025 mg/mL	H_2–CO_2 (80:20 vol/vol)	
	Geovibrio ferrireducens (ATCC 51996)		Intracellular		7	100	0.5–3 h		0.025 mg/mL	H_2–CO_2 (80:20 vol/vol)	
	Desulfitobacterium metallireducens			No precipitation	7	100	0.5–3 h		0.025 mg/mL	H_2–CO_2 (80:20 vol/vol) or N_2-CO_2 (80:20 vol/vol) with lactate	
	Geobacter sulfurreducens (ATCC 51573)			No precipitation	7	100	0.5–3 h		0.025 mg/mL	H_2–CO_2 (80:20 vol/vol) or N_2-CO_2 (80:20 vol/vol) with acetate	
5	*Pseudomonas aeruginosa* PAO1 biofilm		Extracellular and intracellular	<10 nm (intracellular); 1–2 mm within biofilm	acid	20	0.5 h	1×10^{-5} to 5×10^{-3}			Karthikeyan and Beveridge (2002)
6	*Lactobacillus* sp.	Spherical, triangular, hexagonal	Extracellular and intracellular	20–50 nm and >100 nm	4.4	25	3 days	1×10^{-3}			Nair and Pradeep (2002)
		Spherical	Extracellular and intracellular	100–300 nm	4.4	25	3 days	Au + Ag (equimolar)			
7	*Arthrobacter tumescens* IAM 1447 *Bacillus subtilis* IAM 1026				3	30	1 h	5×10^{-5}	15 mg/100 mL cell weight		Nakajima (2003)

(*continued*)

Table 3.2 (continued)

No	Bacteria name	Shape	Extracellular/ intracellular	Size	pH	Temperature (°C)	Period	Initial gold concentrations (mol/L)	Bacterial population (cells/mL)	Experimental condition	References
	Brevibacterium helovolum IAM 1637										
	Corynebacterium equi IAM 1038										
	Deinococcus proteolyticus IAM 1214										
	Escherichia coli IAM 1264										
	Pseudomonas maltophilia IAM 1554										
	Zooglea ramigera IAM 12136										
8	*Acinetobacter calcoaceticus* IAM 12087				3	25	1 h	5×10^{-5}	15 mg/100 mL dry cell weight	Batch test	Tsuruta (2004)
	Arthrobacter simplex IAM 1660				3	25		5×10^{-5}	0.66 g cell weight/g dry weight polyacrylamide	Column tests	
	Arthrobacter tumesseus IAM 1447										
	Bacillus cereus IAM 1656										
	Bacillus licheniformis IAM 11054										
	Bacillus megaterium IAM 1166										
	Bacillus subtilis IAM 1026										
	Bacillus subtilis IAM 1633										
	Bacillus subtilis IAM 11060										

Brevibacterium helovolum IAM 1637
Corynebacterium equi IAM 1038
Enterobacter aerogenes IAM 1183
Erwinia herbicola IAM 1562
Escherichia coli IAM 1264
Micrococcus luteus IAM 1056
Nocardia corallina IAM 12121
Nocardia erythropolis IAM 1399
Nocardia rugosa kccA0193
Pseudomonas aeruginosa IAM 1054
Pseudomonas aeruginosa IAM 1095
Pseudomonas fluorescens IAM 12022
Pseudomonas maltophilia IAM 1554
Pseudomonas putida IAM 1506
Serratia marcescens IAM 1022
Thiobacillus novelus IFO 12443

(*continued*)

Table 3.2 (continued)

No	Bacteria name	Shape	Extracellular/ intracellular	Size	pH	Temperature (°C)	Period	Initial gold concentrations (mol/L)	Bacterial population (cells/mL)	Experimental condition	References
9	Magnetotactic bacteria (cocci, bacilli and multicellular)	Irregular	Extracellular and intracellular	few nm		25	1 day	0.1×10^{-3}		Uncultured bacteria	Keim and Farina (2005)
							>1 day	0.4×10^{-3} (Au) + 12.8×10^{-3} (Ag)			
10	*Ralstonia metallidurans*		Extracellular and intracellular	few nm (intracellular)		30	3 days	5×10^{-2}	10^3 to 1.8×10^7	Inoculate with bacteria in a gold containing growth medim	Reith et al. (2006)
						30	2 days		4.2×10^4 to 1.5×10^8	Inoculate with bacteria in a growth medium without gold	
			Extracellular			30	5 days	5×10^{-2}		Dead cells (lysed)	
11	*Pseudomonas stutzeri* NCIMB 13420 *Bacillus subtilis* DSM 10	Spherical, irregular	Extracellular and intracellular	<10 nm and above	5–6	28	1–3 days	$1.3–10^{-3}$		(1) Sceening process	Gericke and Pinches (2006a) Gericke and Pinches (2006b)
	Pseudomonas putida DSM 291	Spherical	Intracellular	<10 nm	3	28	1–3 days	1.3×10^{-3}		(2) Determine the effect of pH	
		Spherical	Intracellular	<10 nm	5						
		Spherical, irregular	Extracellular and intracellular	<10 nm and above	7						
		spherical, irregular	Extracellular and intracellular	<10 nm and above	9						
		Spherical, irregular	Extracellular and intracellular	<10 nm and above	5	25, 35, and 50	1 day	1.3×10^{-3}	10 mg cells/mL	(3) Determine the effect of temperature	

		Spherical, irregular	Extracellular and intracellular	<10 nm and above		28	1 day	1.3×10^{-3}, 2.5×10^{-3}, and 1.3×10^{-2}		(4) Determine the effect of gold concentrations	
12	*Shewanella algae* ATCC 51181	Irregular	Intracellular	10–20 nm	7	25	1–2 h	1×10^{-4} to 1×10^{-3}	$0.3–4 \times 10^{9}$	H_2-CO_2 (80:20 vol/vol)	Konishi et al. (2006)
				No precipitation	7	25	1–2 h	1×10^{-4} to 1×10^{-3}	$0.3–4 \times 10^{9}$	N_2–CO_2 (80:20 vol/vol) with lactate	
						60	1 h	1.4×10^{-3}		Chemical reaction with citric acid (0.02 mol/L)	
13	*Escherichia coli* DH5α	Mostly spherical, with triangular and quasi-hexagonal	Extracellular	25 ± 8 nm		25	5 days	1×10^{-3}			Du et al. (2007)
14	*Escherichia coli*	Spherical, irregular	Extracellular and intracellular	<10 nm (intracellular), 20–50 nm (extracellular)	7	25	2 h	2×10^{-3}	0.5 mg dry weight/mL	Live bacteria (H_2 and lactate electron donor)	Deplanche and Macaskie (2007)
	Desulfovibrio desulfuricans ATCC 29577				7	25	2 h	2×10^{-3}	0.5 mg dry weight/mL	Live bacteria + copper	
				Negligible precipitation	7	25	2 h			Dead cells (heat-killed)	
				No precipitation	7					Abiotic	
				Red suspension	2	25	2 h	2×10^{-3}	0.5 mg dry weight/mL	Determine the effect of pH	
				Purple suspension	6						
				Dark blue suspension	9						
15	*Rhodopseudomonas capsulata*	Plate, spherical, triangular, hexagonal	Extracellular	10–50 nm (spherical); 50–400 nm (triangular and plate)	4	25	2 days	1×10^{-3}	1 g wet weight/20 mL		He et al. (2007)
					5	25	2 days				
					6	25	2 days				
		Spherical	Extracellular	10–20 nm	7	25	2 days				

(*continued*)

Table 3.2 (continued)

No	Bacteria name	Shape	Extracellular/ intracellular	Size	pH	Temperature (°C)	Period	Initial gold concentrations (mol/L)	Bacterial population (cells/mL)	Experimental condition	References
16	*Pseudomonas aeruginosa* with fluorescent pigment pyoverdin	Spherical	Extracellular	15 ± 5 nm		37	1 day	1×10^{-3}		Live bacteria	Husseiny et al. (2007)
	Pseudomonas aeruginosa with blue pigment pyocyanin			25 ± 15 nm							
	Pseudomonas aeruginosa ATCC 90271			40 ± 10 nm							
				No precipitation		37	1 day	1×10^{-3}		Abiotic	
17	*Rhodobacter capsulatus* (purple non-sulfur bacteria)	Spherical, irregular	Extracellular and intracellular			25	20 h	2×10^{-4}	1×10^{9}	Live bacteria with N_2 gas and lactate	Feng et al. (2008)
				10 nm				4×10^{-4}			
				20–48 nm				8×10^{-4}			
18	*Bacillus licheniformis*	Cubes	Extracellular	10–100 nm		25	2 days	1×10^{-3}	1 g wet weight/ 100 mL	Live bacteria	Kalishwaralal et al. (2009)
19	*Bacillus megatherium* D01	Spherical, irregular, hexagonal, triangular, anisotrophic	Extracellular	<2.5 nm (10–30 min); 1–8 nm (1 h); 1–30 nm (>6 h)	3.2	26	9 h	0.5×10^{-6}	100 mg dry weight/ 100 mL	Live bacteria	Wen et al. (2009)
		Spherical	Extracellular	1–3 nm	3.2	26	9 h	0.5×10^{-6}	100 mg dry weight/ 100 mL	Live bacteria and dodecanethiol as the capping ligand	
		Spherical	Extracellular	1.5–2.5 nm; average 1.9 ± 0.8 nm	3.2	26	4 h	0.5×10^{-6}	1 g dry weight/L	Dried biomass and dodecanethiol as the capping ligand	
20	*Stenotrophomonas maltophilia*	Spherical, irregular	Intracellular	40 nm		25	8 h	1×10^{-3}			Nangia et al. (2009)

Table 3.3 A summary of cyanobacterial interactions with a gold(III)–chloride complex

No	Bacteria name	Shape	Extracellular/ intracellular	Size	pH	Temperature (°C)	Period	Initial gold concentrations (mol/L)	Bacterial population (cells/mL)	Experimental condition	References
1	*Nostoc punctiforme*					25	0.5 h	3×10^{-5}	0.1–0.12 mg/mL dry cell weight	Live cyanobacteria	Karamushka et al. (1991a, b)
	Microcystis aeruginosa										
	Spirulina platensis										
	Phormidium inundatum										
	Anabaena cylindrica										
	Anacystis nidulans										
	Synechococcus elongatus										
	Synechococus parvulus										
	Phormidium boryanum										
2	*Plectonema terebrans*		Extracellular and intracellular			25	14 days	1×10^{-2}		Live cyanobacteria	Dyer et al. (1994)
			Extracellular and intracellular			25	14 days	1×10^{-2}		Dead cells (autoclaved)	
3	*Plectonema boryanum* UTEX 485	Irregular, spherical, octahedral	Extracellular and intracellular	<10 nm (intracellular); 1 µm (extracellular)	1.6–2.2	25	28 days	$(2–2.8) \times 10^{-3}$	8 mg/10 mL dry weight	Cyanobacteria stationary growth phase	Lengke et al. (2006a)
			Extracellular and intracellular	<10 nm (intracellular);	1.6–2.2	60	28 days	$(2–2.8) \times 10^{-3}$			

(*continued*)

Table 3.3 (continued)

No	Bacteria name	Shape	Extracellular/ intracellular	Size	pH	Temperature (°C)	Period	Initial gold concentrations (mol/L)	Bacterial population (cells/mL)	Experimental condition	References
		Irregular, spherical, octahedral		1 μm (extracellular)					8 mg/10 mL dry weight	Cyanobacteria stationary growth phase	
		Irregular, spherical, octahedral	Extracellular and intracellular	<10 nm (intracellular); 1–10 μm (extracellular)	1.6–2.2	100	28 days	$(2–2.8) \times 10^{-3}$	8 mg/10 mL dry weight	Cyanobacteria stationary growth phase	
		Irregular, spherical, octahedral	Extracellular and intracellular	<10 nm (intracellular); 1–10 μm (extracellular)	1.6–2.2	200	1 day	$(2–2.8) \times 10^{-3}$	8 mg/10 mL dry weight	Cyanobacteria stationary growth phase	
				No precipitation		25	28 days	$(2–2.8) \times 10^{-3}$		Abiotic	
				No precipitation		60	28 days	$(2–2.8) \times 10^{-3}$		Abiotic	
		Irregular		25 nm		100	28 days	$(2–2.8) \times 10^{-3}$		Abiotic	
		Irregular		25 nm		200	1 day	$(2–2.8) \times 10^{-3}$		Abiotic	
4	*Plectonema boryanum* UTEX 485	Irregular, spherical, octahedral	Extracellular and intracellular	<10 nm (intracellular); 1.5 μm (extracellular)	1.6–2.2	25	28 days	2×10^{-3}	8 mg/10 mL dry weight	Cyanobacteria stationary growth phase	Lengke et al. (2006b)
		Irregular, spherical, octahedral		<10 nm (intracellular); 1.5 μm (extracellular)	1.6–1.9	60	28 days	2×10^{-3}	8 mg/10 mL dry weight	Cyanobacteria stationary growth phase	
		Irregular, spherical, octahedral		<10 nm (intracellular); 1–10 μm (extracellular)	1.6–1.9	100	28 days	2×10^{-3}	8 mg/10 mL dry weight	Cyanobacteria stationary growth phase	
		Irregular, spherical, octahedral		<10 nm (intracellular); 1–10 μm (extracellular)	1.9–2.2	200	1 day	2×10^{-3}	8 mg/10 mL dry weight	Cyanobacteria stationary growth phase	

		Irregular, spherical, octahedral	Extracellular and intracellular		2.2	25	28 days	2×10^{-3}		Dead cells (autoclaved)	
			No precipitation		2.2	25	28 days	2×10^{-3}		Abiotic	
			No precipitation		2.2	60	28 days	2×10^{-3}		Abiotic	
		Cubic	Precipitation	25 nm	2.2–1.9	100	28 days	2×10^{-3}		Abiotic	
		Cubic	Precipitation	25 nm	2.2–1.6	200	1 day	2×10^{-3}		Abiotic	
5	*Plectonema boryanum* UTEX 485	Irregular, spherical, octahedral	Extracellular and intracellular	<20 nm to 6 µm	1.9–2.2	25	1 day	$(0.8–7.6) \times 10^{-3}$	20 mg/mL dry weight	Cyanobacteria stationary growth phase	Lengke et al. (2006c)
6	*Plectonema boryanum* UTEX 485	Irregular, octahedral	Extracellular and intracellular	<10 nm to 6 µm	1.9	25	2 days	7.6×10^{-3}	20 mg/mL dry weight	Cyanobacteria stationary growth phase	Lengke et al. (2007)
		Irregular, octahedral	Extracellular and intracellular	<10 nm to 6 µm	1.9	60	2 days	7.6×10^{-3}	20 mg/mL dry weight	Cyanobacteria stationary growth phase	
		Irregular, octahedral	Extracellular and intracellular	<10 nm to 6 µm	1.9	80	1 day	7.6×10^{-3}	20 mg/mL dry weight	Cyanobacteria stationary growth phase	
				No precipitation	1.9	25	2 days	7.6×10^{-3}		Abiotic	
				No precipitation	1.9	60	2 days	7.6×10^{-3}		Abiotic	
				No precipitation	1.9	80	1 day	7.6×10^{-3}		Abiotic	

Table 3.4 A summary of algae interactions with a gold(III)–chloride complex

No	Algae	Shape	Extracellular/ intracellular	Size	pH	Temperature (°C)	Period	Initial gold concentrations (mol/L)	Algae concentration	Experimental condition	References
1	*Chlorella vulgaris* biomass				2–7	25	2 h	1×10^{-4} (equimolar of Au^{3+}, Hg^{2+}, Pb^{2+}, Al^{3+}, Zn^{2+}, and Cu^{2+})		Batch experiment with dead cells (lyophilized)	Darnall et al. (1986)
					2–6	25		1×10^{-4} (equimolar of Au^{3+}, Hg^{2+}, Pb^{2+}, Al^{3+}, Zn^{2+}, and Cu^{2+})		Column experiment with dead cells (lyophilized) and polyacrylamide matrix	
2	*Chlorella vulgaris* biomass	Tetrahedral crystals, decahedral, icosahedral structures	Extracellular and intracellular	few nm		25	0.25 h	$(0.1–0.8) \times 10^{-3}$	2 mg/mL	Dead cells (lyophilized)	Hosea et al. (1986)
3	*Chlorella vulgaris* biomass				2–3	25	1 h	1×10^{-4}	5 mg/mL	Dead cells	Greene et al. (1986)
					1–8	25	1 h	1×10^{-4}	5 mg/mL	Dead cells	
4	*Chlorella vulgaris* biomass				3	25	0.5 h			Dead cells (lyophilized)	Watkins et al. (1987)
5	*Sargassum natans* biomass *Sargassum fluitans* biomass *Macrocystis pyrifera* biomass	Spherical, irregular	Extracellular		1–6.3	4–60	0.5–4 h	$0.05–5 \times 10^{-3}$		Dead cells	Kuyucak and Volesky (1989a, b)

	Undaria sp. biomass						
	Laminaria sp. biomass						
	Ascophyllum nodosum biomass						
	Cosium taylori biomass						
	Halimeda opuntia biomass						
	Chondrus crispus biomass						
	Palmaria palmata biomass						
	Porphyra tenera biomass						
6	*Cyanidium caldarium* biomass	5	25	2 days	4.06 $\times 10^{-6}$ and 6.6×10^{-4}	Dead cells	Gardea-Torresdey et al. (1990)
	Eisenia bicyclis biomass						
	Laminaria japonica biomass						
	Spirulina platensis biomass						
	Chlorella pyrenoidosa biomass						

(*continued*)

Table 3.4 (continued)

No	Algae	Shape	Extracellular/ intracellular	Size	pH	Temperature (°C)	Period	Initial gold concentrations (mol/L)	Algae concentration	Experimental condition	References
7	*Chlorella vulgaris* YA-1-1				4–10	25	up to 1 h	3×10^{-5}	0.02–0.08 mg/mL dry weight	Live algae	Karamushka et al. (1991a)
8	*Chlorella vulgaris* LARG-1 *Chlorella vulgaris* LARG-3 *Chlorella vulgaris* N 875 *Chlorella vulgaris* YA-1-1 *Scenedesmus obliquus* *Porphyridium sordidum* *Porphyridium cruentum* *Porphyridium purpureum*				4–10	25	up to 1 h	3×10^{-5}	0.02–0.08 mg/mL dry weight	Live algae	Karamushka et al. (1991b)
9	*Chlorella vulgaris*							0.05 or 0.1×10^{-3}		Live algae, and different treatment applied	Ting et al. (1995)
10	Dealginated seaweed waste	Hexagonal, tetrahedral, rod, irregular, docahedral	Extracellular	20 nm to 5 µm	2–10	25	1 day	5×10^{-6} to 3.8×10^{-3}	3 g/L dry weight	Dead cells	Romero-Gonzãlez et al. (2003)

11	*Saccharomyces cerevisiae* biomass		Extracellular		3	20–60	1 h	5×10^{-4}	2.5 mg/mL dry weight	Dead cells	Lin et al. (2005)
12	*Sargassum wightii* biomass	Spherical	Extracellular	8–12 nm			15 h	1×10^{-3}	0.1 g/L dry weight	Dead cells	Singaravelu et al. (2007)
13	*Fucus vesiculosus* biomass	Irregular, spherical	Extracellular		2–11	23	up to 24 h	5×10^{-4}	1 g/L dry weight	Dead cells	Mata et al. (2009)

The interaction of *Pseudomonas aeruginosa* PAO1 biofilm and a gold(III)–chloride complex resulted in the formation of both extracellular and intracellular gold (Karthikeyan and Beveridge 2002). Most gold particles were precipitated at the cell surfaces with lesser amounts inside the cells and little throughout the exopolymeric substances (EPS). Nair and Pradeep (2002) used *Lactobacillus* sp. to assist the precipitation of gold, silver, and gold–silver alloy. Gold particles were precipitated both within and outside the cells in the range of 20–50 nm and >100 nm forming spherical, triangular, and hexagonal shapes. In the system containing both silver and gold, gold–silver alloy precipitated inside the bacterial cells, forming 100–300 nm crystals within 3 days. Nakajima (2003) and Tsuruta (2004) conducted gold biosorption to determine maximum gold accumulation using 8 and 25 bacterial species, respectively. However, the size and shape of gold accumulation were not described in their studies. *Escherichia coli* and *Pseudomonas maltophilia* have extremely high ability to accumulate gold from a gold(III)–chloride solution at pH 3 and 30°C (Nakajima 2003). Tsuruta (2004) found that some gram-negative bacterial species (e.g., *Acinetobacter calcoaceticus*, *Erwinia herbicola*, *Pseudomonas aeruginosa*, and *Pseudomonas maltophilia*) have high ability to sorb gold at pH 3 and 25°C. Uncultured magnetotactic cocci bacteria, collected from Itaipu lagoon, Rio de Janeiro, Brazil were able to precipitate gold in the capsule and granules (Keim and Farina 2005). 16S ribosomal DNA clones from bacterial biofilms of the secondary gold grains from two sites in Australia (Tomakin Park Gold Mine, New South Wales and the Hit and Miss Gold Mine, Queensland) displayed 99% similarity to *Ralstonia metallidurans* (Reith et al. 2006). The laboratory experiments using the same bacteria confirmed that elemental gold was precipitated during the interaction with a gold(III)–chloride solution with both viable and dead cells. Gericke and Pinches (2006a, b) conducted laboratory experiments using three bacterial species (*Pseudomonas stutzeri* NCIMB 13420, *Bacillus subtilis* DSM 10, and *Pseudomonas putida* DSM 291) to determine the effect of pH (3–9), temperature (25–50°C), and gold concentrations (1.3–13 mol/L) on the size and shape of gold particles. In all cases, gold was precipitated uniformly inside the cells as spherical shapes (<10 nm) at all pH values, but larger particles with irregular, undefined shapes formed at pH 7 and 9. The size and rate of gold precipitation increased with increasing temperature and gold concentrations. Konishi et al. (2006) investigated the reduction and precipitation of gold using *Shewanella algae* ATCC 51181. The results showed that elemental gold was only formed in the presence of bacteria with H_2 electron donor, forming 10–20 nm irregular shape. The biosynthesis of gold nanoparticles was investigated using *Escherichia coli* DH5α by Du et al. (2007). The gold nanoparticles formed on the bacterial surfaces, mostly as spherical with triangular and quasi-hexagonal shapes. Deplanche and Macaskie (2007) achieved gold precipitation intracellularly (<10 nm) and extracellularly (20–50 nm) using both *Escherichia coli* and *Desulfovibrio desulfuricans* with H_2 as the electron donor. Gold particles were not precipitated in the abiotic conditions or the presence of heat-killed cells, and the presence of copper in solution inhibited gold precipitation. At pH 2, red suspension was observed, indicating the formation of smaller gold particles, and at pH 9, dark blue suspension was formed, presumably containing larger gold particles. *Rhodopseudomonas capsulata* was able to precipitate gold from a gold(III)–chloride solution at pH 4–7, forming spherical, plate, triangular, and hexagonal gold with size ranging from 10 to 400 nm (He et al. 2007). Biosynthesis of gold nanoparticles using *Pseudomonas aeruginosa* was achieved and formed extracellular spherical gold with size ranging from 15 to 40 nm (Husseiny et al. 2007). Feng et al. (2008) discovered that *Rhodobacter capsulatus* were able to precipitate gold nanoparticles within and outside the bacterial cells, forming spherical and irregular gold with average size ranging from 10 to 48 nm. *Bacillus licheniformis* precipitated gold nanocubes (10–100 nm) within 2 days at 25°C (Kalishwaralal et al. 2009). Monodispersed gold nanoparticles capped with dodecanethiol were biosynthesized extracellularly by *Bacillus megatherium* D01 at 26°C (Wen et al. 2009). The presence of thiol capping ligand induced the formation of spherical gold nanoparticles with size <2.5 nm. Nangia et al. (2009) reported the biosynthesis of gold nanoparticles by *Stenotrophomonas maltophilia* forming ~40 nm spherical and irregular shapes at 25°C for 8 h.

In the cyanobacterial system, Karamushka et al. (1991a, b) investigated gold biosorption using nine different species, and all of them were able to accumulate gold. Dyer et al. (1994) found that live and dead cells of *Plectonema terebrans* were able to precipitate and accumulate elemental gold. The studies by Karamushka et al. (1991a, b) and Dyer et al. (1994) did not describe the size and shape of the gold formed. *Plectonema boryanum* UTEX 485, a filamentous cyanobacterium, had been reacted with a gold(III)–chloride complex (up to 2.8 mmol/L gold) at 25–100°C for up to ~1 month and at 200°C for 1 day (Lengke et al. 2006a, b, c, 2007). On the addition of a gold(III)–chloride solution to the cyanobacteria, all cyanobacteria were killed within several minutes at all temperatures investigated. A significant increase in the precipitation of gold occurred with increasing temperature from 25 to 60–200°C. Gold nanoparticles were precipitated inside the cells (<10 nm) and also formed octahedral shape in the bulk solution from 1 μm at 25°C to 10 μm at 100°C. For abiotic experiments using a gold(III)–chloride solution, total soluble gold was stable in solution at 25–80°C, but it decreased with time at 100 and 200°C, forming irregular or cubic gold (~25 nm).

In the algae system, most of the published literature focused on the biosorption and biorecovery of gold from solution (e.g., Darnall et al. 1986; Hosea et al. 1986; Watkins et al. 1987); therefore, the size and shape of gold particles were not described in their published papers. Darnall et al. (1986) conducted the biosorption and biorecovery experiments of Au, Hg, Pb, Al, Zn, and Cu on *Chlorella vulgaris* biomass at pH 2–7. Between pH 5 and 7, these metals bound strongly to the cell surfaces, but most of these algae-bound metals were desorbed back into solution by lowering the pH to 2, except for Au, Hg, and Ag. Hosea et al. (1986) also conducted the biosorption and biorecovery experiments of gold using *Chlorella vulgaris* biomass. Elemental gold was precipitated inside and outside the cells forming nanometer-scale of irregular and spherical gold. Biosorption of gold by *Chlorella vulgaris* biomass reached maximum binding at pH 3 (Greene et al. 1986). Inhibition and reversal of gold binding by strong ligands were pH dependent, with the order of effectiveness: thiourea > cyanide > mercaptoethanol > bromide. Watkins et al. (1987)

confirmed that *Chlorella vulgaris* biomass has high affinity for a gold(III)–chloride solution. Eleven species of brown, green, and red algae were tested for their ability to sorb gold from a gold(III)–chloride solution, and the maximum gold sorption was shown by *Sargassum natans* at pH 2.5 (Kuyucak and Volesky 1989a, b). The rates of gold biosorption increased at higher temperature from 4 to 60°C. The presence of other cations such as U, Fe, Zn, Ni, Ca, Ag, and Co did not affect the gold biosorption of *Sargassum natans* biomass at pH 2.5; however, anions such as sulfate, nitrate, and phosphate affected the biosorption ability. Gardea-Torresdey et al. (1990) showed that the gold binding capacity of five alga biomass increased as the algal carboxyl groups were esterified. Karamushka et al. (1991a, b) investigated gold biosorption using nine different species of algae and all of them were able to accumulate gold. The uptake of gold (III)–chloride solution was enhanced by several treatments such as acid, alkali, heat, and formaldehyde over the live/pristine cells (Ting et al. 1995). Gold precipitation by dealginated seaweed waste has been studied to elucidate the mechanisms of gold uptake from solution at pH 2–9 by Romero-Gonzãlez et al. (2003). In this study, gold was precipitated as hexagonal, tetrahedral, rod, irregular, and decahedral shapes with size ranging from ~20 nm to 5 μm. Lin et al. (2005) conducted a study of gold biosorption by *Saccharomyces cerevisiae* and determined that the gold bound on the cell wall had been reduced to elemental gold. Biosynthesis of gold nanoparticles was performed using *Sargassum wightii* biomass, collected from Mandapam Camp, Tamil Nadu, India (Singaravelu et al. 2007). The gold particles were precipitated as monodisperse spherical gold with size ranging from 8 to 12 nm. Mata et al. (2009) investigated gold biosorption and bioreduction using *Fucus vesiculosus* and reported that the maximum gold uptake occurred between pH 4 and 9, with optimum uptake at pH 7. The precipitated gold formed irregular or spherical shapes.

3.4 Mechanisms of Biosynthesis of Gold Nanoparticles

The mechanisms for the biosynthesis of gold particles by bacteria, cyanobacteria, and algae from two gold complexes have been tested using several methods including laboratory-based experiments, microscopy technique [transmission electron microcopy (TEM) or scanning electron microscopy (SEM)], Fourier transform infrared spectroscopy (FT-IR), and/or X-ray absorption spectroscopy (XAS), as discussed below.

3.4.1 Gold(I)–Thiosulfate Complex

The mechanisms of gold precipitation from a gold(I)–thiosulfate complex by *Acidithiobacillus thiooxidans*, SRB, and *Plectonema boryanum* UTEX 485 are summarized here. Gold(I)–thiosulfate was entered into the cell of *Acidithiobacillus* *thiooxidans* as part of a metabolic process (Lengke and Southam 2005). This gold complex was initially decomplexed to Au(I) and thiosulfate ($S_2O_3{}^{2-}$) ions. Thiosulfate was used as energy source and Au(I) was presumably reduced to elemental gold within the bacterial cells. During the late stationary growth phase, the gold nanoparticles that were initially precipitated inside the cells were released from the cells, resulting in the formation of gold particles at the cell surface. Finally, the gold particles in the bulk solution were grown into micrometer-scale wire and octahedral gold.

The precipitation of gold(I)–thiosulfate complex by SRB was caused by three possible mechanisms: (1) iron sulfide formation, (2) localized reducing conditions, and (3) a metabolic process (Lengke and Southam 2006, 2007). In the iron system, the formation of iron sulfide generated by SRB could have adsorbed a gold(I)–thiosulfate complex onto freshly forming surfaces, leading to the precipitation of elemental gold. The localized reducing conditions generated by SRB were associated with metabolism. Thiosulfate ion from a gold(I)–thiosulfate complex was initially reduced to hydrogen sulfide (HS^-), as the end product of metabolism. The release of hydrogen sulfide through the outer membrane pores decreased redox conditions around the cells and caused the precipitation of elemental gold. The precipitation of elemental gold by SRB through metabolic process was initiated when a gold(I)–thiosulfate entered the bacterial cells and was decomplexed to Au(I) and thiosulfate ($S_2O_3{}^{2-}$) ions. Thiosulfate was used as energy source and Au(I) was presumably reduced to elemental gold within the bacterial cells. During the late stationary growth phase or death phase, the gold nanoparticles that were initially precipitated inside the cells were released into the bulk solution and formed sub-octahedral to octahedral, sub-spherical to spherical aggregates resembling framboids, and ultimately millimeter-thick gold foil at longer experimental duration.

In the cyanobacterial system (*Plectonema boryanum* UTEX 485) with the addition of gold(I)–thiosulfate complex, gold was precipitated as thin nanoparticles associated with the surfaces of membrane vesicles at 25°C (Lengke et al. 2006a). *Plectonema boryanum* UTEX 485 exhibits the characteristics of gram-negative bacteria which can produce membrane vesicles. When the cyanobacteria interacted with relatively high concentrations of gold(I)–thiosulfate complex, the cells released membrane vesicle as a protective shield to prevent the uptake of gold (I)–thiosulfate from solutions and to keep gold(I)–thiosulfate away from sensitive cellular components. The interaction of gold(I)–thiosulfate complex with membrane vesicle caused the precipitation of elemental gold, possibly through the reaction with phosphorus, sulfur, or nitrogen ligands of outer membrane proteins, lipopolysaccharide, periplasmic proteins, phospholipids, DNA, and RNA. In the experiments at 60–200°C, gold nanoparticles were precipitated both intracellularly (<10 nm) and extracellularly (~10–25 nm), the latter with a distinct cubic shape and admixed with gold sulfide from 60 to 100°C. The stress on cyanobacteria caused by increasing temperature presumably decreased the cell sensitivity to receiving gold(I)–thiosulfate, and this gold complex was then reduced to gold sulfide and gold inside the cells. During the death of cyanobacteria, nanoparticles of gold sulfide and gold produced inside the cells were released through the cell membrane into solutions, as indicated by the precipitation of gold nanoparticles around the cells.

3.4.2 Gold(III)–Chloride Complex

In the bacterial system using a gold(III)–chloride solution, gold was precipitated intracellularly (<10 nm) and extracellularly (~1 to 10 μm) (e.g., Southam and Beveridge 1994, 1996; Karthikeyan and Beveridge 2002; Nair and Pradeep 2002; Reith et al. 2006; Gericke and Pinches 2006a, b; Deplanche and Macaskie 2007; Feng et al. 2008). The presence of intracellular gold nanoparticles suggests that gold entered the cells as a gold(III)–chloride complex and was then reduced to elemental gold. These bacteria were killed and the resulting release of organics caused further precipitation of gold (Southam and Beveridge 1996). A role of sulfur and phosphorus has been linked to the precipitation of octahedral gold at acidic pH by *Bacillus subtilis* 168 (Southam and Beveridge 1996). The precipitation of gold by magnetotactic cocci bacteria occurred in the Phosphorus–Sulfur–Iron (PSFe) granules which suggests the association of gold with these elements (Keim and Farina 2005). The reduction and precipitation of gold by dissimilatory iron(III) reducing bacteria were catalyzed by H_2 electron donor and not by lactate, indicating the involvement of hydrogenase (Kashefi et al. 2001). Deplanche and Macaskie (2007) further investigated the hydrogenase enzyme on the role of gold precipitation by *Escherichia coli* and *Desulfovibrio desulfuricans* ATCC 29577. They suggested that the periplasmic hydrogenases were involved in the gold precipitation but were not essential; however, the cytoplasmic hydrogenases and/or cytochrome c3 could be a complementary mechanism of gold reduction.

In the cyanobacterial system, the mechanisms of gold reduction by *Plectonema boryanum* UTEX 485 from gold(III)–chloride solutions have been studied at several gold concentrations (0.8–7.6 mmol/L) and at 25–80°C, using both fixed-time laboratory and real-time synchrotron radiation XAS experiments (Lengke et al. 2006c, 2007). The XAS results showed that Au(III) was reduced to Au(I) in a very fast reaction (within minutes), and Au(I) was immediately coordinated with sulfur atoms from cyanobacteria forming gold(I)–sulfide for all gold concentrations and temperatures. Within the cyanobacteria, sulfur presumably was present as cysteine or methionine groups of the outer membrane or periplasmic proteins. Sulfur from the cysteine or methionine groups was released into the bulk solutions through the outer membrane and immediately bound with the reduced gold forming gold(I)–sulfide on the cells or at the cell walls. The fast reduction of Au(III) to Au(I) and the fast release of organic sulfur from the dying and dead cyanobacteria at the higher temperatures investigated (60 and 80°C) resulted in the presence of gold (I)–sulfide as a major phase at the initial stage in the reaction. The reduction of gold (I)–sulfide to elemental gold was slower at 25°C than at 60 and 80°C. The cysteine or methionine within the outer membrane or periplasmic proteins also contained carbon and nitrogen, and this may explain indirect relationship between nitrogen and gold. The steps of mechanism of gold reduction and precipitation by cyanobacteria are deduced:

$$\text{gold(III)} - \text{chloride}(\text{AuCl}_4{}^{-}) \rightarrow \text{gold(I)} - \text{sulfide}(\text{Au}_2\text{S}) \rightarrow \text{gold(Au)} \quad (3.1)$$

In the algae system, the mechanisms of gold reduction by *Chlorella vulgaris* biomass from gold(III)–chloride solutions have been studied using XAS (Watkins et al. 1987). The XAS results showed that Au(III) was partly reduced to Au(I) and Au(I) was coordinated with sulfur atoms from free sulfhydryl residues and also to a light-atom element, probably nitrogen. Kuyucak and Volesky (1989b) showed that elemental gold was mostly precipitated on the cell wall of *Sargassum natans* biomass and suggested that the carbonyl ($C \equiv O$) groups of the cellulosic materials were the main functional group in the gold binding with N-containing groups involved in a lesser degree. Lin et al. (2005) suggested that the hydroxyl group of saccharides, the carboxylate anion of amino-acid residues, from the peptidoglycan layer on the cell wall appeared to be the sites for gold binding. However, the gold uptake by algal biomass increased after esterification, suggesting that carboxyl groups played a minor role in gold binding (Gardea-Torresdey et al. 1990). Romero-Gonzãlez et al. (2003) studied the mechanisms of gold biosorption by dealginated seaweed biomass using FT-IR and XAS. Although FT-IR showed the presence of carboxylate groups on the surface of the biomass, XAS showed that the reduction of gold species occurred on the biomass surfaces to form gold nanoparticles and was followed by retention of Au(I) at the sulfur containing sites. Therefore, the steps of mechanism of gold reduction and precipitation by algae are similar to cyanobacteria (Reaction 3.1).

3.5 Application of Gold Nanoparticles

The properties of gold nanoparticles remarkably differ from the bulk gold because of quantum size confinement imposed by nano-size regimen (Link et al. 1999; Reddy 2006). The electronic, magnetic, and catalytic properties of gold nanoparticles depend mainly on their size and shape (Link et al. 1999). For example, spherical gold nanoparticles show a strong absorption band in the visible region of electromagnetic field (~520 nm) but is absent for very small particles ($\leq$2 nm) as well as in the bulk gold. With a variety of unique properties, when gold nanoparticles are manipulated effectively, it can be applied to many different applications across the field of biology and medicine, environment, and technology (e.g., Oldenburg et al. 1998; Vieira and Volesky 2000; Salata 2004; Sperling et al. 2008; Chen et al. 2008; Cai et al. 2008).

Ancient cultures in Egypt, India, and China have used gold to treat diseases such as smallpox, skin ulcers, syphilis, and measles (Huaizhi and Yuantao 2001; Richards et al. 2002; Gielen and Tiekink 2005; Kumar 2007; Chen et al. 2008). Gold is currently used for medical devices including pacemakers and gold plated stents (Edelman et al. 2001; Svedman et al. 2005), for the management of heart disease, middle ear gold implants, and gold alloys in dental restoration (Svedman et al. 2006). Organogold compounds are widely used for the treatment of rheumatoid arthritis but at high doses, side effects such as proteinuria and skin reactions have been observed (Sun et al. 2007; Chen et al. 2008).

3.5.1 Biology and Medicine

Gold nanoparticles have been primarily used for labeling and bioimaging applications (Sperling et al. 2008; Chen et al. 2008). The gold nanoparticles are directed and enriched at the region of interest, providing contrast for observation and visualization. With the characteristic of strongly absorption and scattering visible light, the light energy excites the free electrons in the gold nanoparticles to a collective oscillation, known as surface plasmon. The excited electron gas relaxes thermally by transferring the energy to the gold lattice, and finally the light absorption leads to heating of the gold nanoparticles. The interaction of gold nanoparticles with light can be used for the visualization of particles using optical microscopy, fluorescence microscopy, photothermal, and photoacoustic imaging. In addition, the interaction of gold nanoparticles with both electron waves and X-rays can also be used for visualization, e.g., using TEM. Other noninvasive diagnostic tools such as magnetic resonance imaging (MRI) and X-ray computed tomography (X-ray CT) have also utilized gold nanoparticles as contrasting agent due to the ease of surface modification and higher X-ray absorption coefficient, respectively (Debouttiére et al. 2006; Kim et al. 2007).

Gold nanoparticles have been used for a long time for delivery of molecules into cells (Sperling et al. 2008; Chen et al. 2008). The molecules are adsorbed on the surface of gold nanoparticles and then are introduced into the cells using gene guns or particle ingestion. Inside the cells, these molecules will eventually detach themselves from the gold nanoparticles. Gene guns have been used for the introduction of plasmic DNA into plant cells and animal cells, which result in expression of the corresponding proteins inside the cells.

Gold nanoparticles can also be used as a heat source (Sperling et al. 2008; Cai et al. 2008). When gold particles absorb light, the free electrons in the gold particles are excited. Excitation at the plasmon resonance frequency causes a collective oscillation of the free electrons. During the interaction between the electrons and the crystal lattice of the gold nanoparticles, the electrons relax and the thermal energy is transferred to the lattice. The heat from the gold particles can be used for manipulating the surrounding tissues, e.g., hyperthermia, optically triggered opening of bonds, and opening of containers. Cells are sensitive to small increases in temperature and an increase of a few degrees can lead to cell death. If gold nanoparticles can be directed to the localized cancer tissue and is then heated by external stimuli, the cells in the vicinity of the gold particles can be selectively killed. Photo-induced heating of gold nanoparticles can also be used for the opening of chemical bonds (e.g., melting double stranded DNA and disassembling protein aggregates). Finally, photo-induced heating of gold nanoparticles can also be used for remotely controlled release of cargo molecules from capsules inside living cells. A newly functionalized gold nanoparticle (dendrimers) has been designed for not only targeting and killing tumors but also to fight cancer (Nam et al. 2009; Escosura-Muńiz et al. 2009). Gold nanoparticle is engineered not only to identify, target, and kill tumors but also to carry the additional drug to slow down the growth of cancer cells or kill the cancer cells. Dendrimers acts as an arm to the gold nanoparticles so that different molecules are attached to the arms. Once the cancer cells are surrounded by gold nanoparticles, lasers or infrared light heats the gold particles and the dendrimers release the various molecules to kill the tumors.

Gold nanoparticles can also be used for active sensor applications (Sperling et al. 2008). The objectives for sensor applications are to determine the presence of analyte and to provide its concentration. The plasmon resonance frequency is a reliable feature of gold nanoparticles that can be used for sensing. The binding of molecules to the particle surface can change the plasmon frequency directly. On the other hand, the plasmon resonance frequency is changed when the average distance among gold nanoparticles is reduced by forming small aggregates. The effect of plasmon coupling can be used for colorimetric detection of the analyte, known as a gold-based sensor. In the presence of target sequence, the gold nanoparticles bind to the target by hybridization of complementary strands of DNA which lead to a change in the plasmon resonance and the solution appears to be a violet/blue color. When the sample is heated, single sequence mismatches result in a different melting temperature of the aggregates and cause color change. The same concept applied for DNA assays can also be used for RNA- and peptide-based sequences and enzyme. The color changes can also be used to measure lengths, known as “rulers on the nanometer scale”. The fluorescence quenching occurs when many fluorophores are in close proximity to gold surfaces and this effect can be used for several sensor strategies. Raman scattering is enhanced if the analyte is close to a gold surface, called as surface-enhanced Raman scattering. Gold nanoparticles modified with Raman-active reporter molecules have been used for the detection of DNA (Krug et al. 1999), protein (Ni et al. 1999), and two-photon excitation (Kneipp et al. 2006). Gold nanoparticles can also be used for the transfer of electrons in redox reactions (Willner et al. 2006). The enzyme is conjugated to the surface of the gold particles and is immobilized on the surface of an electrode (Xiao et al. 2003). An electrode covered with a layer of gold nanoparticles has a much higher surface roughness and larger surface area which lead to higher currents. In addition, due to the presence of small gold particles, the contact of the gold nanoparticles with the enzyme can be more intimate, i.e., located in a close proximity to the reactive center, which can facilitate the electron transport.

3.5.2 Environment

Gold nanoparticle based technologies are currently being developed for the environmental applications to pollution control and water purification (Das et al. 2009). Bimetallic gold–palladium nanoparticles provide an active catalyst to degrade trichloroethene (TCE), one of the major pollutants in groundwater to a non-toxic form (Wong et al. 2009). Palladium catalyst has been shown to degrade TCE in water but the cost is significant to be widely adopted. Although gold is more expensive than palladium, a combination of gold–palladium nanoparticles is much more reactive to remove TCE, resulting in more cost-effective application. Gold nanoparticles incorporated in a water purification device can effectively capture and remove halocarbon-based pesticides from drinking water (Das et al. 2009) and can also enhance the oxidation of mercury generated from coal power plants (Pradeep and Anshup 2009). A mixture of gold nanoparticles as well as the traditional platinum and palladium has been developed for automotive catalysts in diesel engines to increase hydrocarbon oxidation activity by U.S. Nanostellar (http://www.nanostellar.com). The use of gold nanoparticles as a catalyst has a major role to play in green chemistry (Dahl et al. 2007; Herzing et al. 2008). Most industrial oxidation processes tend to use chlorine or organic peroxides which result in large amounts of chloride salts and chlorinated organic byproducts. Gold nanoparticles supported on carbon active molecular oxygen in air are able to convert alkenes to partial oxidation products such as epoxides at atmospheric pressure and at 60–80°C (Hughes et al. 2005). Gold nanoparticles have been developed for selective oxidation of the biomass-derived chemicals, furfural and hydroxymethylfurfural, to form methyl esters. These chemicals are used for flavor and fragrance applications, in plastics and industrial solvents (Taarning et al. 2008).

3.5.3 Technology

Gold nanoparticles have been designed to improve computer memory (Lee et al. 2007). A three-dimensional computer memory device composed of layers of gold nanoparticles has been developed to increase the memory capacity of a single chip. The device is built on a base of silicon that is coated with hafnium oxide. Then, alternating layers of 16-nm sized gold nanoparticles and insulating polymers are formed on top. Another development of computer memory using gold nanoparticles is an organic nonvolatile bistable memory, which is a mixture of plastic and gold (Lin et al. 2007). Organic nonvolatile memories have been developed using plastic and other carbon-based chemicals but the organic memory devices tend to break down in air and under the stress of many read–write cycles. Therefore, a new memory consisting of gold nanoparticles mixed into a polymer and sandwiched between two aluminum electrodes is considered essential to be implemented in flexible electronics, such as radio-frequency identification, smart cards, e-paper, and flexible displays.

3.6 Future Directions

During the past two decades, the interaction of a variety of bacteria and two gold solutions [gold(I)–thiosulfate and gold(III)–chloride] have been well investigated, although the focus of these studies is not necessarily on the biosynthesis of gold nanoparticles. Living and dead bacteria/cyanobacteria/algae have huge potential for the production of gold nanoparticles; however, the previous studies are still largely in the discovery phase. Given the anticipated wide application of gold nanoparticles for commercial applications, consideration of the material design, processes, and applications using bacteria/cyanobacteria/algae that minimize hazard and waste will be essential for the transition of nanoscience discoveries to commercial products of nanotechnology. Future work should implement systematic experiments which include development of gold nanoparticles of well-defined size and shape. Better understanding of the mechanisms of gold biosynthesis will enable us to achieve better control over size, shape, and monodispersivity which will lead to the development of high precision in the production level and the application of nanoparticles for commercial scale applications.

3.7 Conclusions

We provide a comprehensive review of research conducted on the biosynthesis of gold nanoparticles by bacteria, cyanobacteria, and algae using gold(I)–thiosulfate [$Au(S_2O_3)_2^{3-}$] and gold(III)–chloride [$AuCl_4^-$] complexes. In general, many bacteria, cyanobacteria, and algae have the ability to produce gold nanoparticles with properties similar to chemically synthesised materials. Intracellular synthesis of gold nanoparticles, as well as extracellular formation of nanoparticles in the presence of these microorganisms has been successfully demonstrated. The shape of gold particles precipitated by bacteria/cyanobacteria/algae includes spherical, oval, spongy clots, mushroom, irregular, triangular, tetragonal, hexagonal, octahedral, rod, cubic, docahedral, icosahedral, coil or wire, plate, and thin foil, with size ranging from 1 nm to several millimeters. The mechanisms of gold precipitation from a gold(I)–thiosulfate complex by *Acidithiobacillus thiooxidans* and SRB are directly or indirectly associated with metabolism. For the dissimilatory iron(III) reducing bacteria using gold(III)–chloride complex, the involvement of cytoplasmic hydrogenases and/or cytochrome c3 could be a complementary mechanism of gold reduction. For the cyanobacteria and algae using gold(III)–chloride complex, Au(III) was reduced to Au(I), and Au(I) was immediately coordinated with sulfur atoms from the cysteine or methionine groups, forming gold(I)–sulfide. The reduction of gold(I)–sulfide to elemental gold was a slower step mechanism than the formation of gold(I)–sulfide.

Previous work on the biosynthesis of gold nanoparticles is still largely in the discovery phase. Given the anticipated wide application of gold nanoparticles for commercial applications, continuing work is recommended to focus on the mechanisms of the biosynthesis of gold nanoparticles and the development of gold nanoparticles of well-defined size and shape.

References

Ahmad A, Senapati S, Khan MI, Kumar R, Sastry M (2005) Extra-/intracellular biosynthesis of gold nanoparticles by alkalotolerant fungus, *Trichothecium* sp. J Biomed Nanotechnol 1 (1):47–53

Aylmore MG, Muir DM (2001) Thiosulfate leaching of gold – a review. Miner Eng 14(2):135–174

Brust M, Walker M, Bethell D, Schiffrin DJ and Whyman R (1994) Synthesis of thiol derivatised gold nanoparticles in a two-phase liquid/liquid system. Chem Commun: 801–802

Cai W, Gao T, Hong H, Sun J (2008) Applications of gold nanoparticles in cancer nanotechnology. Nanotechnol Sci Appl 1:17–32

Canizal G, Ascencio JA, Gardea-Torresday J, Jose-Yacaman M (2001) Multiple twinned gold nanorods grown by bio-reduction techniques. J Nanopart Res 3:475–481

Chen PC, Mwakwari SC, Oyelere AK (2008) Gold nanoparticles: from nanomedicine to nanosensing. Nanotechnol Sci Appl 1:45–66

Dahl JA, Maddux BLS, Hutchison JE (2007) Toward greener nanosynthesis. Chem Rev 107:2228–2269

Daniel M-C, Astruc D (2004) Gold nanoparticles: assembly, supramolecular chemistry, quantum size-related properties, and applications toward biology, catalysis and nanotechnology. Chem Rev 104:293–346

Darnall DW, Greene B, Henzl MT, Hosea JM, McPherson RA, Sneddon J, Alexander MD (1986) Selective recovery of gold and other metal ions from an algal biomass. Environ Sci Technol 20 (2):206–208

Das SK, Das AR, Guha AK (2009) Gold nanoparticles: microbial synthesis and application in water hygiene management. Langmuir 25(14):8192–8199

Debouttiére P-J, Roux S, Vocanson F, Billotey C, Beuf O, Favre-Réguillon A, Lin Y, Pellet-Rostaing S, Lamartine R, Perriat P, Tillement O (2006) Design of gold nanoparticles for magnetic resonance imaging. Adv Funct Mater 16(18):2330–2339

Deplanche K, Macaskie LE (2007) Biorecovery of gold by *Escherichia coli* and *Desulfovibrio desulfuricans*. Biotechnol Bioeng 99(5):1055–1064

Dermont G, Bergeron M, Mercier G, Richer-Lafléche M (2008) Metal-contaminated soils: remediation practices and treatment technologies. Pract Periodical Hazard Toxic Radioactive Waste Manage 12(3):188–209

Du L, Jiang H, Liu X, Wang E (2007) Biosynthesis of gold nanoparticles assisted by *Escherichia coli* DH5α and its application on direct electrochemistry of hemoglobin. Electrochem Commun 9:1165–1170

Dyer BD, Krumbein WE, Mossman DJ (1994) Accumulation of gold in the sheath of *Plectonema terebrans* (filamentous marine cyanobacteria). Geomicrobiol J 12:91–98

Edelman ER, Seifert P, Groothuis A, Morss A, Bornstein D, Rogers C (2001) Gold-coated NIR stents in porcine coronary arteries. Circulation 103:429–34

Ehrlich HL (2002) Geomicrobiology, 4th edn. New York, Marcel Dekker, p 800

Emery JF, Leddicotte GW (1961) The radiochemistry of gold. National Academy of Sciences - National Research Council, Washington DC, p 34

Escosura-Muńiz ADL, Sánchez-Espinel C, Díaz-Freitas B, González-Fernández A, Costa MM, Merkoci A (2009) Rapid identification and quantification of tumor cells using an electrocatalytic method based on gold nanoparticles. Anal Chem 81:10268–10274

Feng Y, Lin X, Wang Y, Wang Y, Hua J (2008) Diversity of aurum bioreduction by *Rhodobacter capsulatus*. Mater Lett 62:4299–4302

Gardea-Torresdey JL, Becker-Hapak MK, Hosea JM, Darnall DW (1990) Effect of chemical modification of algal carboxyl groups on metal ion binding. Environ Sci Technol 24(9):1372–1378

Gardea-Torresdey JL, Tiemann KJ, Gamez G, Dokken K, Tehuacanero S, Jose-Yacaman M (1999) Gold nanoparticles obtained by bio-precipitation from gold(III) solutions. J Nanoparticles Res 1:397–404

Gardea-Torresdey JL, Tiemann KJ, Gamez G, Dokken K, Cano-Aguilera I, Furenlid LR, Renner MW (2000) Reduction and accumulation of gold(III) by *Medicago sativa* alfalfa biomass: X-ray absorption spectroscopy, pH, and temperature dependence. Environ Sci Technol 34:4392–4396

Gardea-Torresdey JL, Parsons JG, Gomez E, Peralta-Videa J, Troini HE, Santiago P, Jose-Yacaman M (2002) Formation and growth of Au nanoparticles inside live alfalfa plants. Nano Lett 2(4):397–401

Gericke M, Pinches A (2006a) Microbial production of gold nanoparticles. Gold Bull 39(1):22–28

Gericke M, Pinches A (2006b) Biological synthesis of metal nanoparticles. Hydrometallurgy 83:132–140

Gielen M, Tiekink ERT (2005) Metallotherapeutic drugs and metal-based diagnostic agents. The use of metals in medicine. Wiley, Hoboken, New York

Greene B, Hosea M, McPherson R, Henzl M, Alexander MD, Darnall DW (1986) Interaction of gold(I) and gold(III) complexes with algal biomass. Environ Sci Technol 20(6):627–632

Handley DA (1989) Methods for synthesis of colloidal gold, Chap. 2. In: Hayat MA (ed) Colloidal gold: principles, methods and application, vol 1. Academic, San Diego, pp 13–33

He S, Guo Z, Zhang Y, Zhang S, Wang J, Gu N (2007) Biosynthesis of gold nanoparticles using the bacteria *Rhodopseudomonas capsulata*. Mater Lett 61:3984–3987

Heath GR (1981) Ferromanganese nodules of the deep sea. Economic Geology 75th Anniversary Volume, 735–765.

Herzing AA, Kiely CJ, Carley AF, Landon P, Hutchings GJ (2008) Identification of active gold nanoclusters on iron oxide supports for CO oxidation. Science 321:1331–1335

Hosea M, Greene B, McPherson R, Henzl M, Alexander MD, Darnall DW (1986) Accumulation of elemental gold on the alga *Chlorella vulgaris*. Inorg Chim Acta 123:161–165

Huaizhi Z, Yuantao N (2001) China’s ancient gold drugs. Gold Bull 34:24–9

Hughes MD, Xu YJ, Jenkins P, McMorn P, Landon P, Enache DI, Carley AF, Attard GA, Hutchings GJ, King F, Stitt EH, Johnston P, Griffin K, Kiely CJ (2005) Tunable gold catalysts for selective hydrocarbon oxidation under mild conditions. Nature 437:1132–1135

Husseiny MI, El-Aziz MA, Badr Y, Mahmond MA (2007) Biosynthesis of gold nanoparticles using *Pseudomonas aeruginosa*. Spectrochim Acta A 67:1003–1006

Kalishwaralal K, Deepak V, Pandian SRK, Gurunathan S (2009) Biological synthesis of gold nanocubes from *Bacillus licheniformis*. Biosource Technol 100:5356–5358

Karamushka VI, Ul’berg ZR, Gruzina TG, Sukhovii NV, Tsarenko PM (1991a) Characteristics of the concentration of trivalent gold by microalgal cells in an energized state. Biotekhnologiya 2:65–68

Karamushka VI, Ulberg ZR, Gruzina TG, Dukhin AS (1991b) ATP-dependent gold accumulation by living chlorella cells. Acta Biotechnol 11(3):197–203

Karthikeyan S, Beveridge TJ (2002) *Pseudomonas aeruginosa* biofilms react with and precipitate toxic soluble gold. Environ Microbiol 4(11):667–675

Kashefi K, Tor JM, Nevin KP, Lovley DR (2001) Reductive precipitation of gold by dissimilatory Fe(III)-reducing bacteria and archaea. Appl Environ Microbiol 67(7):3275–3279

Keim CN, Farina M (2005) Gold and silver trapping by uncultured magnetotactic cocci. Geomicrobiol J 22:55–63

Kim D, Park S, Lee JH, Jeong YY, Jon S (2007) Antibiofouling polymer-coated gold nanoparticles as a contrast agent for in vivo X-ray computed tomography imaging. J Am Chem Soc 129 (24):7661–7665

Kneipp J, Kneipp H, Kneipp K (2006) Two-photon vibrational spectroscopy for biosciences based on surface-enhanced hyper-Raman scattering. Proc Natl Acad Sci USA 103(46):17149–17153

Konishi Y, Tsukiyama T, Ohno K, Saitoh N, Nomura T, Nagamine S (2006) Intracellular recovery of gold by microbial reduction of $AuCl_4^-$ ions using the anaerobic bacterium *Shewanella algae*. Hydrometallurgy 81:24–29

Korobushkina YeD, Korobuskhin IM (1986) Interaction of gold with bacteria and the generation of new gold. Dokl Akad Nauk SSSR 287(4):978–980

Krug JT, Wang GD, Emory SR, Nie S (1999) Efficient Raman enhancement and intermittent light emission observed in single gold nanocrystals. J Am Chem Soc 121(39):9208–9214

Kumar CSSR (2007) Nanomaterials for cancer diagnosis. Wiley, Weinheim, Germany

Kuyucak N, Volesky B (1989a) Accumulation of gold by algal biosorbent. Biorecovery 1:189–204

Kuyucak N, Volesky B (1989b) The mechanism of gold biosorption. Biorecovery 1:219–235

Lee JS, Cho J, Lee C, Kim I, Park J, Kim YM, Shin H, Lee J, Caruso F (2007) Layer-by-layer assembled charge-trap memory devices with adjustable electronic properties. Nat Nanotechnol 2:790–795

Lengke MF, Southam G (2005) The effect of thiosulfate-oxidizing bacteria on the stability of the gold-thiosulfate complex. Geochim Cosmochim Acta 69(15):3759–3772

Lengke MF, Southam G (2006) Bioaccumulation of gold by sulfate-reducing bacteria cultured in the presence of gold(I)-thiosulfate complex. Geochim Cosmochim Acta 70:3646–3661

Lengke MF, Southam G (2007) The deposition of elemental gold from gold(I)-thiosulfate complex mediated by sulfate-reducing bacterial conditions. Econ Geol 102(1):109–126

Lengke MF, Fleet ME, Southam G (2006a) Morphology of gold nanoparticles synthesized by filamentous cyanobacteria from gold(I)-thiosulfate and gold(III)-chloride complexes. Langmuir 22(6):2780–2787

Lengke MF, Fleet ME, Southam G (2006b) Bioaccumulation of gold by filamentous cyanobacteria between 25 and 200°C. Geomicrobiol J 23:591–597

Lengke MF, Ravel B, Fleet ME, Wanger G, Gordon RA, Southam G (2006c) Mechanisms of gold bioaccumulation by filamentous cyanobacteria from gold(III)-chloride complex. Environ Sci Technol 40(20):6304–6309

Lengke MF, Ravel B, Fleet ME, Wanger G, Gordon RA, Southam G (2007) Precipitation of gold by the reaction of aqueous gold(III) chloride with cyanobacteria at 25–80°C – studied by x-ray absorption spectroscopy. Can J Chem 85(10):651–659

Lin Z, Wu J, Xue R, Yang Y (2005) Spectroscopic characterization of Au^{3+} biosorption by waste biomass of *Saccharomyces cerevisiae*. Spectrochim Acta A 61:761–765

Lin HT, Pei Z, Chen JR, Hwang GW, Fan JF, Chan YJ (2007) A new nonvolatile bistable polymer-nanoparticle memory device. IEEE Electron Device Lett 28(11):951–953

Link S, Mohamed MB, El-Sayed MA (1999) Simulation of the optical absorption spectra of gold nanorods as a function of their aspect ratio and the effect of the medium dielectric constant. J Phys Chem B 103:3073–3077

Lloyd JR (2002) Bioremediation of metals; the application of micro-organisms that make and break minerals. Microbiol Today 29:67–69

Masala O, Seshadri R (2004) Synthesis routes for large volumes of nanoparticles. Annu Rev Mater Res 34:41–81

Mata YN, Torres E, Blāzquez ML, Ballester A, Gonzālez F, Muńoz JA (2009) Gold(III) biosorption and bioreduction with the brown alga *Fucus vesiculosus*. J Hazard Mater 166:612–618

Mohanpuria P, Rana NK, Yadav SK (2008) Biosynthesis of nanoparticles: technological concepts and future applications. J Nanopart Res 10:507–517

Mukherjee P, Ahmad D, Mandal D, Senapati S, Saikar SR, Khan MI, Ramani R, Parischa R, Ajaykumar PV, Alam M, Sastry M, Kumar R (2001) Bioreduction of $AuCl_4^-$ ions by the fungus, *Verticillium* sp. surface trapping gold nanoparticles formed. Angew Chem Int Ed 40 (19):3585–3588

Mukherjee P, Senapati S, Mandal D, Ahmad A, Khan MI, Kumar R, Sastry M (2002) Extracellular synthesis of gold nanoparticles by the fungus *Fusarium oxysporum*. Chembiochem 5:461–463

Nair B, Pradeep T (2002) Coalescence of nanoclusters and formation of submicron crystallites assisted by *Lactobacillus* strains. Cryst Growth Des 2(4):293–298

Nakajima A (2003) Accumulation of gold by microorganisms. World J Microbiol Biotechnol 19:369–374

Nam J, Won N, Jin H, Chung H, Kim S (2009) pH-induced aggregation of gold nanoparticles for photothermal cancer therapy. J Am Chem Soc 131:13639–13645

Nangia Y, Wangoo N, Sharma S, Wu J, Dravid V, Shekhawat GS, Suri CR (2009) Facile biosynthesis of phosphate capped gold nanoparticles by a bacterial isolate *Stenotrophomonas maltophilia*. Appl Phys Lett 94(23):1–3

Nash JT, Granger HC, and Adams SS (1981) Geology and concepts of genesis of important types of uranium deposits. Economic Geology 75th Anniversary Volume, 63–116.

Ni J, Lipert RJ, Dawson GB, Porter MD (1999) Immunoassay readout method using extrinsic Raman labels adsorbed on immonogold colloids. Anal Chem 71:4903–4908

Nicol MJ, Fleming CA, Paul RL (1987) The chemistry of the extraction of gold. In: Stanley GG (ed) The extractive metallurgy of gold in South Africa, vol 2. South Africa Institute of Mining and Metallurgy, Johannesburg, South Africa, pp 831–905

Oldenburg SJ, Averitt RD, Westcott SL, Halas NJ (1998) Nanoengineering of optical resonances. Chem Phys Lett 288:243–247

Pradeep T, Anshup (2009) Noble metal nanoparticles for water purification: a critical review. Thin Solid Films 517(24):6441–6478

Puddephatt RJ, Vittal JJ (1994) Gold: inorganic and coordination chemistry. In: King RB (ed) Encyclopedia of inorganic chemistry. Wiley, Chichester, UK, pp 1320–1331

Ran Y, Fu J, Rate AW, Gikes RJ (2002) Adsorption of Au(I, III) complexes on Fe, Mn oxides and humic acid. Chem Geol 185:33–49

Reddy VR (2006) Gold nanoparticles: synthesis and applications. Synlett 11:1791–1792

Reith F, Rogers SL, McPhail DC, Webb D (2006) Biomineralization of gold: biofilms on bacterioform gold. Science 313:233–236

Richards DG, McMillin DL, Mein EA, Nelson CD (2002) Gold and its relationship to neurological/glandular conditions. Int J Neurosci 112(1):31–53

Romero-Gonzãlez ME, Williams CJ, Gardiner PHE, Gurman SJ, Habesh S (2003) Spectroscopic studies of the biosorption of gold(III) by dealginated seaweed waste. Environ Sci Technol 37 (18):4163–4169

Salata OV (2004) Application of nanoparticles in biology and medicine. J Nanobiotechnol 2:3–9

Selvakannan PR, Mandal S, Phadtare R, Pasricha R, Sastry M (2003) Capping of gold nanoparticles by the amino acid lysine renders them water-dispersible. Langmuir 19:3545–3549

Senanayake G, Perera WN, Nicol MJ (2003) Thermodynamic studies of the gold(III)/(I)/(0) redoc system in ammonia-thiosulfate solutions at 25°C. In: Yong CA, Alfantazi AM, Anderson CG, Dreisinger DB, Harris B, James A (eds) Hydrometallurgy 2003 - Fifth International Conference in Honor of Professo Ian Ritchie, Vancouver, vol 1. TMS, Warrendale, Pennsylvania, pp 155–168

Shankar SS, Ahmad A, Pasricha R, Sastry MJ (2003) Bioreduction of chloroaurate ions by geranium leaves and its endophytic fungus yields gold nanoparticles of different shapes. J Mater Chem 13:1822–1826

Shankar SS, Rai A, Ankamwar B, Singh A, Ahmad A, Sastry M (2004) Biological synthesis of triangular gold nanoprisms. Nature 3:482–488

Singaravelu G, Arockiamary JS, Ganesh Kumar V, Govindaraju K (2007) A novel extracellular synthesis of mondisperse gold nanoparticles using marine alga, *Sargassum wightii* Greville. Colloids Surf, B 57:97–101

Southam G, Beveridge TJ (1994) The in vitro formation of placer gold by bacteria. Geochim Cosmochim Acta 58(20):4527–4530

Southam G, Beveridge TJ (1996) The occurrence of sulfur and phosphorus within bacterially derived crystalline and pseudocrystalline octahedral gold formed in vitro. Geochim Cosmochim Acta 60(22):4369–4376

Sperling RA, Gil PR, Zhang F, Zanella M, Parak WJ (2008) Biological application of gold nanoparticles. Chem Soc Rev 37:1896–1908

Sun RW-Y, Ma D-L, Wong EL-M, Che C-M (2007) Some uses of transition metal complexes as anti-cancer and anti-HIV agents. Dalton Trans 43:4884–4892

Svedman C, Tillman C, Gustavsson CG, Moller H, Frennby B, Bruze M (2005) Contact allergy to gold in patients with gold-plated intracoronary stents. Contact Dermat 52(4):192–196

Svedman C, Dunér K, Kehler M, Moller H, Gruvberger B, Bruze M (2006) Lichenoid reactions to gold from dental restorations and exposure to gold through intracoronary implant of a gold-plated stent. Clin Res Cardiol 95:689–91

Taarning E, Nielsen IS, Egeblad K, Madsen R, Christensen CH (2008) Chemicals from renewables: aerobic oxidation of furfural and hydroxymethylfurfural over gold catalysts. ChemSusChem 1:75–78

Ting YP, Teo WK, Soh CY (1995) Gold uptake by *Chlorella vulgaris*. J Appl Phycol 7:97–100

Tsuruta T (2004) Biosorption and recycling of gold using various microorganisms. J Gen Appl Microbiol 50:221–228

Vieira RHSF, Volesky B (2000) Biosorption: a solution to pollution. Int Microbiol 3:17–24

Watkins JW II, Elder RC, Greene B, Darnall D (1987) Determination of gold binding in an algal biomass using EXAFS and XANES spectroscopies. Inorg Chem 26(7):1147–1151

Wen L, Lin Z, Gu P, Zhou J, Yao B, Chen G, Fu J (2009) Extracellularbiosynthesis of monodispersed gold nanoparticles by a SAM capping route. J Nanopart Res 11:279–288

Willner B, Katz E, Willner I (2006) Electrical contacting of redox proteins by nanotechnological means. Curr Opin Biotechnol 17:589–596

Wong MS, Alvarez PJJ, Fang YL, Akcin N, Nutt MO, Miller JT, Heck KN (2009) Cleaner water using bimetallic nanoparticle catalysts. J Chem Technol Biotechnol 84:158–166

Xiao Y, Patolsky F, Katz E, Hainfeld JF, Willner I (2003) Plugging into enzymes: nanowiring of redox enzymes by a gold nanoparticle. Science 299(5614):1877–1881

Rev Environ Sci Biotechnol (2010) 9:199–204
DOI 10.1007/s11157-010-9188-5

PROJECT UPDATE

A green chemical approach for the synthesis of gold nanoparticles: characterization and mechanistic aspect

Sujoy K. Das · Enrico Marsili

Published online: 4 February 2010
© Springer Science+Business Media B.V. 2010

Abstract This IRCSET-EMPOWER (Irish Research Council for Science, Engineering and Technology Postdoctoral Research Grant) project aims to improve current methodology for the synthesis of metal nanoparticles (NPs). The development of efficient methodology for metal nanomaterials synthesis is an economical and environmental challenge. While the current methods for NPs synthesis are often energy-intensive and involve toxic chemicals, NPs biosynthesis can be carried on at circumneutral pH and mild temperature, resulting in low cost and environmental impact. Nanomaterial biosynthesis has been already observed in magnetotactic bacteria, diatoms, and S-layer bacteria, however, controlled NPs biosynthesis is a relatively new area of research with considerable potential for development. A thorough understanding of the biochemical mechanism involved in NPs biosynthesis is needed, before biosynthetic methods can be economically competitive. The analysis and identification of active species in the nucleation and growth of metal NPs is a daunting task, due to the complexity of the microbial system. This project work focuses on the controlled biosynthesis of gold NPs by fungal microorganisms and aims to determine the biochemical mechanism involved in nucleation and growth of the particles.

Keywords Nanobiotechnology · Gold nanoparticles · Microbial synthesis · Living nanofactory · Green chemical approach

1 Introduction

The synthesis of metal nanoparticles (NPs) is a growing area of research in materials science because they exhibit unique properties (Gratzel 2001; Xia et al. 2003), different from those of bulk metals due to their unique size and shape dependent characteristics. Because of stability, oxidation resistance, and biocompatibility, gold NPs find wide applications in electronics and photonics, catalysis, information storage, chemical sensing and imaging, drug delivery and biological labeling (Elghanian et al. 1997; Cao et al. 2002). For each application, NPs of different size and shape are needed (Jin et al. 2001; Sun and Xia 2002), thereby synthetic protocols for the production of size and shape controlled monodisperse NPs are required. Since Faraday's pioneering work in 1857 on the synthesis of colloidal gold by reducing $NaAuCl_4$ with a solution of phosphorus in carbon disulphide (Fig. 1) (The Royal Institution of Great Britain 2008; Thomson 2007), several physical and chemical methods have been developed to produce gold NPs. Synthetic techniques based on the reduction of metal ions with sodium citrate or sodium borohydride, followed by surface modification of the

---

S. K. Das · E. Marsili (✉)
School of Biotechnology, Dublin City University,
Collins Avenue, Dublin 9, Ireland
e-mail: enrico.marsili@dcu.ie

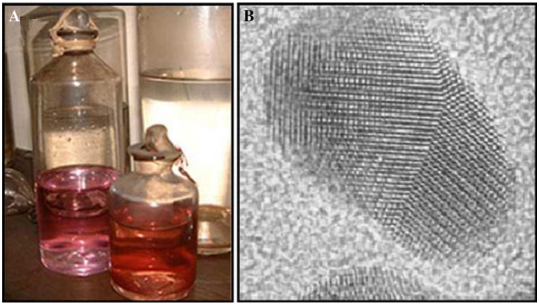

Fig. 1 Faraday's colloidal suspension of gold (**a**) (The Royal Institution of Great Britain 2008); High resolution transmission electron microscopic image (**b**) of individual colloidal gold particles (at a magnification of 10^7 ×), prepared according to Faraday's recipe (Edwards, Thomas 2007)

produced particles with suitable capping ligands and organic solvents (Niemeyer et al. 1998; Lévy et al. 2004), raised environmental concerns, because of the toxic compounds used in the process. Also, it is difficult to obtain NPs of defined size and shapes (e.g., spheres, rod, cubes, hexagons, etc.) in high yield. Current synthetic methods result in mixed-shape NPs that require expensive and low-yield purification procedures, such as differential centrifugation (Murphy 2002). These limitations invite new eco-friendly ("green chemistry") methodology for production of nanocrystals with desired shape.

Natural processes such as biomineralization may be mimicked to design efficient NP synthesis techniques. Biomineralization processes exploit biomolecular templates that interact with the inorganic material throughout its formation resulting in the synthesis of particles with defined shape and size (Mann 1993). Bones, teeth and shells are typical examples of structural materials produced by natural biomineralization processes. A general scheme for NP synthesis in microorganisms is illustrated in Fig. 2.

The adoption of biomineralization methods in the synthesis of nanostructured materials is expected to yield novel and more complex structural entities compared to those obtained with conventional methods (Brown et al. 2000; Klaus et al. 1999; Mukherjee et al. 2001; Xie et al. 2007a, 2007b). Both uni and multicellular microorganisms are reported to produce inorganic nanomaterials either intra- or extracellularly. Some well-known examples (Mann et al. 1990; Oliver et al. 1995; Sleytr et al. 1999) of microbial mediated synthesis of inorganic materials include magnetotactic bacteria *Magnetospirillum magnetotacticum* (which synthesize magnetite NPs), S-layer bacteria *Synechococcus* sp., *Bacillus stearothermophilus* (which produce gypsum and calcium carbonate layers), and diatoms *Coscinodiscus* sp., *Cylindrotheca fusiformis* (which synthesize siliceous materials). However, the use of microorganisms in the deliberate and controlled NP synthesis is a new area of research.

1.1 Bacteria in nanoparticle synthesis

Among the microorganisms, prokaryotes have received the most attention in the area of NP biosynthesis. Beveridge and Murray (1980) have demonstrated that gold NPs readily precipitate in bacterial cells following incubation of the cells with Au^{+3} ions under ambient temperature and pressure. Organic phosphate compounds play a role in the in vitro development of octahedral Au, possibly as bacteria–Au complexing agents. Fe^{+3} reducing bacteria *Shewanella algae* can reduce Au^{+3} ions in anaerobic environments. In the presence of *S. algae* and hydrogen gas, the Au ions are completely reduced and 10–20 nm gold NPs are formed (Konishi et al. 2004). Klaus–Joerger and co-workers (Klaus et al. 1999) have demonstrated that *Pseudomonas stutzeri* AG259 isolated from a silver mine reduces Ag^{+} ions and forms silver NPs of well-defined size and morphology, ranging from a few to 200 nm or more, within the periplasmic space.

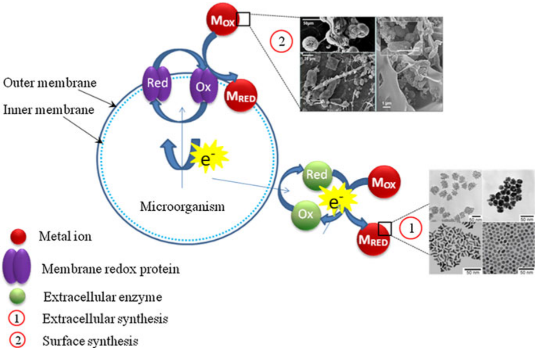

Fig. 2 Schematic of biomineralization process for nanoparticle synthesis

1.2 Fungi in nanoparticle synthesis

The use of fungi in the synthesis of NPs is a relatively recent addition and holds promise for large scale NP production. In fact, fungi secrete large amounts of the enzymes involved in NP synthesis and are simpler to grow both in the laboratory and at industrial scale. Different fungal and actinomycete species, i.e., *Fusarium oxysporum*, *Verticillium* sp., *Thermomonospora* sp., *Rhodococcus* sp. have been reported (Ahmad et al. 2003; Mandal et al. 2006) to synthesize NPs intra- or extracellularly. Shankar et al. (2004) synthesized gold nanoplates by fungal extracts.

A brief over view on microbial synthesis of metal NPs is given in Table 1.

1.3 Mechanism of nanoparticle synthesis

While a large number of microbial species are capable of producing metal NPs, the mechanism of nanoparticle biosynthesis has not been established. The metabolic complexity of viable microorganisms complicates the analysis and identification of active species in the nucleation and growth of metal NPs. Recent works by Xie et al. (2007a) demonstrated that proteins are the principal biomolecules involved in the algal

Table 1 Synthesis of nanoparticles by different microorganisms

Microorganisms	Metal nanoparticle	References
Bacteria		
Bacillus subtilis	Gold	Beveridge and Murray (1980)
Shewanella algae	Gold	Konishi et al. (2004)
Pseudomonas stutzeri	Silver	Klaus et al. (1999)
Lactobacillus	Gold, silver, Au–Ag alloy	Nair and Pradeep (2002)
Escherichia coli	Gold	Brown et al. (2000)
Rhodococcus	Gold	He et al. (2007)
Fungi		
Verticillium	Gold, silver	Mukherjee et al. (2001)
Fusarium oxysporum	Gold, silver, Au–Ag alloy	Ahmad et al. (2003); Mandal et al. (2006); and there in
Colletotrichum sp.	Gold	Shankar et al. (2003)

synthesis of gold NPs. Other researchers (Ahmad et al. 2003; He et al. 2007) have postulated that microorganisms secrete enzymes, which may be responsible for the reduction of metal ions, which result in the NPs nucleation and growth. Ahmad et al. (2003) postulated that a NADH-dependent reductase is involved in Ag NPs synthesis by *Fusarium oxysporum*. However, the biochemical mechanism of metal ion reduction and subsequent NP formation remains unexplored.

The elucidation of the biochemical pathways leading to gold biomineralization is necessary to develop a rational approach to NP biosynthesis. A number of issues need to be addressed from the nanotechnology and microbiological points of view before such biosynthetic procedures can compete with the conventional protocols.

Preliminary experiments (Fig. 3) carried out in our laboratory demonstrated the synthesis of single crystal gold NPs from $HAuCl_4$ when incubated with mycelia or cell-free extract of *Rhizopus oryzae* (Das et al. 2008, 2009).

'Green chemistry' aims to employ environmentally benign solvents and nontoxic chemicals in synthetic methods, thereby reducing their environmental impact (Anastas and Warner 1998). This IRCSET-EMPOWER project will adopt such 'green chemistry' approach to synthesize gold NPs using microorganisms as a 'living nano-factory' by avoiding any chemical agents, to determine the biochemical mechanisms involved in the biomineralization process, and to isolate and purify the enzymes involved in the NP formation.

2 Methodological approaches

The present project work aims to (1) synthesize gold NPs through room temperature reduction of gold ions by *R. oryzae*; and (2) determine of the biochemical mechanism involved in the nucleation and growth of gold NPs. *R. oryzae* will be grown in the laboratory as previously described (Das et al. 2009) and the cell-free

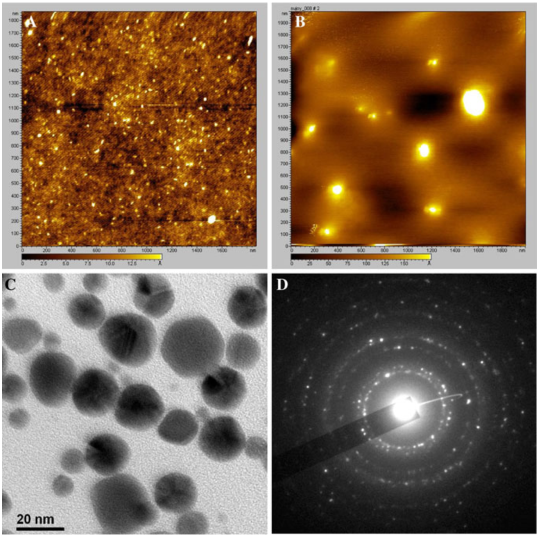

Fig. 3 Atomic force microscopic images (**a**–**b**) of gold nanoparticles synthesized on the surface of the fungal mycelia (**a** low resolution; **b** high resolution); high resolution transmission electron microscopic image (**c**) shows that the average particles size is 20 nm; selected area electron diffraction (SAED) pattern (**d**) indicates that the synthesized gold nanoparticles are single crystal

extract will be prepared from *R. oryzae* mycelia following harvesting from the growth medium. The cell-free extract will then be used for the synthesis of gold NPs.

The NP will be characterized through Transmission Electron Microscopy (TEM), Atomic Force Microscopy (AFM), X-ray photoelectron spectroscopy (XPS), UV–visible and Fourier Transform Infrared spectroscopy (FTIR). The crystal structure of the NPs will be determined with the selected area electron diffraction (SAED) pattern obtained from TEM image.

The biochemical pathway involved in the NP biosynthesis will be assessed using heat inactivated or metabolically inhibited microorganisms (e.g., through sodium cyanide, formaldehyde, and 2,4-dinitrophenol) as control experiment. The enzyme(s) responsible for reduction of Au^{+3} to Au^0 will be obtained from the cell-free extract through several purification steps: ammonium sulphate fractionation, anion-exchange chromatography, chromatofocusing, and gel filtration. The purified enzyme(s) will then be used for the synthesis of gold NPs as described above. Kinetic measurements of enzyme activity for gold NP synthesis will then be undertaken at the optimal pH and temperature, as determine in separate experiments. The shape controlled synthesis of gold NPs by purified enzyme(s) will be also performed using varying reaction conditions, such as the concentration of gold ions, the pH of the solution, and the incubation period. All these conditions control the crystal growth kinetics and final NP morphology. Since the enzyme(s) secreted by *R. oryzae* act both as reducing and capping agent, the adsorption of such enzyme(s) on the growing crystals and their reducing activity changes with the above mentioned conditions, thereby resulting in different crystal shapes.

3 Impact of the proposed research

Metal NPs are relevant to numerous emerging technologies. The development of high yield and low cost methods for NP production is therefore an important challenge. Current methods for metal NP production require harsh chemicals and energy-intensive processes. It is consequently important to develop an eco-friendly sustainable ("green chemistry") alternative to the existing chemical methods. The microbial-mediated synthesis of metal NPs may replace some of the current physical and chemical methods in use for NP production. However, several issues need to be addressed before such biosynthetic procedures can compete with established protocols. Comprehension of biochemical mechanism involved in gold nanoparticle formation is crucial to the development of innovative and low-energy NPs production processes. This IRCSET-EMPOWER project deals with pioneer research on the synthesis of gold nanostructures employing microorganism simultaneously as the reducing and capping agent. This environmental-friendly methodology may be applied in various pharmaceutical and biomedical formulations, as well as in cellular imaging, biosensing, and drug delivery.

Acknowledgment Funding source: IRCSET-EMPOWER 2009 Postdoctoral Research Grant.

References

Ahmad A, Mukherjee P, Senapati S, Mandal D, Khan MI, Kumar R, Sastry M (2003) Extracellular biosynthesis of silver nanoparticles using the fungus *Fusarium oxysporum*. Colloids Surf B Biointerfaces 28:313–318

Anastas PT, Warner JC (1998) Green chemistry: theory and practice. Oxford University Press, New York, p 30

Beveridge TJ, Murray RGE (1980) Site of metal deposition in the cell wall of *Bacillus subtilis*. J Bacteriol 141:876–887

Brown S, Sarikaya M, Johnson EA (2000) Genetic analysis of crystal growth. J Mol Biol 299:725–735

Cao YC, Jin R, Mirkin CA (2002) Nanoparticles with Raman spectroscopic fingerprints for DNA and RNA detection. Science 297:1536–1540

Das SK, Das AR, Guha AK (2008) Synthesis of gold nanoparticles: a green chemical approach. International conference on soft system ICSS-2008, Kolkata, India, 3–15 February 2008

Das SK, Das AR, Guha AK (2009) Gold nanoparticles: microbial synthesis and application in water hygiene management. Langmuir 25:8192–8199

Edwards PP, Thomas JM (2007) Gold in a metallic divided state—from faraday to present-day nanoscience. Angew Chem Int Ed 46:5480–5486

Elghanian R, Storhoff JJ, Mucic RC, Letsinger RL, Mirkin CA (1997) Selective colorimetric detection of polynucleotides based on the distance-dependent optical properties of gold nanoparticles. Science 277:1078–1081

Gratzel M (2001) Photoelectrochemical cells. Nature 414:338–344

He S, Guo Z, Zhang Y, Zhang S, Wang J, Gu N (2007) Biosynthesis of gold nanoparticles using the bacteria *Rhodopseudomonas capsulate*. Mater Lett 61:3984–3987

Jin R, Cao Y, Mirkin CA, Kelly KL, Schatz GC, Zheng JG (2001) Photoinduced conversion of silver nanospheres to nanoprisms. Science 294:1901–1903

Klaus T, Joerger R, Olsson E, Granqvist C-G (1999) Silver-based crystalline nanoparticles, microbially fabricated. Proc Natl Acad Sci USA 96:13611–13614

Konishi Y, Nomura T, Tsukiyama T, Saitoh N (2004) Microbial preparation of gold nanoparticles by anaerobic bacterium. Trans Mater Res Soc Jpn 29:2341–2343

Lévy R, Thanh NTK, Doty RC, Hussain I, Nichols RJ, Schiffrin DJ, Brust M, Ferning DG (2004) Rational and combinatorial design of peptide capping ligands for gold nanoparticles. J Am Chem Soc 126:10076–10084

Mandal D, Bolander ME, Mukhopadhyay D, Sarkar G, Mukherjee P (2006) The use of microorganisms for the formation of metal nanoparticles and their application. Appl Microbiol Biotechnol 69:485–492

Mann S (1993) Molecular tectonics in biomineralization and biomimetic materials chemistry. Nature 365:499–505

Mann S, Sparks NHC, Frankel RB, Bazylinski DA, Jannasch HW (1990) Biomineralization of ferrimagnetic greigite (Fe_3O_4) and iron pyrite (FeS_2) in a magnetotactic bacterium. Nature 343:258–260

Mukherjee P, Ahmad A, Mandal D, Senapati S, Sainkar SR, Khan MI, Parischa R, Ajayakumar PV, Alam M, Kumar R, Sastry M (2001) Fungus mediated synthesis of silver nanoparticles and their immobilization in the mycelial matrix: a novel biological approach to nanoparticle synthesis. Nano Lett 1:515–519

Murphy CJ (2002) Nanocubes and nanoboxes. Science 298:2139–2141

Nair B, Pradeep T (2002) Coalescence of nanoclusters and formation of submicron crystallites assisted by *Lactobacillus* strains. Cryst Growth Des 2:293–298

Niemeyer CM, Burger W, Peplies I (1998) Covalent DNA-streptavidin conjugates as building blocks for novel biometallic nanostructures. Angew Chem Int Ed 37:2265–2268

Oliver S, Kupermann A, Coombs N, Lough A, Ozin GA (1995) Lamellar aluminophosphates with surface patterns that mimic diatom and radiolarian microskeletons. Nature 378:47–50

Shankar SS, Ahmad A, Parischa R, Sastry M (2003) Bioreduction of chloroaurate ions by geranium leaves and its endophytic fungus yields gold nanoparticles of different shapes. J Mater Chem 13:1822–1826

Shankar SS, Rai A, Ankamwar B, Singh A, Ahmad A, Sastry M (2004) Biological synthesis of triangular gold nanoprisms. Nature Mat 3:482–488

Sleytr UB, Messner P, Pum D, Sara M (1999) Crystalline bacterial cell surface layers (S layers): from supramolecular cell structure to biomimetics and nanotechnology. Angew Chem Int Ed 38:1035–1054

Sun Y, Xia Y (2002) Shape-controlled synthesis of gold and silver nanoparticles. Science 298:2176–2179

The Royal Institution of Great Britain, cited 18 Dec 2008. Available from: http://www.rigb.org/rimain/heritage/faradaypage.jsp

Thomson D (2007) Michael Faraday's recognition of ruby gold: the birth of modern nanotechnology. Gold Bulletin 40:267–269

Xia Y et al (2003) One-dimensional nanostructures: synthesis, characterization, and applications. Adv Mater 15:353–389

Xie J, Lee JY, Wang DIC, Ting YP (2007a) Silver nanoplates: from biological to biomimetic synthesis. ACS Nano 1:429–439

Xie J, Lee JY, Wang DIC, Ting YP (2007b) High-yield synthesis of complex gold nanostructures in a fungal system. J Phys Chem C 111:16858–16865

Bioprocess Biosyst Eng (2012) 35:637–643
DOI 10.1007/s00449-011-0646-4

ORIGINAL PAPER

Mycogenesis of gold nanoparticles using a phytopathogen *Alternaria alternata*

**Joy Sarkar · Sandipan Ray · Dipankar Chattopadhyay ·
Aparna Laskar · Krishnendu Acharya**

Received: 29 July 2011 / Accepted: 7 October 2011 / Published online: 19 October 2011
© Springer-Verlag 2011

Abstract The development of an eco-friendly and reliable process for the synthesis of gold nanomaterials (AuNPs) using microorganisms is gaining importance in the field of nanotechnology. In the present study, AuNPs have been synthesized by bio-reduction of chloroauric acid ($HAuCl_4$) using the fungal culture filtrate (FCF) of *Alternaria alternata*. The synthesis of the AuNPs was monitored by UV–visible spectroscopy. The particles thereby obtained were characterized by UV, dynamic light scattering (DLS), X-ray diffraction (XRD), energy dispersive X-ray (EDX) analysis, Fourier transform infrared (FTIR) spectroscopy, atomic force microscopy (AFM) and transmission electron microscopy (TEM). Energy-dispersive X-ray study revealed the presence of gold in the nanoparticles. Fourier transform infrared spectroscopy confirmed the presence of a protein shell outside the nanoparticles which in turn also support their stabilization. Treatment of the fungal culture filtrate with aqueous Au^+ ions produced AuNPs with an average particle size of 12 ± 5 nm. This proposed mechanistic principal might serve as a set of design rule for the synthesis of nanostructures with desired architecture and can be amenable for the large scale commercial production and technical applications.

Keywords *Alternaria alternata* · Fungal culture filtrate · Gold nano

Abbreviations

FCF	Fungal culture filtrate
DLS	Dynamic light scattering
XRD	X-ray diffraction
EDX	Energy dispersive X-ray
FTIR	Fourier transform infrared
AFM	Atomic force microscopy
TEM	Transmission electron microscopy
$HAuCl_4$	Chloroauric acid
AuNPs	Gold nanoparticles

Introduction

Nanotechnology, the powerful tool for the creation of new objects in nanoscale dimensions, is a cutting edge technology having important applications in modern biomedical research [1–4]. As the dimension of nanoscale devices is similar to cellular components such as DNA and proteins [5, 6], the tools developed through nanotechnology may utilize AuNPs to detect several diseases at the molecular level [7]. But in the past few years, researchers have began to realize the possible toxicities of AuNPs which are to some extent traced back to the chemical ingredient used in conventional method [8]. Conventional synthetic methods of AuNPs have involved a number of chemical methods [9, 10]. With the rapid development of these chemical

---

J. Sarkar · S. Ray · K. Acharya (✉)
Molecular and Applied Mycology and Plant Pathology Laboratory, Department of Botany,
University of Calcutta, Kolkata 700019, India
e-mail: krish_paper@yahoo.com

D. Chattopadhyay
Department of Polymer Science and Technology,
University College of Science and Technology,
University of Calcutta, Kolkata 700009, India

A. Laskar
Transmission Electron Microscopy Section (Infectious Disease and Immunology), Indian Institute of Chemical Biology,
Kolkata 700032, India

methods, concern for environmental contaminations is regularly heightened as the chemical procedures involved in the synthesis of nanomaterials generates a large amount of hazardous by-products. Thus, there is an urgent need for 'green chemistry' that includes clean, nontoxic and environment-friendly methods of nanoparticle synthesis with precise control over the shape and size. In the recent years, 'green synthesis' of the nanoparticles has paid much more attention in the rapidly growing area of nanoscience and nanotechnology [11–15].

Biological systems have been widely utilized to synthesize and assemble a range of inorganic nanomaterials from bacteria [16], algae [17] and fungi [18]. Many microbes are known to produce highly structured metallic nanoparticles with very similar properties to that of chemically synthesized materials, while having precise control over size, shape and monodispersity [19]. Filamentous fungi in general possess some distinctive advantage over bacteria and algae, because of their high metal tolerance and bioaccumulation ability [20]. Additional benefits of using fungi in nanoparticle synthesis are ease in their scale-up, downstream processing, handling of biomass and economic viability. Besides these, fungi are extremely efficient secretor of extracellular enzymes; it is thus possible to easily obtain large-scale production of enzymes. Literature survey showed a number of fungi to produce nanoparticles either intracellularly or extracellularly [18, 21–23]. Gold nanoparticles are of interest, mainly due to their stability under atmospheric conditions, resistance to oxidation and biocompatibility [24–27]. These unique properties can potentially be exploited in a diverse range of industrial applications using their optical and electronic properties in optics, electronics, medical diagnostic and treatments, senders and coating [24, 26, 28]. Earlier attempts have been made for extracellular biosynthesis of AuNPs using different filamentous fungi like *Verticillium* sp. [29], *Fusarium oxysporum* [30], *Aspergillus flavus* [31], *Colletotrichum* sp. [32], *Aspergillus clavatus* [19], *Trichothecium* sp. [33].

In this context, we present the single step 'green synthesis' protocol for the production of AuNPs utilizing culture filtrate of a phytopathogenic fungus *Alternaria alternata* (strain number: MAMP/C/51).

Materials and methods

Isolation of the pathogen and culture maintenance

The pathogen, *A. alternata* (strain number: MAMP/C/51) isolated previously by Maiti et al. [34] was grown aerobically in 50 ml of fully autoclaved potato-dextrose broth (HiMedia Laboratories Pvt. Ltd., Mumbai, India) in Erlenmeyer flasks having the capacity of 250 ml and kept for 12 days at 30 °C temperature. After the incubation period, the media was filtered with Whatman filter paper No. 1. 100 ml of that fungal culture filtrate (FCF) was taken in a sterilized Erlenmeyer flask which was further used for the reduction of the chloroauric acid aqueous solution.

Synthesis of gold nanoparticles

The chemical chloroauric acid ($HAuCl_4$) was purchased from Sigma, St. Louis, MO, USA. 100 ml of FCF was taken in each different Erlenmeyer flask and mixed with chloroauric acid solution (3 mM final concentration). The FCF containing flask was agitated for 24 h at room temperature. Simultaneously, only the culture filtrate of *A. alternata* and only chloroauric acid solution were maintained under same conditions.

The gold nanoparticles were separated out by centrifugation at 12,000*g* for 10 min, and the settled nanoparticles were washed with deionized water (three times). The purified AuNPs were resuspended in deionized water and ultrasonicated by Piezo-u-sonic ultrasonic cleaner (Pus-60w). Synthesis of AuNPs was repeated for three times ($n = 3$) and subsequently utilized for characterization of the particles.

UV–visible spectroscopy

The absorption at 540 nm (maximum absorbance observed in the full range scan) was measured continuously to determine the stability of the solution. The UV–visible spectra of the solution were kinetically monitored in the range of 200–900 nm recorded in a Hitachi 330 spectrophotometer. Deionized water was used as blank.

Size measurement by dynamic light scattering (DLS) experiment

Particle size was measured by laser diffractometry using a nano size particle analyzer (Zen 1600 Malvern USA) in the range between 0.6 nm and 6.0 μm, under the following conditions: particle refractive index 1.590, particle absorption coefficient 0.01, water refractive index 1.33 and temperature 25 °C.

X-ray diffraction (XRD) analysis

After bio-reduction, the liquid reaction mixture was dried at 45 °C in a vacuum drying oven. The vacuum-dried mixture was then collected and used for powder XRD analysis. The spectra were recorded in a PW. 3040/60 PANalytical X-ray diffractometer (Cu Kα radiation,

λ 1.54443) running at 45 kV and 30 mA. The diffracted intensities were recorded from 30° to 90° 2θ angles.

Energy dispersive X-ray (EDX) analysis

Energy-dispersive X-ray (EDX) analysis was carried out by the Hitachi S 3400 N instrument (Japan) and employed to know the elemental compositions of the particles. Samples were filtered and dried before measurements.

Fourier transform infrared spectroscopic (FTIR) analysis

For FTIR analysis, the vacuum-dried culture filtrate and AuNPs and culture filtrate were mixed separately with potassium bromide (KBr) at a ratio of 1:100 and the spectra were recorded with a Shimadzu 8400S fourier transform infrared spectrophotometer using a diffuse reflectance accessory. The scanning data were obtained from the average of 50 scans in the range between 4,000 and 400 cm^{-1}.

Atomic force microscopic (AFM) observation of gold nanoparticles

The size and surface topography of the drop coated film of the AuNPs was investigated with atomic force microscope [Nanoscope (R) 111a Veeco multimode, USA] and high resolution surface images were produced. In AFM characterization, the tapping mode with RTESP tip was used. The resonance frequency was 287.64 and the scanning range was 1.25 μm.

Transmission electron microscopic (TEM) observation of gold nanoparticles

TEM samples of the aqueous suspension of AuNPs were prepared by placing a drop of the suspension on carbon-coated copper grids and allowing the water to evaporate. The micrographs were obtained by Tecnai G^2 spirit Biotwin (FP 5018/40) TEM, operated at 80 kV accelerating voltage.

Results and discussion

Production and characterization of gold nanoparticles

The culture filtrate mediated synthesis of AuNPs was validated by visually monitoring the three flasks containing only the culture filtrate of *A. alternata*, reaction mixture of the culture filtrate with chloroauric acid and only chloroauric acid solution. Only the reaction mixture displayed a time dependent color change, whereas the fungal culture filtrate and the chloroauric acid solution were observed to retain their original color (Fig. 1 inset). At the beginning, the reaction mixture was light yellow and became pinkish after 1 h of incubation at room temperature; the pinkish color changed to dark red gradually at 24 h and then the red color did not change with increasing incubation time. The appearance of the red color indicated the occurrence of the reaction and the formation of Au nanoparticles.

UV–visible spectroscopic analysis

The characteristic red color of the reaction solution was due to the excitation of the surface plasmon vibration of Au^0 particles and provided a convenient spectroscopic signature of their formation. Both the control set showed no significant color change in the same experimental conditions. The reduction of chloroauric acid was subjected to spectral analysis by using the UV–visible spectrophotometer. This showed an absorbance peak at 540 nm (Fig. 1), which was specific for gold nanoparticles [19].

Particle size measurement

Particle size was determined by dynamic light scattering measurement. Laser diffraction revealed that particle size obtained in the range of 2–30 nm (Fig. 2).

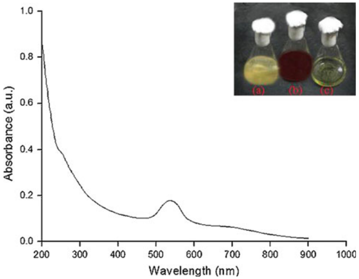

Fig. 1 UV–visible spectra recorded as a function of reaction time of an aqueous solution of 3 mM $\mathrm{HAuCl_4}$ with the fungal culture filtrate (FCF). Inset: Represents three flasks containing only the culture filtrate of *Alternaria alternata* (**a**), reaction mixture of the culture filtrate with chloroauric acid (**b**) and only chloroauric acid solution (**c**). The appearance of red color only in the flask (**b**) due to the addition of *Alternaria alternata* FCF to 3×10^{-3} M aqueous $\mathrm{HAuCl_4}$ solution after 24 h incubation period

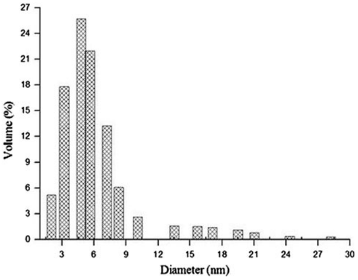

Fig. 2 Histogram of particle size distribution as obtained from light scattering of the gold nanoparticles produced by *Alternaria alternata*

XRD analysis

In order to confirm the mono-crystalline nature of the AuNPs, XRD analysis was performed. Figure 3 shows the X-ray diffraction pattern obtained from the AuNPs. The Bragg reflections obtained from the AuNPs clearly correspond to the fcc crystalline structure of gold. The XRD pattern exhibited four identical diffraction peaks corresponding to the [111], [200], [220] and [311] appearing at $2\theta = 38.2°$, 44.5°, 65.6° and 78.6° of metal gold, respectively (International Center for Diffraction Data, ICDD No. 04–0783), indicating that the precipitate was composed of pure crystalline gold [19]. As per the XRD pattern, a very intense Bragg reflection for the [111] lattice was observed, suggesting that the [111] oriented AuNPs were lying flat [19] on the planar surface, while the reflections correspond to [220] and [311] with lattice spacing of 1.44 and 1.23 Å was specific for the triangular morphology, respectively. It was also notable that the ratio of intensity between the [200] and [111] diffraction peaks for the prepared sample was much lower than the standard (0.042 vs. 0.33), and this rationally decreased as the particles size increased. These observations confirmed that as-formed AuNPs were primarily dominated by [111] facets [19], which were quite consistent with the above electron diffraction observation.

EDX observation of gold nanoparticles

An elemental composition analysis employing EDX showed the presence of a strong signal from gold atoms (Fig. 4). Moreover, the presence of sharp optical absorption peak in the range of 2–3 keV which is typical for the absorption of metallic gold nanocrystallites [35]. This analysis indicated that the nanostructures were composed solely of gold. However, there were other EDX peaks for C, O, K and N, suggesting that they were mixed precipitates from the culture filtrate.

FTIR analysis of gold nanoparticles

FTIR absorption spectra of vacuum dried fungal culture filtrate and reduced chloroauric acid by culture filtrate are shown in Fig. 5a, b, respectively. Both the spectra showed the presence of bonds due to O–H stretching (around $\sim$3,430 cm^{-1}) and aldehydic C–H stretching (around $\sim$2,920 cm^{-1}) [36]. These peaks indicated the presence of proteins and other organic residues, which might have produced extracellularly during the growth of *A. alternata*.

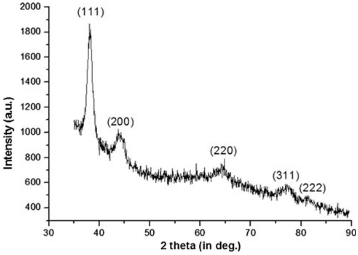

Fig. 3 Representative XRD patterns of gold nanoparticles synthesized by the reaction of 3 mM aqueous $HAuCl_4$ solution with *Alternaria alternata* culture filtrate

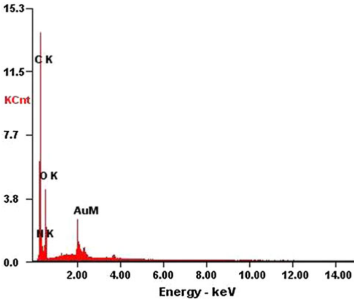

Fig. 4 EDX spectrum recorded showing sharp peak in between 2 and 3 keV confirming the presence of gold

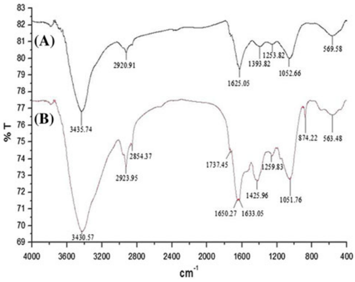

Fig. 5 FTIR absorption spectra of FCF after (**a**) and before (**b**) bioreduction of chloroauric acid

FTIR spectrum of fungal culture filtrate showed absorption band at 1,625 cm^{-1}, corresponding to the amide I of polypeptides [36]. Following reaction with HAuCl$_4$ solution, the amide I band appeared at 1,633 and 1,650 cm^{-1} [36]. The intense band found in Fig. 5b at 1,425 and 874 cm^{-1} corresponding to the C–H in plane deformation with aromatic ring stretching [37, 38]. The FTIR peak at around 1,240–1,260 cm^{-1} present in both the cases signified amide III band of the random coil of protein [39]. Band at 1,052 cm^{-1} in both the spectra indicated C–O stretching [37]. The bands visible in between 500 and 749 cm^{-1} signified the presence of R-CH group [40]. Some other significant bands appeared after bioreduction in the FTIR spectra were at 2,854 cm^{-1} and 1,737 cm^{-1} corresponding to the aromatic C–H anti-symmetric stretching vibration [41] and C=O stretching vibration [37], respectively. These findings supported the results of Goel et al. [42], who reported that proteins can bind to nanoparticles either through amino groups or cysteine residue or through electrostatic attraction. Furthermore, Ahmad et al. [43] and Xie et al. [44] reported that protein can interact with AuNPs either through free amine, carboxyl or phosphate groups to stabilize them. Thus, it can be concluded that the AuNPs are stabilized by surface bound protein molecules that also prevent aggregation. In addition to that microscopic fungi can generate extracellular AuNPs by a process involving NADH-reductase [45, 46].

Atomic force microscopy

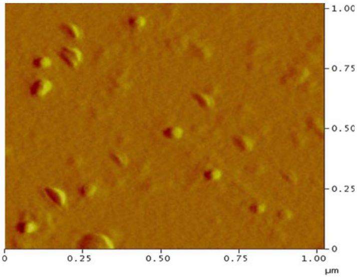

Fig. 6 Tapping Mode AFM phase image presented as two-dimensional graphics showing the clean spherical and triangular shaped gold nanoparticles

Results obtained from AFM study (Fig. 6) represent a clear concept regarding shape as shown in the picture. Majority of the particles were spherical and triangular in shape, well distributed without aggregation and monodispersity was an important characteristic of nanoparticles. The sizes of the AuNPs were found to be similar with the data collected from the DLS study (Fig. 2) and the variation in size of nanoparticles were commonly found during biological synthesis.

TEM image of gold nanoparticles

Transmission electron microscopic (TEM) image shown in Fig. 7 recorded different sizes of AuNPs which arose from the bio-reduction of chloroauric acid by culture filtrate at room temperature (37 °C) for 24 h. These observations revealed that spherical, triangular as well as hexagonal structures of the AuNPs were formed in the reaction solution. The diameters of these AuNPs were measured and

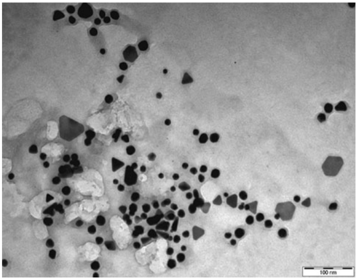

Fig. 7 Transmission electron micrograph of gold nanoparticles after bio-reduction of chloroauric acid

the size was in the range of 2–30 nm. The average diameter of these AuNPs was of 12 ± 5 nm.

Conclusion

In summary, we have demonstrated the biosynthesis of AuNPs using a phytopathogenic fungus *A. alternata*. The fungal reduction of chloroauric acid by *A. alternata* yielded AuNPs in the range of 2–30 nm. The present investigation suggests extracellular biosynthesis and stabilization of AuNPs by proteins present in the culture filtrate. The advantage of biosynthesis of nanoparticles using this protocol over other methods currently in use is that the nanoparticles are quite stable in solution. This study may therefore lead to the development of a simple bioprocess for the synthesis of AuNPs. It is expected that with further work on understanding the biochemistry of the fungal system and complete cataloging of biomolecules in the culture filtrate which participate in AuNPs formation, a green process using microorganisms as "nanofactories" may be developed to produce metal nanocrystals of increasingly complex and yet controllable structure.

Acknowledgments The authors (Krishnendu Acharya and Dipankar Chattopadhyay) would like to thank Center for Research in Nanoscience and Nanotechnology, University of Calcutta (Sanction no. Conv/043/Nano Pr. 2009) for financial support and Anirban Chakraborty for carrying out AFM images and for AFM machine facility given by Raja Bazar Science College, University of Calcutta.

References

1. Parak WJ, Gerion D, Pellegrino T, Zanchet D, Micheel C, Williams CS, Boudreau R, Le Gros MA, Larabell CA, Alivisatos PA (2003) Biological applications of colloidal nano crystals. Nanotechnol 14:15–27
2. Gao X, Yang L, Petros JA, Marshall FF, Simons JW, Nie S (2005) In vivo molecular and cellular imaging with quantum dots. Curr Opin Biotechnol 16:63–72
3. Alivisatos PA (2004) The use of nanocrystals in biological detection. Nat Biotechnol 2:47–52
4. Salata OV (2004) Applications of nanoparticles in biology and medicine. J Nanobiotechnol 2:3
5. Prescher JA, Bertozzi CR (2005) Chemistry in living systems. Nat Chem biol 1:13–21
6. Thrall JH (2004) Nanotechnology and Medicine. Radiol 230:315–318
7. El-Sayed IH, Huang X, El-Sayed MA (2005) Surface plasmon resonance scattering and absorption of anti-EGFR antibody conjugated AuNPs in cancer diagnostics: applications in oral cancer. Nano Lett 5:829–834
8. Das RK, Gogoi N, Bora U (2011) Green synthesis of gold nanoparticles using *Nyctanthes arbortristis* flower extract. Bioprocess Biosyst Eng 34:615–619
9. Sun Y, Xia Y (2002) Shape-controlled synthesis of gold and silver nanoparticles. Science 298:2176–2179
10. Selvakannan PR, Mandal S, Pasricha R, Adyanthaya SD, Sastry M (2002) One-step synthesis of hydrophobized gold nanoparticles of controllable size by the reduction of aqueous chloroaurate ions by hexadecylaniline at the liquid–liquid interface. Chem Commun 13:1334–1335
11. Korbekandi H, Iravani S, Abbasi S (2009) Production of nanoparticles using organisms. Crit Rev Biotech 29:279–306
12. Basu N, Bhattacharya R, Mukherjee P (2008) Protein-mediated autoreduction of gold salts to gold nanoparticles. Biomed Mater 3:34105
13. Kim J, Rheem Y, Yoo B, Chong Y, Bozhilov KN, Kim D, Sadowsky MJ, Hur HG, Myung NV (2010) Peptide-mediated shape- and size-tunable synthesis of gold nanostructures. Acta Biomater 7:2681–2989
14. Verma VC, Kharwar RN, Gange AC (2010) Biosynthesis of antimicrobial silver nanoparticles by the endophytic fungus *Aspergillus clavatus*. Nanomed 5:33–40
15. Huang P, Kong Y, Li Z, Gao F, Cui D (2010) Copper selenide nanosnakes: bovine serum albumin-assisted room temperature controllable synthesis and characterization. Nanoscale Res Lett 5:949–956
16. Narayanan KB, Sakthivel N (2010) Biological synthesis of metal nanoparticles by microbes. Adv Colloid Interfac 156:1–13
17. Chakraborty N, Banerjee A, Lahiri S, Panda A, Ghosh AN, Pal R (2009) Biorecovery of gold using cyanobacteria and an eukaryotic alga with special reference to nanogold formation–a novel phenomenon. J Appl Phycol 21:145–152
18. Acharya K, Sarkar J, Deo SS (2009) Mycosynthesis of nanoparticles. In: Bhowmik PK, Basu SK, Goyal A (eds) Advances in biotechnology. Bentham Science, USA, pp 204–215
19. Verma VC, Singh SK, Solanki R, Prakash S (2011) Biofabrication of anisotropic gold nanotriangles using extract of endophytic *Aspergillus clavatus* as a dual functional reductant and stabilizer. Nano Res Lett 6:16–23
20. Sastry M, Ahmad A, Khan I, Kumar R (2003) Biosynthesis of metal nanoparticles using fungi and actinomycete. Curr Sci 85:162–170
21. Saha S, Sarkar J, Chattopadhyay D, Patra S, Chakraborty A, Acharya K (2010) Production of silver nanoparticles by a phytopathogenic fungus *Bipolaris nodulosa* and its antimicrobial activity. Dig J Nanomater Biostruct 5:887–895
22. Sarkar J, Chattopadhyay D, Patra S, Deo SS, Sinha S, Ghosh M, Mukherjee A, Acharya K (2011) *Alternaria alternata* mediated synthesis of protein capped silver nanoparticles and their genotoxic activity. Dig J Nanomat Biostruct 6:563–573
23. Sarkar J, Dey P, Saha S, Acharya K (2011) Mycosynthesis of selenium nanoparticles. Micro Nano Lett 6:599–602
24. Corti CW, Holliday RJ, Thompson DT (2002) Developing new industrial applications for gold: gold nanotechnology. Gold Bull 35:111–117
25. Corti CW, Holliday RJ (2004) Commercial aspects of gold applications: from materials science to chemical science. Gold Bull 37:20–26
26. Cortie MB (2004) The weird world of nanoscale gold. Gold Bull 37:12–19
27. Huang H, Yang X (2005) One-step shape control synthesis of gold nanoparticles stabilized by 3-thiopheneacetic acid. Coll Surf A: Physicochem Eng Asp 255:11–17
28. Daniel M-C, Astruc D (2004) Gold nanoparticles: assembly, supramolecular chemistry, quantum-size related properties, and applications toward biology, catalysis, and nanotechnology. Chem Rev 104:293–346
29. Mukherjee P, Ahmad A, Mandal D, Senapati S, Sainkar SR, Khan MI, Ramani R, Parischa R, Kumar PAV, Alam M, Sastry M, Kumar R (2001) Bioreduction of $AuCl_4^-$ Ions by the fungus,

Verticillium sp. and surface trapping of the gold nanoparticles formed. Angew Chem Int Ed 40:3585–3588

30. Mukherjee P, Senapati S, Mandal D, Ahmad A, Khan MI, Kumar R, Sastry M (2002) Extracellular synthesis of gold nanoparticles by the fungus *Fusarium oxysporum*. Chem Bio Chem 3:461–463
31. Bhambure R, Bule M, Shaligram N, Kamat M, Singhal R (2009) Extracellular biosynthesis of gold nanoparticles using Aspergillus niger–its characterization and stability. Chem Eng Technol 32:1036–1041
32. Shankar SS, Ahmad A, Pasricha R, Sastry M (2003) Bioreduction of chloroaurate ions by geranium leaves and its endophytic fungus yields gold nanoparticles of different shapes. J Mater Chem 13:1822–1826
33. Ahmad A, Satyajyoti S, Khan MI, Rajiv K, Sastry M (2005) Extra-/intracellular biosynthesis of gold nanoparticles by an alkalotolerant fungus, *Trichothecium* sp. J Biomed Nanotechnol 1:47–53
34. Maiti CK, Sen S, Acharya R, Acharya K (2007) First report of *Alternaria alternata* causing leaf spot on *Stevia rebaudiana*. Plant Pathol 56:723
35. Song JY, Jang H-K, Kim BS (2009) Biological synthesis of gold nanoparticles using *Magnolia kobus* and *Diopyros kaki* leaf extracts. Proc Biochem 44:1133–1138
36. Sathyavathi R, Krishna MB, Rao SV, Saritha R, Rao DN (2010) Biosynthesis of silver nanoparticles using *Coriandrum Sativum* leaf extract and their application in nonlinear optics. Adv Sci Lett 3:01–06
37. Renuga Devi TS, Gayathri S (2010) FTIR and FT-Raman spectral analysis of paclitaxel drugs. Int J Pharm Sci Rev Res 2:106–110
38. Pandey KK (1999) A study of chemical structure of soft and hardwood and wood polymers by ftir spectroscopy. J Appl Pol Sci 71:1969–1975
39. Cai S, Singh BR (2004) A distinct utility of the amide III infrared band for secondary structure estimation of aqueous protein solutions using partial least squares methods. Biochem 43:2541–2549
40. Singh AK, Talat M, Singh DP, Srivastava ON (2010) Biosynthesis of gold and silver nanoparticles by natural precursor clove and their functionalization with amine group. J Nanopart Res 12:1667–1675
41. Sanghi R, Verma P (2009) Biomimetic synthesis and characterization of protein capped silver nanoparticles. Biores Technol 100:501–504
42. Gole A, Dash C, Ramakrishnan V, Sainkar SR, Mandle AB, Rao M (2001) Pepsin-gold colloid conjugates: preparation, characterization, and enzymatic. Langmuir 17:1674–1679
43. Ahmad A, Senapati S, Khan MI, Kumar R, Sastry M (2003) Extracellular biosynthesis of monodisperse gold nanoparticles by a novel extremophilic actinomycete, *Thermomonospora* sp. Langmuir 19:3550–3553
44. Xie J, Lee JY, Wang DIC, Ting YP (2007) High-yield synthesis of complex gold nanostructures in a fungal system. J Phys Chem C 111:16858–16865
45. Kumar SA, Abyaneh MK, Gosavi SW, Kulkarni SK, Ahmad A, Khan MI (2007) Sulfite reductase-mediated synthesis of gold nanoparticles capped with phytochelatin. Biotechnol Appl Biochem 47:191–195
46. Kumar SA, Abyaneh MK, Gosavi SW, Kulkarni SK, Pasricha R, Ahmad A, Khan MI (2007) Nitrate reductase-mediated synthesis of silver nanoparticles from $AgNO_3$. Biotechnol Lett 29:439–445

J Clust Sci (2011) 22:661–665
DOI 10.1007/s10876-011-0412-4

ORIGINAL PAPER

Biological Synthesis of Gold Nanoparticles by Fungus *Epicoccum nigrum*

Zeinab Sheikhloo · Mojtaba Salouti · Farzad Katiraee

Received: 28 May 2011 / Published online: 15 September 2011
© Springer Science+Business Media, LLC 2011

Abstract Gold nanoparticles exhibit unique optical, thermal, chemical and physical properties. The microorganisms have high potential for production of nanoparticles with wide applications. Application of fungi to produce nanoparticles is potentially exciting because of their ability to secrete large amounts of enzymes. In this study, we investigated biosynthesis of gold nanoparticles by the fungus *Epicoccum nigrum* isolated from Andalian gold mine in north-west of Iran. The gold nanoparticles were produced intra and extracellular by reaction of an aqueous solution of chloroauric acid with the biomass of fungus *E. nigrum*. The produced gold nanoparticles were in the size range of 5–50 nm in spherical and rod shapes. This is the first report on the biosynthesis of gold nanoparticles by the fungus *E. nigrum*.

Keywords Nanoparticles · Gold · Biosynthesis · Fungi · *Epicoccum nigrum*

Introduction

Gold nanoparticles have found many potential applications in many fields such as catalysis, sensors, drugs and gene delivery systems [1]. Nanoparticles can be synthesized by physical and chemical methods [2]. The problems of these methods are often experienced with low stability of the nanoparticle preparations, difficult control of the crystal growth and aggregation of the particles [3–5]. One of the most important criteria of nanotechnology is development of clean, nontoxic and

---

Z. Sheikhloo · M. Salouti (✉)
Department of Microbiology, Faculty of Sciences, Zanjan Branch, Islamic Azad University,
Moallem St., Etemadieh, 4515658145 Zanjan, Iran
e-mail: saloutim@yahoo.com

F. Katiraee
Mycology Research Center, Faculty of Veterinary Medicine, University of Tehran, Tehran, Iran

environmentally acceptable green chemistry procedures [6, 7]. Many biological organisms have known to produce inorganic materials either intra or extracellular [8, 9]. Some well-known examples include formation of iron oxides and various metal nanoparticles using bacteria, fungi or plants [10]. The use of eukaryotic organisms such as fungi in the synthesis of nanoparticles with different chemical composition and size is in progress due to their ability to secrete large amounts of enzymes. The fungi possess some advantages over bacteria. The first is that the most filamentous fungi have a high tolerance towards metals and a high wall-binding capacity, as well as intracellular metal uptake capabilities. In addition, they are easy to culture on a large scale, thus making it possible to easily obtain enough biomass for processing [11]. In an interesting study, Bhambure et al. [11] have reported that the fungus *Aspergillus niger* NCIM616, when placed in a concentrated aqueous solution of $HAuCl_4$, resulted in formation of extracellular gold nanoparticles with the size of 12.79 ± 5.61 nm. In an another recent study, Binupriya et al. [12] demonstrated that the fungus *Rhizopus stolonifer*, when placed in aqueous solution of 1 mM $HAuCl_4$, resulted in the extracellular formation of gold nanoparticles. Here, we report the biosynthesis of gold nanoparticles by a novel metal resistance fungus biomass, *Epicoccum nigrum*, isolated from Andalian gold mine in north-west of Iran. *E. nigrum* is an species of fungus that finds in soil and food. Application of fungi for synthesis of gold nanoparticles has already been reported [11, 12]. However, there is no report on the synthesis of gold nanoparticles using *E. nigrum*. The results showed that this fungus is a good candidate for the simple and clean synthesis of gold nanoparticles.

Experimental

Isolation and Growth of Fungi

Many samples of soil were collected from Andalian gold mine in north-west of Iran in sterilized falcon tubes. Five grams of each sample was diluted with 45 mL of sterile distilled water and placed onto the Sabouraud's dextrose agar (SDA) plates. The plates were then incubated at 27 °C for 5–10 days. All of the isolated fungi were tested for synthesis of gold nanoparticles. Then, the fungus that was found to be able to produce gold nanoparticles was identified based on morphological features, slide culture and growth parameters on malt extract agar or oatmeal agar [13, 14]. The emerged colonies on the petri dishes were purified by single spore isolation. The single spores were maintained on SDA slants at 27 °C. The stock cultures were maintained by subculturing at monthly intervals.

Biosynthesis of Gold Nanoparticles

The isolated fungi were grown aerobically in 250 mL Erlenmeyer flasks containing 100 mL MYPG medium (malt extract 0.3%, yeast extract 0.3%, peptone 0.5% and glucose 1% at pH 5.5–6). The culture was agitated on an orbital shaker (160 rpm) at 27–29 °C for 96 h. The biomass was separated from the culture broth by centrifugation (5,000 rpm) at 10 °C for 20 min. The biomass was washed extensively with distilled water to remove medium components. The fresh and clean biomass (5 g of wet biomass) was suspended in 100 mL of 10^{-3} M aqueous $HAuCl_4$ solution at pH 2.5 in 250 mL Erlenmeyer flasks. The whole mixture was put into a shaker at 27–29 °C for 72 h (160 rpm). The reaction was carried out in the dark.

Characterization of Gold Nanoparticles

The bioreduction of the Au ions in solution was monitored by periodic sampling of aliquots of the aqueous component. The scanning was performed in the range of 400–800 nm by a UV–visible spectrophotometer (Shimadzu, UV Pharma spec 1700 with a resolution 0.72 nm). X-Ray diffraction measurement was carried out using (Philips PW 1800) (XRD). The samples for transmission electron microscopy (Philips model EM 208S) analysis were prepared on carbon-coated copper grids.

Results and Discussion

One out of nine kinds of the isolated fungi was found to be able to synthesize gold nanoparticles. This fungus was identified *E. nigrum*, by morphological features, slide culture and growth parameters on malt extract agar. Colonies of *E. nigrum* are fast growing, suede-like to downy, with a strong yellow to orange-brown diffusible pigmentation. When sporulating numerous black sporodochia (aggregates of conidiophores) are visible. Conidia are formed singly on densely compacted, nonspecialized, determinant, slightly pigmented conidiophores. Conidia are globose pyriform, mostly 15–25 μm diameter with a funnel-shaped base and broad attachment scar, often seceding with a protuberant basal cell; i.e. aleuric or rhexolytic dehiscence of conidia. Conidia become multicellular which divide the conidia into up to 15 cells, darkly pigmented and have verrucose external surface. Pelvinate sporodochia was appearing in 8–10 days, visible as black spots and 100–2,000 μm [15].

By mixing the fungus biomass with the aqueous solution of gold ions, the color of the biomass changed from yellow to purple after 32 h. The color change is a signal for the formation of gold nanoparticles. The reduction of the aqueous chloroaurate ions during exposure to the mycelia was followed by UV–vis spectroscopy [11]. The UV–vis spectra, recorded after completion of the reaction, showed a distinct absorption band centered at 543 nm (Fig. 1) that was very specific for gold nanoparticles.

One of the important ways to characterize nanoparticles is evaluating the XRD spectrum of the sample. The XRD pattern clearly showed that the gold nanoparticles have been formed by the bioreduction of gold ions by the fungus XRD patterns of thin films exposed to $HAuCl_4$, broadening of the intense peaks due to (111), (200), (220) and (311) Bragg reflection at $2\theta = 38.26°$, 44.60°, 64.67° and 77.54°, confirmed the presence of gold nanoparticles (Fig. 2) [9].

The nanostructures synthesized in the fungus cells were further characterized by transmission electron microscopy. The TEM images showed that the gold nanoparticles were formed in spherical and rod shapes both intra and extracellular.

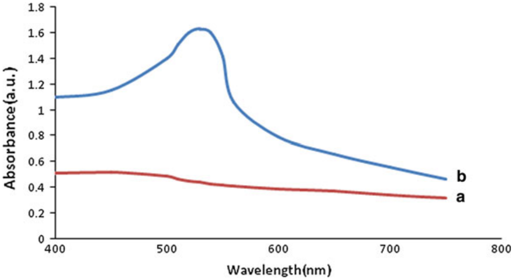

Fig. 1 UV–vis spectra recorded from the fungal cells before (**a**) and after (**b**) exposure to 1 mM aqueous $HAuCl_4$ solution

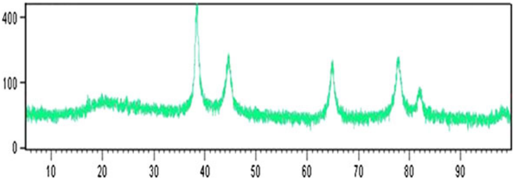

Fig. 2 XRD pattern recorded from an Au nano-*E. nigrum* biofilms

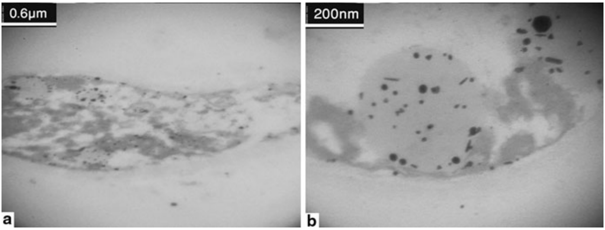

Fig. 3 TEM images at different magnifications of the thin sections of the *E. nigrum* cells after reaction with chloroaurate ions (**a**, **b**). Gold nanoparticles were synthesized both intra and extracellular

The average of nanoparticles size was from 5 to 50 nm. A number of *E. nigrum* cells can be seen in the low magnification of TEM images (Fig. 3). The gold nanoparticles were organized on the cytoplasm and the cell wells.

To our knowledge, this is the first study on the synthesis of gold nanoparticles by *E. nigrum*.

Conclusion

The results showed that the reaction of aqueous chloroaurate ions with the biomass of *E. nigrum* leads to the formation of gold nanoparticles both intra and extracellular.

References

1. S. He, Z. Guo, Z. Yu, and S. Zhang (2007). *Mater. Lett.* **61**, 3984.
2. M. Agnihotri, S. Joshi, K. A. Ravi, S. Zinjarde, and S. Kulkarni (2009). *Mater. Lett.* **63**, 1231.
3. H. Huang and X. Yang (2005). *Colloids Surf. A* **255**, 11.
4. S. Mandal, S. Phadtare, and M. Sastry (2005). *Curr. Appl. Phys.* **5**, 127.
5. D. Mandal, M. E. Bolander, D. G. Mukhopadhyay, and P. Sarkar Mukherjee (2006). *Appl. Microbiol. Biotechnol.* **69**, 485.
6. Z. Ranjbar Navazi, M. Pazouki, and F. Sadat Halek (2010). *Iran. J. Biotechnol.* **8**, 56.
7. I. Maliszewska, L. Aniszkiewicz, and Z. Sadowski (2009). *Acta Phys. Pol. A.* **116**, 163.
8. A. R. Binupriya, M. Sathishkumar, and S. I. Yun (2010). *Colloids Surf. B* **79**, 531.
9. S. S. Shankar, A. Ahmad, R. Pasricha, and M. Sastry (2003). *J. Mater. Chem.* **13**, 1822.
10. P. Mohanpuria, N. K. Rana, and S. K. Yadav (2007). *J. Nanopart. Res.* **10**, 507.
11. R. Bhambure, M. Bule, N. Shaligram, and M. Kamat (2009). *Chem. Eng. Technol.* **32**, 1036.
12. A. R. Binupriya, M. Sathishkumar, and S. I. Yun (2010). *Colloids Surf. B* **79**, 531.
13. R. A. Samson, E. S. Hoekstra, J. C. Frisvad, and O. Filtenborg, *Introduction to Food- and Airborne Fungi*, 6th ed., Chap. 1, p. 118 (Centralbureau voor Schimmelcultures, Delft, 2002).
14. D. H. Larone *Medically Important Fungi—A Guide to Identification*, 3rd ed. (ASM Press, Washington, DC, 1995).
15. D. A. Sutton, A. W. Fothergill, and M. G. Rinaldi *Guide to Clinically Significant Fungi*, 1st ed. (Williams & Wilkins, Baltimore, 1998).

Extracellular Microbial Synthesis of Gold Nanoparticles using Fungus *Hormoconis resinae*

Anuj Narayan Mishra, Seema Bhadauria, Mulayam Singh Gaur, and Renu Pasricha

In this study, the fungus Hormoconis resinae *was screened from soil near a refinery and was found to produce stable gold nanoparticles extracellularly. The kinetics of the reaction was studied using UV–Vis spectroscopy and was further characterized by x-ray diffraction, energy dispersive x-ray (EDX) analysis, and high-resolution transmission electron microscopy. These analyses revealed that the gold nanoparticles are spherical and in nano-regime. The most important feature of* Hormoconis resinae *fungi is the following fact: they have a widespread presence in soil and can produce huge biomass. Such a cheap source of material gives the opportunity for cost-effective preparation of various gold-based nanostructures.*

INTRODUCTION

There is a growing need to develop environmentally benign nanoparticle synthesis processes that do not use toxic chemicals in the synthesis protocol. Even though many biotechnological applications such as remediation of toxic metals employ micro-organisms such as bacteria[1] and yeast,[2] such microorganisms were recently found as possible eco-friendly nanofactories.[3,4] Processes devised by nature for the synthesis of inorganic materials on nano- and micro-length scales have contributed to the development of a relatively new and largely unexplored area of research based on the use of microbes in the biosynthesis of nanomaterials.[5]

Studying nanomaterials biosynthesis offers a valuable contribution to materials chemistry. Many microorganisms can synthesize inorganic nanomaterial intra- or extracellularly[6] and they have received the most attention in the area of biosynthesis of nanoparticles. Early studies have revealed that microbes are able to reduce Au^{3+} ions to produce octahedral gold particles of nanoscale dimensions (5–25 nm) within bacterial cells by incubation of the cells with gold chloride[3,4,7] under ambient temperature and pressure conditions. Microorganisms such as bacteria, yeast, and now fungi play an important role in the remediation of toxic metals through the reduction of the metal ions that have been considered interesting as nanofactories very recently.[3,4]

How would you…

…describe the overall significance of this paper?

In this present work a novel method for the biological synthesis of gold nanoparticles is reported with the fungus Hormoconis resinae *which was isolated from soil near a refinery. Such a cheap source of material provides opportunity for cost-efficient synthesis of various valuable gold-based nanostructures.*

…describe this work to a materials science and engineering professional with no experience in your technical specialty?

In this synthesis method fungus Hormoconis resinae *was used, thus toxic chemicals and pathogenic substances are avoided during nanoparticles synthesis. These nanoparticles are extracellularly synthesized thus they are easy to extract from the solution and this would also contribute to cost-effectiveness of this method.*

…describe this work to a layperson?

In this work synthesis of gold nanoparticles has been reported by simple non-pathogenic fungus and these synthesized nanoparticles are in solution. Due to their resonance in visible regions they can be easily identified and no sophisticated expertise is required for their recovery.

Using the dissimilatory properties of fungi, the biosynthesis of inorganic nanomaterials using eukaryotic organisms, such as fungi, may be used to grow nanoparticles of gold[8] in *Verticillium sp.* fungal cells intracellularly.[9] It has been shown that fungi are excellent candidates in the synthesis of gold.[8,10] The fungus *Verticillium sp.,* when exposed to metal ions, releases enzymes that reduce the metal ions to yield highly stable nanoparticles in solution.[10,11] The extracellular production of metal nanoparticles by several strains of the fungus was described and demonstrated elsewhere.[12] The ability of some microorganisms such as bacteria and fungi to control the synthesis of metallic nanoparticles can be employed in the synthesis of new materials.[13] This extracellular enzyme shows excellent redox properties and it can act as an electron shuttle in the metal reduction. It was evident that electron shuttles or other reducing agents (e.g., hydroquinones) released by microorganisms are capable of reducing ions to nanoparticles. Jose-Yacaman and co-workers have demonstrated the synthesis of gold nanoparticles within live alfalfa plants by gold uptake from solid media.[14]

It has been reported that the Au^{3+} ions are reduced in the solid media to Au^0 by the plant and then the atoms are absorbed into the plant where the nucleation and growth of gold nanoparticles takes place. This method can be very efficient in decontaminating soil polluted with heavy metal ions.[14] Barring the fungus *Fusarium oxysporum*[10,15] and the actinomycete *Thermomonospora sp.,*[16] all other microorganisms and plants investigated thus far when challenged with metal ions have resulted in their reduction and growth of nanoparticles intra-cellularly. Such biosynthetic processes for the synthesis of nanoparticles would be more useful from the application point of view if the nanoparticles can be formed extracellularly. For the reasons mentioned above, monodisperse nanoparticles of gold were previously synthesized by using *Fusarium oxysporum*[17] and silver by *Hormoconis resinae.*[18]

A number of soil fungi have been screened for the efficient and rapid extracellular synthesis of metal nanoparticles and *Hormoconis resinae* (MTCC 368) has been identified as an exciting candidate for the synthesis of gold nanoparticles extracellularly.

See the sidebar for experimental procedures.

RESULTS AND DISCUSSION

In this work, fungus *Hormoconis resinae* was used for the synthesis of gold nanoparticles. Live biomass was prepared by inoculating pure culture in liquid growth medium at 26 ± 1°C, 150 rpm. Then biomass of *Hormoconis* was centrifuged at 5,000 rpm at 10°C for 20 min. and washed with deionized water then filtered. The carefully weighted 0.1 g biomass of *Hormoconis* was added to 50 mL of 1 mM aqueous $HAuCl_4$ solution, in a conical flask of 100 mL content at room temperature. The flasks were thereafter shaken at a rotation rate of 150 rpm at 30°C.

The biomass incubated with deionized water (positive control) retained its original color (i.e., yellow-green) while the gold chloride treated biomass turned purple (as shown in Figure 1) after 24 hours due to the formation of gold nanoparticles extracellularly. As indicated in the experimental section, the bioreduction was carried out at room temperature and clearly, the formation of gold nanoparticles was due to the fungal biomass.

The main groups of the enzyme secreted by biomass that may play an important role in reducing the $AuCl_4^-$ ions include the amino, sulfhydryl, and carboxylic groups[8,10,21] and the $AuCl_4^-$ ions could bind to biomass through these functional groups. The possible role involves the electron shuttle enzymatic metal reduction process. Previous studies[10,11,22] have indicated that NADH and NADH-dependent enzymes are important factors in the biosynthesis of metal nanoparticles. This fungus is known to secrete cofactor NADH and NADH-dependent enzymes that may be responsible for the bioreduction of $Au^{(3+)}$ to $Au^{(0)}$ and the subsequent formation of gold nanoparticles. The reduction seems to be initiated by electron transfer from the NADH by NADH-dependent reductase as electron carrier. Then the gold ions obtain electrons and are reduced to Au^0.[23] The exact mechanism of the reduction of gold ions is yet to be elucidated.

Reduction of the aqueous $AuCl_4^-$ ions during exposure to the fungus *Hormoconis* may easily be followed by UV–Vis spectroscopy. It is well known that gold nanoparticles exhibit an impressive purple color in water; this color arises due to excitation of surface plasmon vibrations in the metal

EXPERIMENTAL PROCEDURES

Fungal strain was isolated from soil samples, collected near a refinery situated at Mathura. Enumeration of the microbes present in the soil was done by serial dilution-agar plating method.[19] Serial dilution of soil suspension was prepared up to 10^{-6} dilution. 1 mL of suspension from dilutions 10^{-3} to 10^{-6} was transferred to the petri dishes containing Czapek's–Dox (CD) agar medium at 23±2°C for 6–8 days and growth was observed after two days. The experiment was set up in triplicate to minimize the deviations.

The fungi isolated on culture medium from soil were purified by spore suspension and streak method. The cultures were routinely (every 6–8 days) transferred onto fresh CD agar plates by streaking. Before fungal cultures were used for inoculation of liquid growth medium, the fungus was subjected to three transfers on CD agar plates by the direct agar transfer method.[20] The culture strains were identified as *Hormoconis resinae* (MTCC 368) IMTECH, Chandigarh. The pure cultures were maintained on czapek's-dox agar medium. The cultures were sealed by wax and kept at 4±1°C temperature in refrigerator.

The fungal biomass of *Hormoconis resinae* (MTCC 368) was cultivated in liquid growth medium using the shake flask method in a shaker cum incubator. Spores and mycelium from the CD spread plate cultures were transferred to 250 mL Erlenmeyer flasks containing 100 mL growth medium. Flasks were incubated at room temperature in a shaker cum incubator at 26 ± 1°C, 150 rpm for 5 days.

The gold chloride ($HAuCl_4$) used in the study was procured from Hi-media Company. In a typical synthesis of gold nanoparticles using *Hormoconis resinae* biomass, the carefully weighted 0.1 g biomass was added to 50 mL of 1 mM aqueous $HAuCl_4$ solution, in a conical flask of 100 mL content at room temperature. The flasks were thereafter shaken at a rotation rate of 150 rpm at 30°C. These synthesized nanoparticles were extracted from the solution by simple centrifugation at 12,000 rpm for 15 min. by REMI Ultra-microcentrifuge.

The bioreduction of Au^+ in aqueous solution was monitored by periodic sampling of aliquots (0.2 mL) of the suspension and then diluting the samples with 2 mL deionized water. Afterwards the UV–Vis spectra of resulting solution have been recorded. The UV–Vis spectroscopy analysis of synthesized gold nanoparticles was carried out as a function of bioreduction time at room temperature by ELICO UV spectrophotometer (Model No. BL-198).

X-ray diffraction (XRD) measurements of the *Hormoconis resinae* reduced gold nanoparticles were carried out on drop-coated films of the respective solutions onto glass substrates by a Phillips PW 1830 instrument operating at a voltage of 40 kV with Cu $K\alpha$ radiation.

The EDX was carried out with a Zeiss EVO 40 Electron Microscope with Bruker EDX. The EDX samples of the aqueous suspension of gold nanoparticles were fabricated by drop coating method. The EDX analysis was carried out in the spot profile mode with a beam diameter of 1 µm at several places on the sample. The results presented in this study are reproducible with the accuracy of ± 5% error.

Samples for high-resolution transmission electron microscopy analysis were prepared on carbon-coated copper grids. The film on the copper grids was allowed to stand for 2 min. and this process was followed with the removal of extra solution through blotting paper. Afterwards the grid was allowed to dry prior to measurement. The analysis was carried out by Tecnai G^2 F30 S-Twin (FEI; Super Twin lens with Cs =1.2 mm) instrument operated at an accelerating voltage of 300 kV (field emission gun) having a point resolution of 0.2 nm and lattice resolution of 0.14 nm.

nanoparticles.[24]

The surface plasmon resonance (SPR) band for gold nanoparticles occurs in the range 510–560 nm respectively in an aqueous medium. It is observed in Figure 2 that the gold surface plasmon resonance band occurs initially at 537 nm after 24 h and subsequently shifts to 541 nm as a function of time of reaction. After completion of the reaction, the wavelength of the surface plasmon band stabilizes at 541 nm. The absorption band for the gold nanoparticles solution is broad and slightly asymmetrical with indications of an additional weaker component at 630 nm. The appearance of this feature indicates either formation of stable aggregates of the gold nanoparticles in solution or shape anisotropy in the particles. Additionally, it is also observed that a weak absorption band above 630 nm also appears during the later stage of reduction of gold ions to form gold nanoparticles. The long wavelength band is observed to extend well into the near infrared region of the electromagnetic spectrum. This is attributed to the significant anisotropy in the shape of the gold nanoparticles with excitation of the in-plane SPR contributing to this feature or to the aggregation of particles in solution[25–28] and is attributed to excitation of the in-plane SPR. After completion of the reaction, the gold nanoparticle solution was separated from the fungal biomass and tested for stability. It was observed that the nanoparticle solution was stable for more than six months, with a little sign of aggregation. Because the proteins were secreted by the biomass,[9,29] the particles were stabilized in solution by a capping agent.

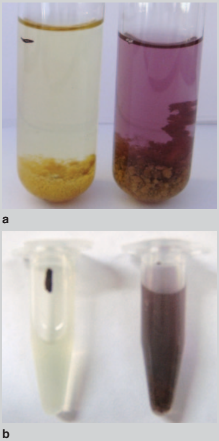

Figure 1. Tubes containing the *Hormoconis* biomass and biomass incubated with $HAuCl_4$ solution (a) after incubation of 24 h in an aqueous solution of $HAuCl_4$, (b) reference and gold nanoparticles after 6 months.

In Figure 3, the particles were confirmed as elemental Au^0 using x-ray diffraction (XRD). A couple of Bragg's reflections are distinctly exhibited, which may be indexed on the basis of the face-centered hexagonal structure of gold. The XRD spectrum shows four intense peaks, which agreed with the Bragg's reflection of gold nanoparticles as reported in the literature.[30] In earlier studies, the biological methods of synthesis gold nanoparticles[14,31] have been successfully carried out and substantiate our present finding of biosynthesis of gold nanoparticles.

The high-resolution transmission electron microscopy (HR-TEM) images illustrated the formation of gold nanoparticles by exposing 0.1g of *Hormoconis* biomass to 50 mL of 1 mM aqueous gold chloride solution at 26°C. The HR-TEM images recorded from drop-coated films of the gold nanoparticles synthesized by treating gold chloride solution with *Hormoconis* for 24 h are shown in Figure 4. A large density of spherical gold nanoparticles can be seen and the nanoparticles are quite ranged in size from 3–20 nm. Some hexagonal shaped particles are also present. Interestingly, particles are quite separated; this may be due to some bioorganic component secreted by the fungus acting as a stabilizing agent for the nanoparticles.

Figure 5 shows the energy dispersive x-ray spectroscopy (EDX) spectrum recorded in the spot-profile mode from one of the densely populated gold nanoparticles. Strong signals from the gold atoms in the nanoparticles are observed, while weaker signals from C, O, and Si atoms were also recorded. The C and O signals are likely to be due to x-ray emission from carbohydrates/proteins/enzymes present in the cell wall of the biomass while the Si signal is due to Si used as a substrate.

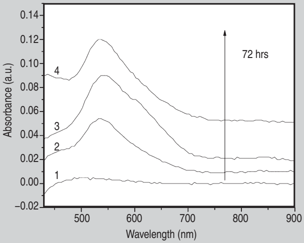

Figure 2. The UV-Vis spectra recorded as a function of reaction time of 1 mM $HAuCl_4$ aqueous solution treated with fungus *Hormoconis resinae*.

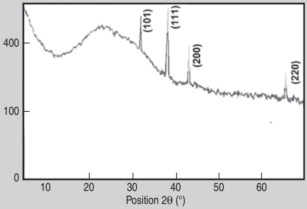

Figure 3. The XRD patterns recorded from drop-coated films of nanoparticles of gold synthesized using *Hormoconis resinae* on glass substrates. The Bragg reflections are indexed on the basis of the fcc structure.

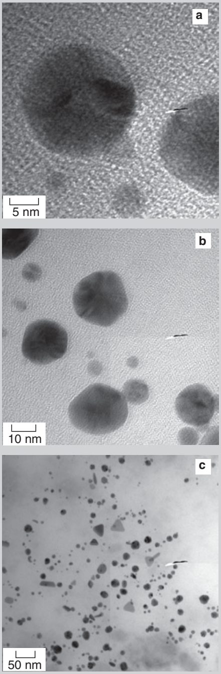

Figure 4. HR-TEM images illustrating the formation of gold nanoparticles by using fungus *Hormoconis resinae*.

CONCLUSION

Our results conclude that the fungus *Hormoconis resinae* is an excellent microbial resource for the extracellular synthesis of gold nanoparticles with appreciable stability in solution. The surface plasmon resonance band at 537 nm in UV-Vis spectrum indicates the primary evidence for synthesis of gold nanoparticles. The presence and size of gold nanoparticles in solution was further confirmed by the EDX and TEM techniques. The XRD spectrum shows that the gold nanoparticles were face-centered crystalline in nature. The sizes of these particles are measured with HR-TEM. To the best of our knowledge this is the first report showing extracellular synthesis of stable gold nanoparticles with *Hormoconis resinae*. The most important feature of *Hormoconis* fungi is the following fact: they have a widespread presence in soil near refinery and can produce a large amount of biomass. Such a cheap source of material gives the opportunity for cost-effective preparation of various gold-based nanostructures. Optimization of microbiological technique for synthesis of gold nanoparticles is yet to be worked upon.

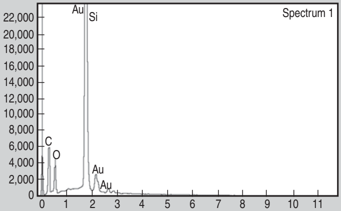

Figure 5. EDX of Au nanoparticles synthesized by treating 10^{-3} M $HAuCl_4$ aqueous solutions with fungus *Hormoconis resinae* and inset the particle targeted for EDX analysis.

ACKNOWLEDGEMENTS

The authors gratefully acknowledge the financial support (SR/S5/NM-22/2006) granted to this research from the Department of Science & Technology, New Delhi under the Nano Science Technology Initiative Scheme. We are also grateful to Principal, R. B. S. College Agra; Director, HCST, Farah (Mathura) and Director, NPL, Delhi for providing laboratory facilities.

References

1. J.R. Stephen and S.J. Maenaughton, *Curr. Opin. Biotechnol.,* 10 (1999), pp. 230–233.
2. R.K. Mehra and D.R. Winge, *J. Cell. Biochem.,* 45 (1991), pp. 30–40.
3. G. Southam and T.J. Beveridge, *Geochim. Cosmochim. Acta,* 58 (1994), pp. 4527–4530.
4. D. Fortin and T.J. Beveridge, in *Biomineralisation,* ed. E. Baeuerlein (Verlag, Germany: Wiley-VCH, 2000), p. 294.
5. M. Sastry, A. Ahmad, M.I. Khan, and R. Kumar, in *Nanobiotechnology,* ed. C.M. Niemeyer and C.A. Mirkin (Weinheim, Germany: Wiley-VCH, 2004), pp. 126–135.
6. S. Mann, *Biomimetic Materials Chemistry* (New York: VCH, 1996).
7. T.J. Beveridge and R.G.E. Murray, *J. Bacteriol.,* 141 (1980), pp. 876–877.
8. P. Mukherjee et al., *Angew. Chem.*, 40 (2001), pp. 3585–3588.
9. M. Sastry, A. Ahmad, N.I. Islam, and R. Kumar, *Current Sci.,* 85 (2003), pp. 162–170.
10. P. Mukherjee et al., *ChemBioChem.*, 5 (2002), pp. 461–463.
11. A. Ahmad et al., *Colloids and Surfaces B: Biointerfaces*, 28 (2003), pp. 313–318.
12. N. Duran et al., *J. Nanobiotechnol.*, 3 (2005), pp. 8–15.
13. D. Mandal et al., *Appl. Microbiol. Biotechnol.*, 69 (2006), pp. 485–492.
14. J. L. Gardea-Torresdey et al., *Nano Lett.*, 2 (2002), pp. 397–401.
15. A. Ahmad et al., *J. Am. Chem. Soc.*, 124 (2002), pp. 12108–12109.
16. A. Ahmad et al., *Langmuir*, 19 (2003), pp. 3550–3553.
17. A.N. Mishra et al., NATCHEE 2010, Proceedings of International Conference, ed. L.D. Khemani and S. Dass (India: Tata McGraw-Hill, 2010), pp. 205–210.
18. R. Varshney et al., *Digest J. Nanomat. and Biostruct.*, 4 (2009), pp. 349–355.
19. S.S. Nigam, in *Laboratory Test Methods in Microbiology* (Issued by Defence Research Laboratory (Materials), Ministry of Defence, Kanpur, 1965).
20. Anonymous, *HERB, IMI, Handbook* (Commonwealth Mycological Institute, Ferry Lane, Kew, Surrey, England, 1960).
21. V. Armendariz et al., *J. Nanoparticle Res.*, 6 (2004), pp. 377–382.
22. S. Senapati et al., *Small*, 1 (2005), pp. 517–520.
23. He Shiying et al., *Materials Letters*, 61 (2007), pp. 3984–3987.
24. P. Mulvaney, *Langmuir*, 12 (1996), pp. 788–800.
25. K.L. Kelly et al., *J. Phys. Chem. B*, 107 (2003), pp. 668–677.
26. M.A. EL-Sayed, *Acc. Chem. Res.*, 34 (2001), pp. 257–264.
27. M. Maye et al., *J. Am. Chem. Soc.*, 124 (2002), pp. 4958–4959.
28. T.J. Norman et al., *J. Phys. Chem. B*, 106 (2002), pp. 7005–7012.
29. S. Shiv Shankar et al., *J. Mater. Chem.*, 13 (2003), pp. 1822–1826.
30. J.W. Jeffrey, *Methods in Crystallography* (New York: Academic Press, 1971).
31. S. Shiv Shankar et al., *Nat. Mater.,* 3 (2004), pp. 482–488.

Anuj Narayan Mishra and Seema Bhadauria are with the Microbiology and Nanotechnology Research Lab, R.B.S. College, Agra, India; Mulayam Singh Gaur is with the Department of Physics, Hindustan College of Science & Technology, Mathura, India; and Renu Pasricha is with the Material Characterization Division, National Physical Laboratory (CSIR Lab.), New Delhi, India. Dr. Mishra can be reached at anujnmishra@rediffmail.com.